

Investigating the Epigenetic Regulation of the Eukaryotic Centromere by the Segregase Enzyme p97

A Thesis Presented to the Faculty of Medical Sciences Division, University of Oxford, for the Degree of Master of Science by Research in Biochemistry

Samuel East
Hertford College
University of Oxford

Supervised by Professor Lars Jansen, University of Oxford

Abstract

The centromere is a vital locus for mediating chromosome segregation. It defines the location where sister chromatids are joined, and constitutes the foundation of the kinetochore, facilitating microtubule binding in mitosis. The position of the centromere is defined by nucleosomes containing CENP-A, a centromere-specific histone which is a necessary and sufficient locus-specifying seed to facilitate deposition of further CENP-A nucleosomes via an epigenetic self-templating feedback loop. Once incorporated into chromatin, CENP-A is stably maintained across multiple cell divisions with a high degree of retention. No turnover of CENP-A has ever been observed, aside from its replicative halving during passage of the DNA replication fork, prior to deposition of newly synthesised CENP-A in G1 following mitosis.

This thesis explores the roles of recently identified proteins which may actively regulate CENP-A. These factors include SENP6, a SUMO protease found to be vital for stable CENP-A maintenance, and p97, a SUMO/ubiquitin segregase whose depletion was found to increase levels of centromeric CENP-A. The latter finding is unexpected, given that CENP-A turnover has not previously been detected. The experiments described herein confirm these initial observations and investigate mechanistic explanations. The increase in centromeric CENP-A levels in p97 depleted cells was found not to be a consequence of increased CENP-A loading, nor of reduction in cell cycle progression. Therefore, this represents the first observation of a factor capable of physiologically destabilising CENP-A nucleosomes. Simultaneous perturbation of SENP6 and p97 was found to fully rescue defects in CENP-A maintenance otherwise caused by SENP6 depletion. These findings lead to the hypothesis that SUMOylation of centromeric proteins destabilises CENP-A with the aid of the p97 segregase, which is kept in check by SENP6 as it cleaves SUMO chains.

Acknowledgements

I would like to sincerely thank Professor Lars Jansen for giving me the opportunity to join his group and work on such an exciting project. It's been a privilege to have such a supportive, insightful supervisor to guide me through this work with patience and humour.

Thank you also to Dr Sreyoshi Mitra for her instruction, her kindness, and for helping me navigate what was at times a very difficult project.

Thank you to all of the members of the Jansen Lab; to Marina, Bas, Sahar, Izma, Puneet and Milind, as well as all former members during my time. It has been a real honour to work alongside such a talented group of scientists, in the incredibly supportive environment that they have created. Thank you for the advice, the fun times, the language lessons, and the falafel!

Thank you to all of my friends – at Hertford, at Exeter, and in Northumberland – for keeping me sane and (sometimes) keeping me distracted.

Thank you to my parents, Robert and Rosie, for their unwavering understanding and care through good times and bad. Thank you to my sister, Meriel, for always knowing what to say. Thank you to Marvin, for always being there.

Table of Contents

Abstract 1

Acknowledgements 2

Table of Contents 3

Chapter 1 - Introduction 5

1.1 – Cell Division 5

1.2 – Chromosome Segregation and the Kinetochore 6

1.3 – The Centromere 8

1.3.1 – Location of the Centromere 8

1.3.2 – The Nucleosome 9

1.3.3 – Epigenetic Inheritance of the Centromere 11

1.3.4 – Regulation and Stability of CENP-A Nucleosomes 13

1.4 – Prior Research on CENP-A Stability 16

1.4.1 – The SNAP-Tag and Associated Protocols 17

1.4.2 – The Role of SENP6 in Centromeric Regulation 20

1.4.3 – The Segregase Enzyme p97 22

1.5 – Research Aims and Hypothesis 24

Chapter 2 – Initial Investigations into the Role of p97 in the Regulation of CENP-A 25

2.1 – Confirmation of Results of the Mitra *et al* Screen 25

2.1.1 – Pulse-Chase Experiments 27

2.1.2 – Confirmation of p97 Knockdown in Pulse-Chase Experiments 35

2.2 – The CENP-A Overloading Hypothesis 37

2.2.1 – Modified Pulse-Chase Experiments 37

2.2.2 – Quench-Chase-Pulse Experiments 39

2.2.3 – Confirmation of p97 Knockdown in Quench-Chase-Pulse Experiments 42

2.3 - Discussion 43

Chapter 3 – Investigating the Role of p97 in Regulation of the Cell Cycle 45

3.1 – The Cell Cycle Delay Hypothesis 45

3.2 – Use of Flow Cytometry to Investigate the Effects of p97 Knockdown in Cycling Populations 46

3.3 – Thymidine Arrest Experiments 49

3.3.1 – Analysis of Cell Counts to Confirm Successful Arrest 52

3.3.2 – Use of EdU Staining to Confirm Successful Arrest 53

3.4 - Discussion 56

Chapter 4 – Investigating the Direct Action of p97 at Centromeric Chromatin 57
4.1 – Hypothesising an Increase in CENP-A Stability 57
4.1.1 – p97 Acting as an Antagonist to SENP6 57
4.1.2 – The Auxin Inducible Degron 59
4.1.3 – SENP6-AID Rescue Experiments using p97 RNAi 60
4.1.4 – SENP6-AID Rescue Experiments using Pharmacological p97 Inhibition 65
4.1.5 – Discussion of SENP6-AID Rescue Experiments 68
4.2 – Investigating the Direct Action of p97 on CENP-A Nucleosomes 68
4.2.1 – CENP-A-AID Rescue Experiments using p97 RNAi 69
4.2.2 – CENP-A-AID Rescue Experiments using Pharmacological p97 Inhibition 72
4.3 – Discussion 73

Chapter 5 – Discussion and Conclusions 75

Chapter 6 – Materials and Methods 81
6.1 – Cell Culture 81
6.2 – RNAi 82
6.3 – CENP-A-SNAP Experiments 82
6.3.1 – Pulse-Chase Protocol 82
6.3.2 – Modified Pulse-Chase Protocol 83
6.3.3 – Pulse-Chase Protocol Alongside Thymidine Arrest 84
6.3.4 – Quench-Chase-Pulse Protocol 84
6.4 – Immunofluorescence 84
6.5 – Immunoblotting 85
6.6 – Microscopy and Image Analysis 85
6.7 – Flow Cytometry 86
6.8 – EdU Staining 87
6.9 – Drug Treatment 87
6.10 – Miscellaneous 87

Bibliography 88

Chapter 1 – Introduction

1.1 – Cell Division

Cell division is a vital process for the propagation of life. The successful division of parental cells is required for countless biological activities; from the maintenance and repair of large multicellular organisms, to their growth and reproduction. Two main forms of cell division have evolved; mitosis and meiosis. In mitotic eukaryotic cells, on which this thesis concentrates, cell division occurs following DNA replication during S-phase, when genomic material exists as two copies known as a pair of sister chromatids. Successfully divided genetic material may then become the genetic basis for the cellular processes in each daughter cell. Therefore, mitosis allows for the production of genetically identical diploid daughter cells (1,2). This process is summarised in Figure 1.1 below.

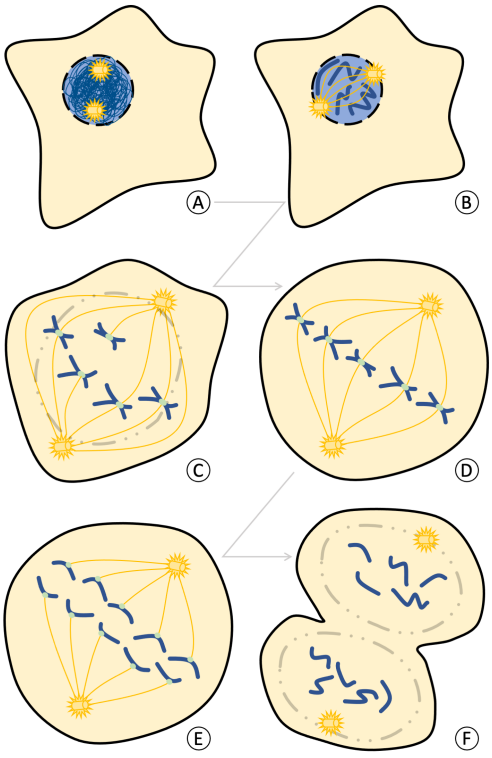


Figure 1.1 – Schematic representing the passage of a eukaryotic cell through mitosis. In Part A, the cell is in G2 phase, having successfully replicated its genome. Chromatin resides in the nucleus alongside the centrosomes (shown as yellow barrels) and remains uncondensed. This then progresses to prophase (Part B) in which chromatin condenses into readily distinguishable chromosomes, and the mitotic spindle begins to form around the centrosomes. Prometaphase (Part C) and metaphase (Part D) then follow, in which the nuclear envelope dissipates, and the spindle fibres extend from the nuclear poles to attach to the sister chromatids of each chromosome, arranging them in a plane through the centre of the cell. During these phases, the cell morphology will typically become more rounded. Once the chromosomes are successfully arranged, anaphase (part E) will follow. During anaphase, separation of the sister chromatids occurs. In the final stages – telophase and cytokinesis (part F) – the new nuclear membranes corresponding to the daughter cells begin to reform, and the cell is cleaved in two (3).

In comparison to mitosis, meiosis is a specialised form of cell division which takes place in sexually reproducing organisms. During meiosis, cells undergo two consecutive cell divisions without intervening DNA replication. This is known as reductionist division, and it produces haploid gametes which carry half of the full genetic information belonging to the individual. These

gametes may then fuse following sexual reproduction. In becoming fertilized, they jointly form the zygote, whose genetic information is a mixture of that from the parental organisms, and which may then develop into their offspring (3,4).

1.2 – Chromosome Segregation and the Kinetochore

A key aspect of all forms of cell division is correct chromosome segregation; this is a process in which genetic information is equally divided between the two poles of the cell, as portrayed in Figure 1.1 above. Overall, chromosome segregation is a process that has evolved intricately; defects in it may lead to aneuploidy, cell death, and the potential for a wide range of genetic and oncological pathologies in an organism and its offspring (5–8).

Successful chromosome segregation is in part governed by the kinetochore; a macromolecular protein assembly which maintains connections from the spindle fibres to the chromatin. This allows the sister chromatids to be mechanically separated, as the disassembly of the microtubules retracts them towards the nuclear poles (7). During DNA replication, the sister chromatids are physically linked by the cohesin ring at multiple locations along the chromosome arms. The cohesin ring is a multiprotein complex which topologically constrains the pair within its tripartite structure until the onset of anaphase (9,10). Dissolution of the cohesin ring is an additional requirement for chromosome segregation; these complexes must become depleted from chromosomes at the site of spindle binding such that they no longer bind sister chromatids together. This allows the tensile forces created as microtubules contract to separate the sister chromatids (11,12). The newly separated DNA contained within may therefore be passed on to progeny, wherein it stores biological information, is transcribed for cellular processes, and is once again capable of acting as a template for its own replication in successive generations of cells (9,13).

Further, the kinetochore acts to monitor and regulate the bi-directionally orientated attachment of the microtubules to chromatin, maintaining the sister chromatids in a state of tension between opposing microtubules during metaphase (9,13–15). The kinetochore is also capable of correcting errors in the binding of these microtubules (16,17), preventing the cell from transitioning from metaphase into anaphase until successful, ordered connections have been made between the chromatin and the spindle poles (18). This mechanism operates via the spindle assembly checkpoint (SAC, also known as the mitotic checkpoint), a biochemical surveillance pathway which is tied to the cell cycle and prevents the onset of anaphase (2,17,19,20).

SAC signalling is primarily driven by the existence of unattached kinetochores, detected by the direct interaction between SAC factors and KNL1, a component of the outer kinetochore (see Figure 1.3) (21). SAC components, produced at the unattached kinetochore, diffuse to then inhibit a downstream E3 ubiquitin ligase known as the anaphase promoting complex (APC) or 'cyclosome' (18,22–24). The APC is a component of the ubiquitin system; it acts by covalently tagging substrates with multiple ubiquitin molecules, creating polyubiquitin chains that mark these substrates for degradation at the 26S proteasome (3,25). Specifically, the APC targets several factors whose action prevents chromosome segregation. One of these factors is securin, an inhibitor of separase; the protease enzyme responsible for dissolution of the cohesin ring, as discussed above (26,27). Crucially, the APC also targets cyclin B, a subunit of the cyclin-B/CDK1 complex, which phosphorylates key substrates in order to prevent mitotic exit (2,20,28). Therefore, securin and cyclin B are stabilised by inactivation of the APC until SAC signalling is terminated. This termination is in turn triggered by the correct attachment of microtubules to the kinetochore, causing the reaction of a mechanical 'switch' which physically separates molecular components in order to disrupt and silence the SAC signalling cascade. This removes the cell cycle block and allows passage through mitosis (19,20,29,30).

1.3 –The Centromere

Of key importance to these processes is the site at which the kinetochore binds to chromatin. At this locus, the kinetochore connects the spindle fibres to chromosomal DNA. This region of the chromosome is known as the centromere (31,32). The centromere also represents the final site of cohesion between the two sister chromatids. It is a bifunctional structure which internally binds the chromatids together until the onset of anaphase, and externally binds to microtubules via the kinetochore. During prophase, cohesin complexes begin to dissociate from the chromosome arms. However, it is not until anaphase that cohesin dissolution occurs at the centromere (33). This grants mitotic chromosomes their characteristic 'X' shape, as the sister chromatids remain topologically associated at the centromere, but not along the arms. The centromere is therefore the locus from which they become bidirectionally orientated and physically separated towards the nuclear poles. It acts as a recognition and assembly site for the kinetochore (13,31,34) via the constitutive centromere-associated network (CCAN), a cluster of proteins which link centromeric chromatin and the inner kinetochore (35–37). Many components of the SAC also assemble atop the kinetochore; the activity of this checkpoint is physically and functionally dependent upon the centromere (30). As such, the centromere – its location, and its biochemical regulation – is of critical importance to the processes of chromosome segregation and mitotic passage, and therefore to cell division as a whole.

1.3.1 – Location of the Centromere

In budding yeast, the location of the centromere is defined genetically; the kinetochore forms atop a small (~125 bp) sequence-specific region of DNA (38,39). Conversely, for most higher eukaryotes, the centromere is significantly larger, and its location is defined *epigenetically* (31,32,40,41). That is to say; the location of the centromere is heritable by offspring yet it is not specified by the underlying DNA sequence (42,43). The locations of eukaryotic centromeres do typically correlate strongly with regions of the genome which consist of repetitive A/T-rich

α-satellite DNA. These sequences often extend for multiple megabases in humans (39,44–46). However, while they have contributing roles, the existence of these sequences is neither necessary nor sufficient to define the centromeric locus. Chromosomal rearrangements have been shown to be capable of 'silencing' – or inactivating – an existing centromere, even if it resides within the A/T-rich regions that may otherwise characterise it (47,48). Additionally, neocentromeres have been observed within regions of the genome that do not contain this α-satellite DNA (49–51). Rather than having a purely genetic basis, it has become clear in recent decades that centromere specification is primarily dependent upon chromatin structure, and in particular that its location is determined by the existence of a specific nucleosomal marker (31).

1.3.2 – The Nucleosome

Nucleosomes are the basic packaging unit of chromatin; a protein octamer comprised of four core histone proteins - H2A, H2B, H3 and H4 – around which DNA is wrapped in a spool-like fashion (52). These structures are chained together on a macromolecular level like 'beads on a string' (53). Each octamer may accommodate just under two turns of DNA, or approximately 147 base pairs. De novo assembly of nucleosomes occurs via a stepwise mechanism in which their separate components are loaded onto the DNA. An H3/H4 heterotetramer is initially deposited, followed by two H2A/H2B dimers (54). This occurs extremely rapidly following replication, with the nucleosome assembling onto the newly synthesised DNA almost immediately as the replication machinery completes a passage long enough to wrap around the octamer (55,56). This assembly occurs via a cascade of reactions during which the histone proteins are bound to and directed by various molecular chaperones, including "chromatin assembly factor 1" (CAF-1, see Section 1.3.4) (56,57). This cascade is additionally mediated by the acetylation of these histone components by B-type histone acetyltransferases (B-type HATs) (58). The crystal structure of a completed nucleosome in complex with DNA is shown below (Figures 1.2a, 1.2b).

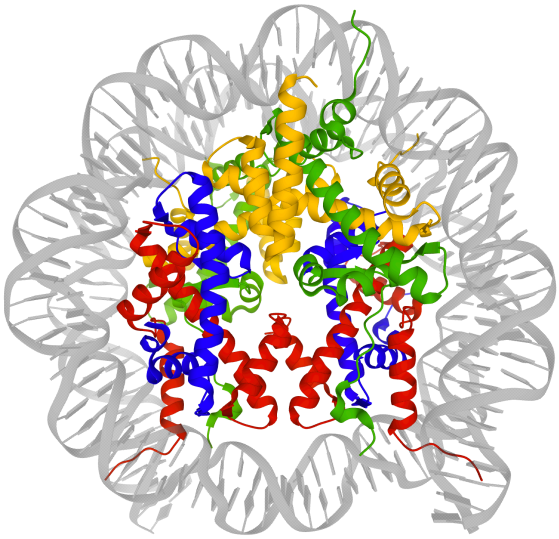


Figure 1.2a – Structure of a nucleosome and the spooling of DNA around it, top-down view

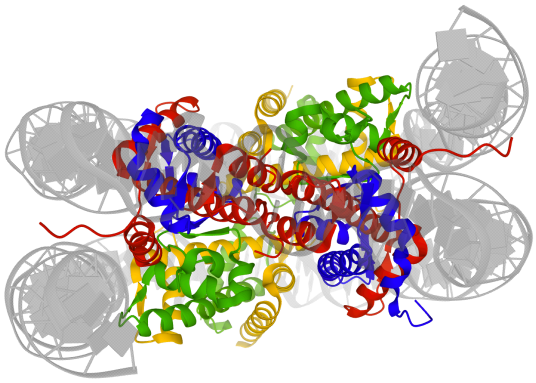


Figure 1.2b – Structure of a nucleosome and the spooling of DNA around it, side-on view

Figures 1.2a and 1.2b show the structure of a completed nucleosome, around which approximately 1.7 turns of DNA is spooled. Individual histone subunits can be identified; histones H2A are shown in green, H2B in yellow, H3 in red, and H4 in blue. DNA is shown in semi-transparent grey. Two copies of each histone protein are readily discernible. Figures 1.2a and 1.2b created with the tools and structures available at the RCSB protein databank (59–61)

Following their assembly, nucleosomal turnover is a highly dynamic process, and one whose kinetics vary across different regions of the genome. Rates of turnover are found to be rapid at transcribed regions of active genes, and at enhancer and promoter regions, where they may turn over several times per cell cycle (62). These rates are correlated with histone methylation and acetylation states (63,64) and depend on the activities of histone chaperones such as anti-silencing function protein 1 (ASF1) (65) and the minichromosome maintenance complex (MCM2, see also Section 1.3.4) (66), shuttling histones away from sites of disruption towards locations where nucleosomes may reassemble (67). Indeed, nucleosome recycling is a core aspect of DNA replication. In general, following the passage of the replication fork (Section 1.3.4) the parental histones disperse to either side and are reincorporated into the DNA, likely reassembled from their individual components following initial segregation of the H3/H4 heterotetramers (68,69). The exact mechanisms of this recycling remain a subject of research and debate, although experiments suggest that CAF-1, ASF1, and MCM2 are key components of this pathway (65,66,70).

Once incorporated into chromatin, nucleosomes carry out a variety of vital roles within the cell. On a macromolecular level, they allow for the efficient packaging of DNA into condensed forms of chromatin. Linker histones define the conformation and density of the histone octamers, and therefore may condense the associated DNA into tightly bound units for efficient packaging and storage. Alternatively, they may instead be instructed to adopt a more open conformation, so as to allow cellular machinery – such as that required for replication or transcription – to access the genetic material. Further, nucleosomes are vital components of many well-established regulatory processes. Covalent modifications to their surfaces act as signals to enhance or inhibit cellular processes on associated DNA, thus altering the phenotype of an organism without modifying its genetic code (71–73). These signals may be considered epigenetic in nature if their resultant phenotype is inheritable by offspring in the continued absence of DNA changes (42,43).

1.3.3 – Epigenetic Inheritance of the Centromere

An example of the utility of nucleosomes as epigenetic markers is their regulation at centromeres. The centromeric locus is defined by the presence of nucleosomes in which the canonical histone H3 (shown in Figures 1.2a, 1.2b above) has been replaced by a centromere-specific variant protein, known as centromere-protein A (CENP-A) (31,34,74–76). This replacement acts as a reliable marker for centromere location (77). CENP-A was initially discovered as a histone-like protein which associated with centromeric chromatin (74,75,78) in a wide variety of eukaryotic organisms (49). CENP-A nucleosomes are functionally similar to canonical nucleosomes, and retain their classical octameric structure (76). Crucially, the presence of CENP-A nucleosomes has been shown to be both necessary and sufficient for centromere formation (79). In *Drosophila*, targeting of genetically modified CENP-A-GFP-LacI fusion proteins to LacO sequences in non-centromeric regions of chromatin was sufficient to cause the formation of functional centromeres and kinetochores at those sites. Further, these artificial neocentromeres were heritable, and capable of recruiting wild-type (untagged) CENP-A (80). Analogous results were

obtained in chicken cells (81), and in human cells via the tethering of the CENP-A histone chaperone HJURP (Holliday junction recognition protein) (82). This malleable and inducible heritability occurs due to the fact that CENP-A nucleosomes are deposited in a self-templating epigenetic feedback loop, whereby the presence of existing CENP-A facilitates the deposition of new CENP-A in a cell-cycle controlled manner (83). The structural relationship between CENP-A nucleosomes and the CCAN and kinetochore is summarised below (Figure 1.3). Note that an additional key centromeric protein – CENP-B – is known. However, CENP-B does not form a part of the CCAN, and instead binds directly to α-satellite DNA. This is further discussed in Section 2.1.1 below.

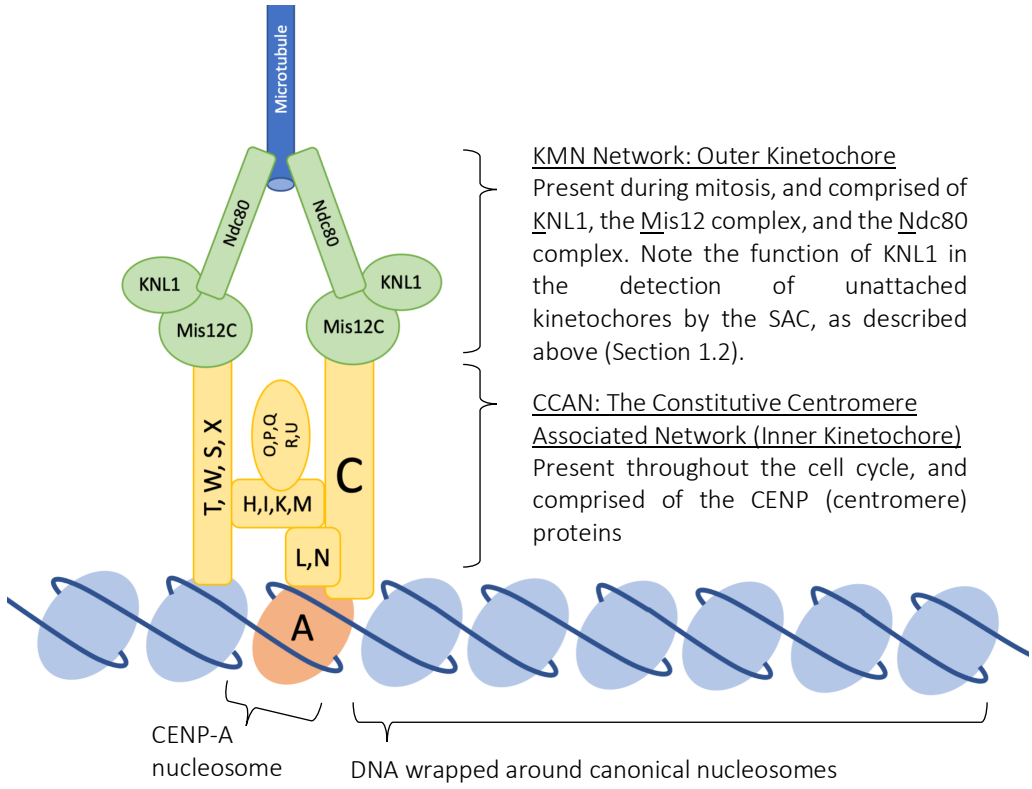


Figure 1.3 – Schematic representing the structure of the inner and outer kinetochore. Produced based upon "Critical Foundation of the Centromere: The Constitutive Centromere Associated Network (CCAN)" (37).

Highlighted in Figure 1.3 is the KMN network. As indicated, this consists of KNL1, the Mis12 complex, and the Ndc80 complex. Collectively, the KMN network acts as a core binding region to connect centromeric DNA to microtubules via the kinetochore (17,84). This network forms on top of centromeres during prophase, before dissipating in telophase (17,85). As mentioned

previously, KNL1 (CASC5/blinkin) plays a role in the mitotic checkpoint; it has been shown to bind to BUB1 and BUBR1, two components of the SAC (21). It has also been shown to bind directly to microtubules (84), and is itself recruited by the Mis12 complex; the "keystone" of the outer kinetochore (35,85). The Mis12 complex broadly serves as a foundation for outer kinetochore architecture. It binds directly to CENP-C (86), thus joining the KMN network to the CCAN. Whilst it has not been shown to bind to microtubules itself, it does enhance the microtubule binding affinities of KNL1 and the Ndc80 complex (84,85). The Ndc80 complex – the final key component of the KMN network – is crucial for correct interaction between the kinetochore and the microtubules. It is capable of directly binding microtubules *in vitro,* and this affinity is significantly strengthened when in complex with the full KMN network (84,87). It also has a role in error correction at the kinetochore. Ndc80/Hec1, a component of this complex, is regulated to promote both the binding and detachment of microtubules to the kinetochore. This is controlled by the phosphorylation of Hec1 by Aurora B kinase, an enzyme which broadly acts to maintain the fidelity of correct microtubule attachment (84,87,88), and which may also play a role in SAC signalling; evidence suggests that the detection of tension by Aurora B in correctly aligned chromosomes contributes to the downregulation of this pathway, and so allows passage through anaphase (89).

Having established an overview of the key components of the kinetochore and their modes of operation within the broader perspective of chromosome segregation, this thesis now focuses on the regulation and dynamics of CENP-A chromatin.

1.3.4 – Regulation and Stability of CENP-A Nucleosomes

CENP-A is regulated in a precise and controlled manner throughout the cell cycle. During DNA replication in S-phase, new CENP-A containing nucleosomes are not deposited during the large-scale assembly of new histones that accompanies this process (90,91). Instead, CENP-A nucleosomes are evenly divided to either side of the progressing replication fork, with

nucleosomes containing H3.3 – a variant of histone H3 – incorporated as placeholders (92). This is shown schematically below (Figure 1.4).

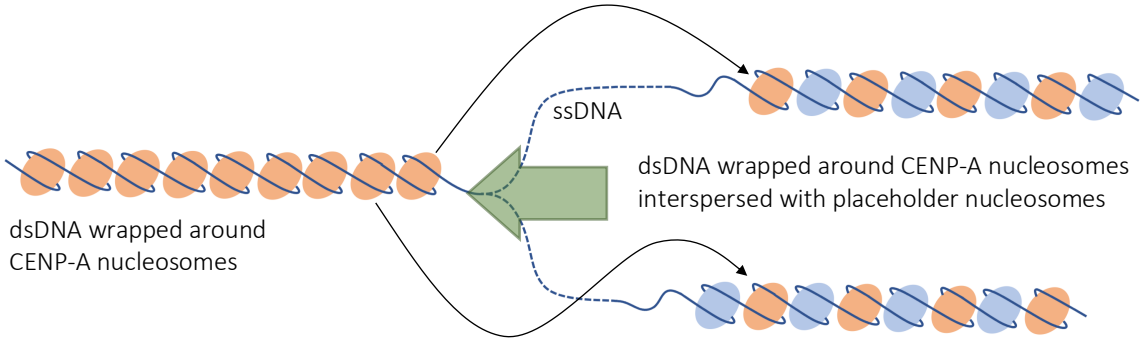


Figure 1.4 – Simplified schematic showing the passage of the replication fork at centromeric chromatin. CENP-A nucleosomes (shown in orange) are faithfully transmitted from the parental dsDNA to the leading and lagging strands, as indicated by the black arrows. Placeholder H3.3 nucleosomes (shown in blue) are deposited alongside these CENP-A nucleosomes after the passage of the fork, resulting in a 50% reduction in CENP-A levels at chromatin. Direction of passage of the fork is indicated by the green arrow. Single-stranded DNA is indicated by the dashed lines.

It is not until G1 following the mitotic exit that placeholder H3.3 nucleosomes are removed, and CENP-A nucleosomes are deposited in their place to restore centromeric CENP-A to prior levels (Figure 1.5a) (91,93). Crucially, the existence of nearby CENP-A nucleosomes serves as a marker for this replacement, such that the positions of parental centromeres define the positions of those of the daughters (94). Notably, CENP-A nucleosomes are extremely stable once incorporated into centromeric chromatin; they have been shown to have a significantly longer biological half-life than their canonical H3-containing counterparts (93) (Section 1.3.2) with no appreciable turnover having been detected, save the 50% 'dilution' that occurs alongside the replication fork during DNA replication (Figures 1.4, 1.5b) (91,93,95). However, the biochemical origins of this very high stability are not yet fully understood.

It is noteworthy that this lack of appreciable turnover implies that CENP-A nucleosomes are not only stable, but that they are in fact stably transmitted from one generation to another across multiple cell division cycles with a very high degree of retention at the centromere (93,95). This is an intrinsically surprising observation, given that CENP-A nucleosomes are subject to a wide host

of interfering forces; forces which would otherwise be expected to displace them from the centromere.

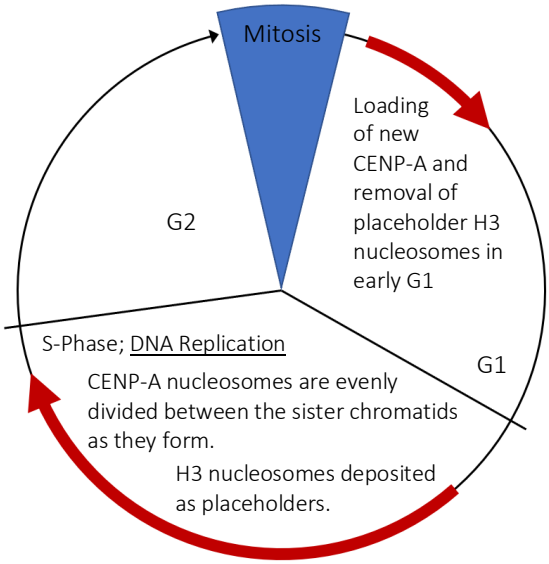


Figure 1.5a – Overview of CENP-A dynamics across the cell cycle

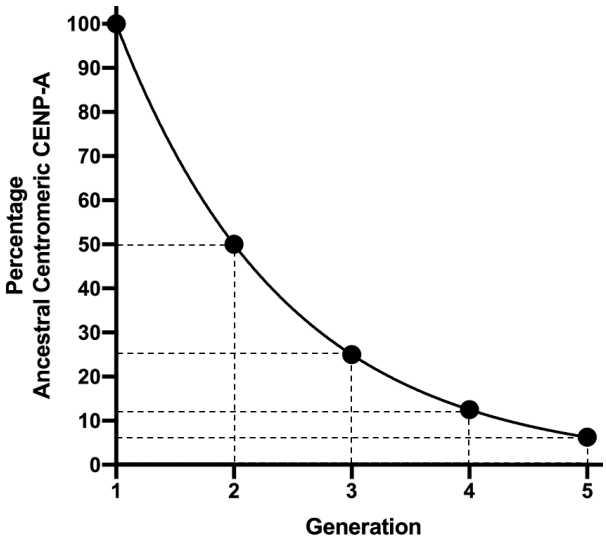


Figure 1.5b – Schematic model showing theoretical results of successive 50% dilutions of ancestral CENP-A nucleosomes across generations. Note that this does not result in a depletion of total centromeric CENP-A levels, as newly synthesised CENP-A is reincorporated during early G1

At a minimum, all nucleosomes must be displaced from chromatin at the replication fork during DNA replication, regardless of where they sit along the chromosome. Stages in the replication process include the unwinding of the DNA duplex by the minichromosome maintenance helicase complex (MCM2-7) (96–98) and the passing of the leading and lagging strands of this newly unwound DNA through polymerases such as Polδ and Polε – which carry out the majority of DNA synthesis – and Polα, which acts to prime the lagging strand for this subsequent synthesis (99). This machinery is tethered in place by the proliferating cell nuclear antigen (PCNA); a homotrimeric ringed protein which encircles double-stranded DNA and recruits a histone chaperone protein known as chromatin assembly factor 1 (CAF-1) following the passage of the replisome. This allows the reassembly of histone proteins at the chromatin (100,101). It is not feasible that these processes could occur on DNA which remained wrapped around nucleosomes.

Indeed, replication requires 'naked' DNA, with stretches of ~300bp long nucleosome-free regions having been observed before and after the replication fork (102).

In comparable circumstances, the nucleosome also presents a barrier to the passage of transcriptional machinery (103). Histone presence on the DNA inhibits initiation and elongation of transcription (104), in which RNA polymerases bind to promoter regions of the DNA and synthesise mRNA from the template strand respectively. Nucleosomes must be displaced to alleviate this block (105). Further, whilst centromeres typically reside at gene-free regions of the chromosome (32,106), evidence suggests that centromeric regions of chromatin are transcribed to some extent, producing non-coding RNA strands at low levels which bind to and stabilise key kinetochore proteins. This promotes the formation of the kinetochore at the centromere (107–110). Transcription is expected to displace nucleosomes; canonical nucleosomes have been shown to transfer out of the path of transcribing polymerases (111). Therefore, the observation that CENP-A nucleosomes are stably transmitted and do not relocate away from the centromere at any point during the cell cycle is intriguing, especially given that this observation is not mirrored in canonical nucleosomes. The highly reliable maintenance of CENP-A nucleosomes at centromeric loci despite myriad stresses that would otherwise displace them remains an open question.

1.4 – Prior Research on CENP-A Stability

Recently, a paper has been published by Dr Sreyoshi Mitra and colleagues in which light is shed on a variety of genes responsible for the stable transmission of CENP-A nucleosomes across generations (112). Mitra *et al* conducted a high-throughput screen, searching for factors involved either in the loading of nascent CENP-A at the centromere during G1 phase, or in the maintenance of the ancestral chromatin-bound 'pool' of pre-existing centromeric CENP-A. A custom siRNA library was assembled to target 1046 genes, known in literature to code for proteins involved in a wide range of nuclear regulatory processes, but which had not necessarily been previously

associated with the maintenance or loading of CENP-A at the centromere. The effects of knockdown of these genes on centromeric CENP-A was observed, and a range of proteins identified which showed evidence of involvement in CENP-A regulation; as factors that load CENP-A to nucleosomes at centromeric loci, and/or as factors that regulate and stabilise its presence there through the cell cycle (112).

1.4.1 – The SNAP-Tag and Associated Protocols

A key requirement for Mitra *et al*'s study was technology to enable researchers to selectively measure – and distinguish between – the retention of prebound centromeric CENP-A and the incorporation of newly-synthesised CENP-A into chromatin. This requirement was met using the SNAP-tag. This molecular labelling technique, pioneered by Juillerat *et al* (113) was built around a suicide enzyme bioengineered for use with small reporter molecules. Directed evolution was used to produce mutants of AGT (O^6-alkylguanine DNA alkyltransferase); a human DNA repair protein. In vivo, AGT protects cells from mutagenesis by acting upon DNA to convert O^6-methlyguanine – a commonly occurring DNA lesion – to guanine. It achieves this by removing the erroneous methyl group from the DNA base via an S_N2 mechanism at its reactive Cys145 residue. Following a single use, the alkylated AGT enzyme is targeted by the ubiquitin pathway, and degraded at the proteasome (114). In the case of the artificial SNAP-tag labelling process, genes expressing proteins of interest may be targeted in-frame for genetic fusion with an AGT mutant which no longer acts upon DNA, but which does react with artificial O^6-alkylguanine substrates. The alkyl groups on these substrates may carry a variety of small molecular probes – typically fluorophores – which are then transferred to the protein of interest at a time varying by experimental setup (113,115), as shown schematically in Figure 1.6 below. This allows pools of the protein of interest to be differentiated according to the times at which they are synthesised.

Further, it allows the fates of these nascent and ancestral protein pools to be distinguished, granting key information regarding protein turnover and dynamics (116).

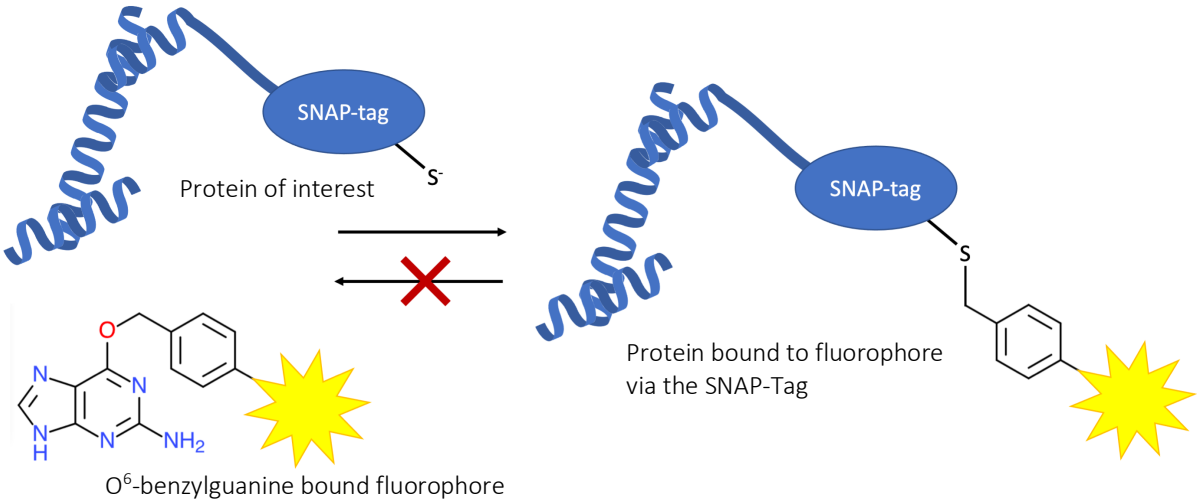


Figure 1.6 – Schematic representing the mode of action through which the SNAP-tag allows the fluorescent labelling of a protein of interest.

Mitra *et al* utilised two key SNAP-tag protocols; the pulse-chase setup, and the quench-chase-pulse setup (112). In a pulse-chase experiment, the fluorescent labelling capability of the SNAP-tag is utilised to observe the fate of a pre-existing SNAP-tagged pool of the protein of interest in live cells. This pool is initially 'pulsed' by labelling existing protein with a membrane permeable O^6-alkylguanine bound fluorophore, such as TMR-Star. This fluorophore is irreversibly bound to the protein of interest by the enzymatic activity of the SNAP-tag. Following washing steps and the removal of the dye, the cells are left to proliferate for a set amount of time, known as the 'chase.' Cells are then microscopically analysed to determine the remaining quantity and/or subcellular localisation of the fluorophore-bound protein (116).

Conversely, in a quench-chase-pulse experiment, the SNAP-tag is used to analyse a newly synthesised population of a protein of interest. This protocol begins by 'quenching' any pre-existing protein of interest by labelling it with a non-fluorescent SNAP blocking substrate. As the SNAP enzyme retains the irreversible mode of action of AGT, this prevents any tagged protein present at this time from appearing in later fluorescence analysis. The cells are then 'chased' for

a set period of time as in a pulse-chase protocol. Any protein of interest synthesised during this time will retain its unreacted SNAP-tag, as it has not been quenched with the blocking substrate. This newly synthesised pool may then be observed by pulsing the cells with a fluorescent SNAP substrate and microscopically imaging them. This allows quantification of the amounts and subcellular localisations of any protein of interest synthesised during the chase window (116). These procedures are outlined and compared below (Figure 1.7).

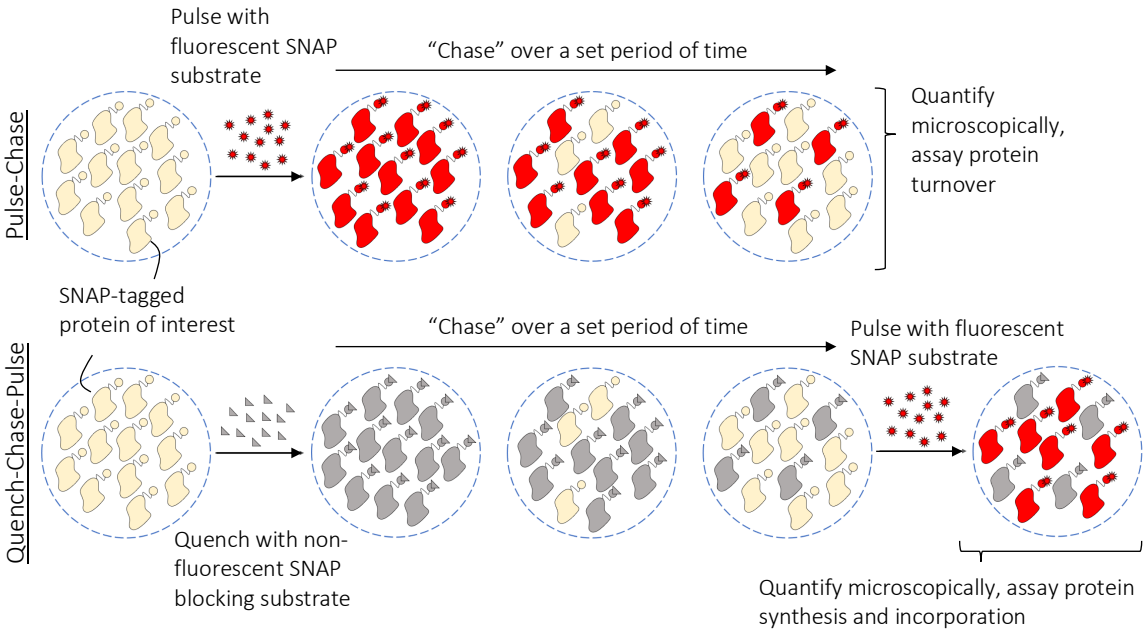


Figure 1.7 – Overview of pulse-chase and quench-chase-pulse experimental protocols.

Created with reference to schematics found in Mitra *et al* (112).

Mitra *et al* used these strategies to investigate the effects of targeted gene knockdown on CENP-A dynamics, using HeLa cells expressing CENP-A-SNAP. This line was originally created by Jansen *et al*, who stably integrated a CENP-A-SNAP transgene via retroviral transfection, such that it is constitutively overexpressed alongside unmodified CENP-A (91). Pulse-chase experiments were tied to knockdown during the chase in order to determine the effects of this knockdown on pre-existing chromatin-bound CENP-A. In other words, this probed for the effects of these genes on the maintenance of centromeric CENP-A nucleosomes. Further, the simultaneous assessment of this knockdown with a quench-chase-pulse protocol allowed investigation into the effects of

these genes on the loading of new CENP-A nucleosomes at the centromere. Amalgamated results of this screen are presented and discussed below (Figures 1.8a, 1.8b)

Figure 1.8a

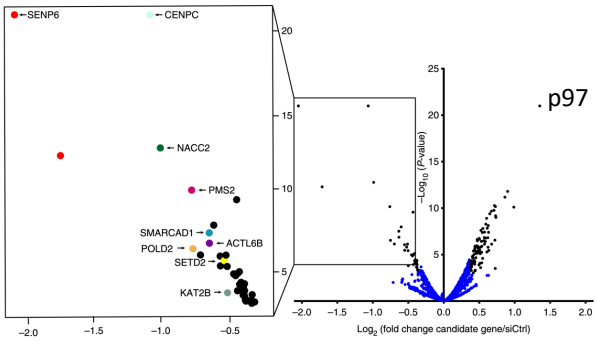


Figure 1.8b

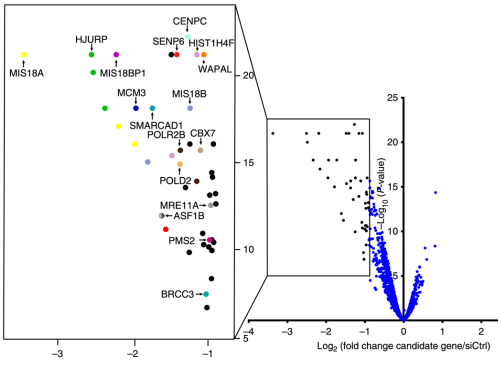


Fig 1.8a - Results of pulse-chase experiments in the siRNA screen conducted by Mitra et al. Changes in centromeric CENP-A intensity are plotted on the x-axis on a log2 scale as a measure of CENP-A stability and maintenance relative to control during knockdown of each gene of interest. Biological reproducibility is shown on the y-axis, with p-values (n=5) plotted on a -Log10 scale.

Fig 1.8b - Analogous results for a quench-chase-pulse setup. Changes in centromeric CENP-A intensity on the x-axis now represent changes in CENP-A loading at the centromere relative to control during the experiment.

Figures 1.8a and 1.8b reproduced with permission from Mitra et al (112). Fig 1.8a modified to highlight p97 in order to facilitate discussion below. Boxes represent artificial cut-off points for changes in centromeric CENP-A and in confidence intervals.

1.4.2 – The Role of SENP6 in Centromeric Regulation

A key result obtained by Mitra *et al* was the discovery of a novel maintenance factor of centromeric CENP-A (112). Depletion of SENP6 – a SUMO-specific protease – resulted in a significant reduction in observed levels of centromeric CENP-A under a pulse-chase protocol compared to control. Thus, SENP6 depletion hindered the ability of the cell to maintain CENP-A nucleosomes which had already been loaded onto chromatin; SENP6 is required to stably maintain centromeric CENP-A. This observation extended throughout the cell cycle. SENP6 is required at all times as a CENP-A maintenance factor (112).

SENP6 is in fact required to stabilise a multitude of CCAN proteins. Mukhopadhyay *et al* (2010) demonstrated that maintenance of the CENP-H/I/K complex (see Figure 1.3) is dependent upon

SENP6 (117). Mitra *et al* showed that, in addition to CENP-A, this is also the case for CENP-C and CENP-T. This indicates that the foundation of the CCAN is actively maintained by SENP6. Mitra *et al* continued on to demonstrate that while depletion of SENP6 causes loss of CENP-A from the centromere, it does not affect its total cellular levels, implying that SENP6 regulates the localisation of CENP-A to the centromere, but not its degradation (112).

As a SUMO protease, SENP6 is a member of a family of enzymes whose activities play roles in numerous cellular processes. Analogous to the ubiquitin system, target proteins in this network are modified by covalent conjugation with SUMO (small ubiquitin-like modifier) proteins via activating (E1), conjugating (E2), and ligase (E3) enzymes; either as SUMO monomers or further extended to polySUMO chains (118,119). However, unlike some ubiquitin chains, SUMOylation is not necessarily a marker for degradation; the SUMO pathway is a multifunctional and malleable control system which broadly orchestrates the interactions of its target proteins with other peptides in the cell. It regulates a wide range of biochemical networks, and its impedance can cause diverse physiological defects, up to and including cell death (120–122). It has also been found working in conjunction with the ubiquitin network, with polySUMOylation capable of promoting downstream polyubiquitination (119). SUMOylation is a reversible modification; SUMO proteases such as SENP6 cleave SUMO species from target proteins, creating a dynamic cycle of SUMOylation and deSUMOylation (123). By deSUMOylating their substrates, SUMO proteases have been demonstrated to regulate the activities of a diverse range of transcription factors; including those that regulate genes managing oxidative-stress response (124), development and metabolism (125–127), apoptosis (128), Notch signalling (129) and immune response (130). SUMO regulation has also been demonstrated playing a role in cell cycle control (131–133) and in mitochondrial fission (134).

Notably, Mitra *et al* found evidence of polySUMOylation of CENP-C and CENP-I, with the accumulation of SUMO chains at these peptides dependent upon loss of SENP6. However, SUMOylation of CENP-A was not observed (112). These results, backed up by cooccurring studies (135,136) suggest the hypothesis that centromeric CENP-A levels are indirectly maintained by the stabilising activity of SENP6 on other core CCAN proteins, but that CENP-A is not itself a direct target of the SUMO pathway.

This finding is in contrast to the role of the SUMO pathway in the regulation of CENP-A (Cse4) in *Saccharomyces cerevisiae*. Cse4 is directly SUMOylated near its N-terminal (Lys65) by the E3 ligases Siz1 and Siz2, resulting in its subsequent ubiquitylation and proteolysis; this mechanism prevents the mislocalisation of Cse4 to noncentromeric regions (137,138). In addition, the C-terminal SUMOylation of Cse4 at Lys215/216 has instead been shown to promote the deposition of Cse4 into chromatin (139). As such, in yeast, the direct SUMOylation of Cse4 acts as bidirectional control network, promoting the loading of Cse4 at the centromere and preventing its misloading elsewhere, thus maintaining the integrity of the *Saccharomyces* centromere.

Therefore, whilst evidence suggests that CENP-A is not directly SUMOylated in higher eukaryotes, the role of the SUMO pathway in broader centromeric regulation in these species remains an open avenue of research.

1.4.3 – The Segregase Enzyme p97

Whilst not yet remarked upon in publication, another enzyme known to play a role in the SUMO pathway was also flagged by the screen run by Mitra *et al* (personal communication). The enzyme ‘p97’, alternatively known as ‘valosin containing protein’ (VCP), or as ‘cell division control protein 48’ (CDC48) in *Saccharomyces,* is an ATP-dependent segregase involved in a vast range of known biochemical processes. An extremely abundant protein (140), p97 acts broadly within the cell to

segregate individual proteins and extract them from larger clusters and assemblies (141). This is usually initiated by polyubiquitination of the proteins in question, and is often – but not always – followed by their degradation (142,143). It has a homohexameric barrel-like structure subdivided into two layered concentric rings, with a pore running through the centre (144,145) (Figures 1.9a, 1.9b). Further, p97 is already known to act upon centromeric chromatin; it has a role in mitosis, extracting Aurora B from the centromere once this kinase has fulfilled its roles in spindle attachment and cytokinesis. The removal of Aurora B is necessary for the reformation of the nucleus in the daughter cells (146,147). Whilst p97 generally acts upon polyubiquitinated proteins, it has been shown to target its segregase activity towards polySUMOylated substrates, including at proteins involved in the repair of DNA double-strand breaks (148).

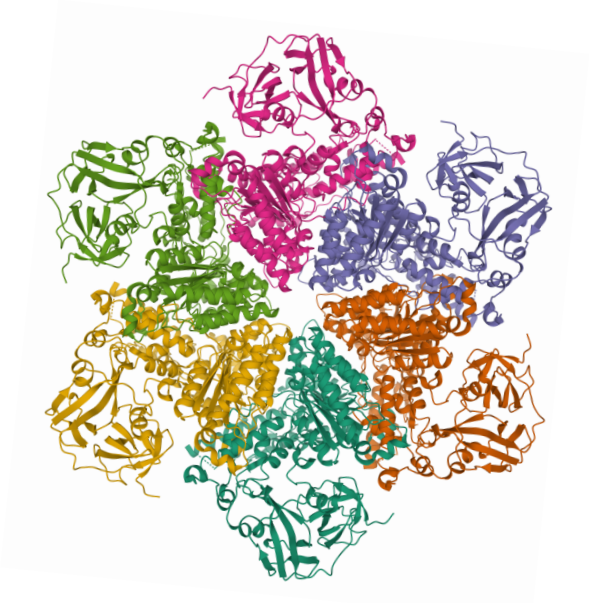


Figure 1.9a – Structure of p97; top-down view highlighting the central pore and hexameric structure. Colouring indicates monomeric subunits

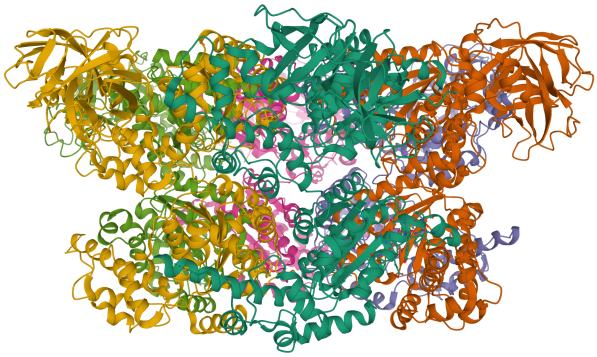


Figure 1.9b – Structure of p97; side-on view highlighting the barrelled structure and layered concentric rings

Figures 1.9a and 1.9b created with the tools and structures available at the RCSB protein databank (149,150,61)

1.5 – Research Aims and Hypothesis

In the screen run by Mitra *et al,* depletion of p97 was noted to have an opposing effect to that of SENP6 (Figure 1.8a). That is to say; its knockdown had a stabilising effect on ancestral centromeric CENP-A. This is a surprising observation, given previously noted and well established research demonstrating that CENP-A is already extremely stable (93), and invited further investigation. The ability of p97 to act upon SUMOylated substrates strengthened this thread of inquiry, given the known activity of SENP6 on core CCAN proteins (112,135,136). It was hypothesised that p97 may act antagonistically to SENP6; this would support the results observed by Mitra *et al* and indicate a key role for p97 in the regulation of CENP-A nucleosomes, and therefore the centromere as a whole. Dr Mitra was until recently also a member of Professor Lars Jansen's research group in the University of Oxford. The aims of this work are as follows, with results presented here as a thesis.

1. Confirm the results of p97 knockdown on CENP-A-SNAP fluorescence, as indicated by Mitra *et al*.
2. Investigate whether these observations are due to increased loading of CENP-A-SNAP at the centromere.
3. Investigate whether these observations may result from perturbances in the cell cycle.
4. Explore mechanistic explanations for these phenomena.

Chapter 2 – Initial Investigations into the Role of p97 in the Regulation of CENP-A

2.1 – Confirmation of Results of the Mitra *et al* Screen

In order to investigate a potential role for p97 in the regulation of centromeric CENP-A, it was first necessary to directly replicate and confirm the results of the high-throughput siRNA screen conducted by Mitra *et al*. As described above, this screen suggested that knockdown of p97 causes a significant increase in the fluorescence of ancestrally inherited CENP-A at the centromere during a pulse-chase protocol. That is to say; p97 knockdown led to an apparent increase in the stability of centromeric CENP-A, possibly by reducing the turnover of CENP-A nucleosomes at the centromere over the course of the experiment (Figure 2.1).

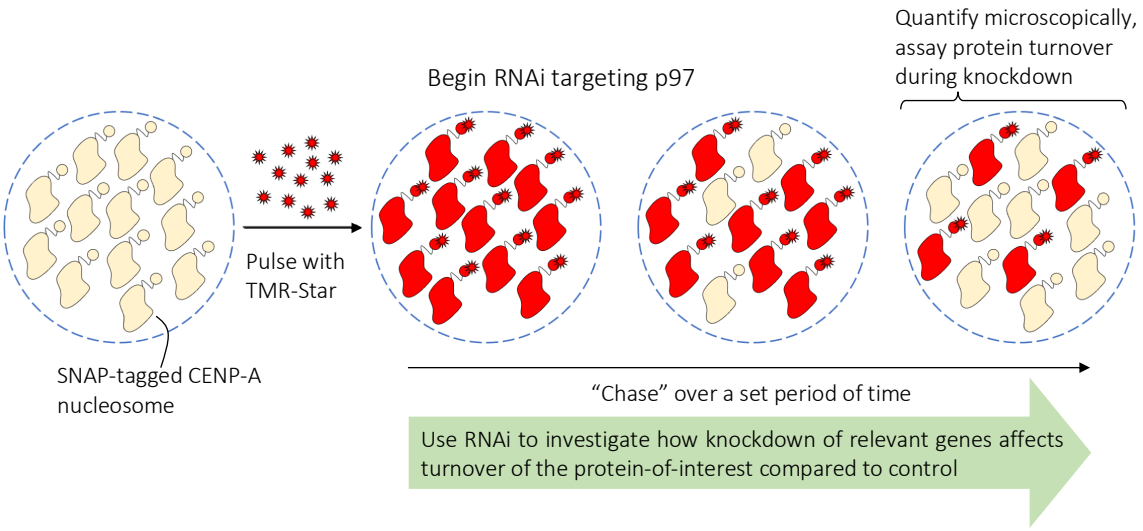


Figure 2.1 – Interpretation of a pulse-chase experiment alongside RNAi. Quantification of residual TMR-Star bound SNAP-tagged CENP-A present at the conclusion of the chase period allows the assaying of centromeric CENP-A turnover under p97-depleted conditions compared to control.

This is a very surprising result within the wider body of current literature. As discussed previously, CENP-A is already believed to be maximally stable once it has been incorporated into chromatin. In their 2007 paper, Jansen *et al* established HeLa cell lines expressing CENP-A-SNAP and so were able to measure the decay rate of ancestral centromeric CENP-A over a number of cell division cycles by use of a pulse-chase protocol (91). They demonstrated that fluorescent signal from these nucleosomes turned over at a rate of roughly 50% per division. This indicated that CENP-A nucleosomes are passed on to daughter cells with a very high rate of retention at the centromere, and no statistically significant turnover was detected other than that resulting from S-phase

'dilution' of centromeric chromatin during DNA replication (see Figures 1.4 and 1.5b). CENP-A nucleosomes are therefore believed to be 'maximally stable'. In this same publication, it was through the use of quench-chase-pulse experiments (Section 1.4.1) that Jansen *et al* demonstrated that the loading of new CENP-A nucleosomes at chromatin occurs only in G1.

Conversely, Mitra *et al* demonstrated that knockdown of p97 in HeLa CENP-A-SNAP cells resulted in a roughly 2.6-fold increase in levels of ancestrally inherited centromeric CENP-A after 48 hours compared to control under a pulse-chase protocol (Figure 2.2). This could be interpreted as a demonstration that knockdown of p97 results in a dramatic increase in the stability of centromeric CENP-A, a finding which is not in agreement with Jansen *et al* as it implies that there must be active turnover of CENP-A nucleosomes at the centromere under normal conditions.

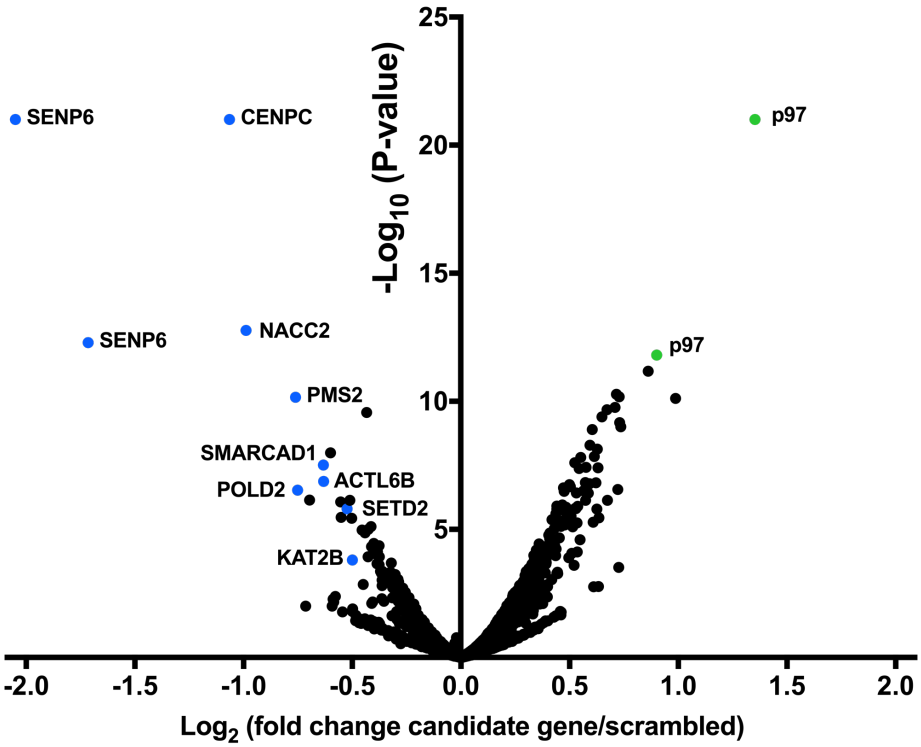


Figure 2.2; Volcano plot modified from Mitra et al as discussed in Fig 1.8a. Key genes are highlighted. Effects of the knockdown of p97 are highlighted in green. Note that some genes appear twice in this plot owing to the use of multiple available siRNAs to target them, each generating different data. Mitra *et al* found that centromeric CENP-A was drastically stabilised under p97 knockdown over a 48-hour period, with a high degree of reproducibility (n=5).

Note that these results specifically demonstrate changes in the levels of CENP-A-SNAP at the centromere, rather than across the nucleus or cytoplasm as a whole. This is due to the nature of fluorescence imaging in these experiments (see Section 2.1.1) whereby centromeric foci are quantitatively imaged, and neither nuclear nor cytoplasmic fluorescence levels are readily distinguished above background noise. Soluble pools of CENP-A-SNAP are nonetheless hypothesised to exist; potential effects of p97 knockdown on these pools is further discussed in Section 2.2 below.

2.1.1 – Pulse-Chase Experiments

To begin research into this, a more direct pulse-chase study on a smaller scale was used in an attempt to confirm the results obtained by Mitra *et al*. It is noteworthy that alternative labelling technologies (such as the HaloTag) have been more recently developed and may offer advantages over the SNAP-Tag, such as increased membrane permeability of associated dyes (151). However, attempts made during the course of this project to genetically tag endogenous CENP-A with the HaloTag did not result in viable cells, and work throughout this project focused on the same HeLa CENP-A-SNAP line produced by Jansen *et al* and employed by Mitra *et al*.

Cycling HeLa CENP-A-SNAP cells were 'pulsed' with a rhodamine-based SNAP substrate fluorophore ('TMR-Star') for 15 minutes and then 'quenched' with a non-fluorescent SNAP blocking substrate ('BTP') upon removal of this dye in order to ensure that all SNAP present was fully labelled, thus preventing any trace residual TMR-Star from reacting with newly synthesising CENP-A-SNAP peptides. These cells were then transfected with two different siRNAs targeting p97 (with these siRNAs distinguished hereafter as sip97-1 and sip97-2) as well as siNeg9, as a non-gene-targeting scrambled negative control, and siSENP6 as a positive control for the destabilisation of CENP-A nucleosomes at the centromere, as discussed above (Section 1.4.2). siMis18α was also included, as a negative control for a gene relevant to centromeric CENP-A.

Mis18α is a protein known to be vital for the loading of CENP-A nucleosomes; it forms part of the Mis18 complex, which binds to HJURP – the CENP-A chaperone – and facilitates the targeted deposition of nascent CENP-A at the centromere. However, it plays no role in CENP-A maintenance; thus its knockdown was not expected to have any effect on CENP-A fluorescence in a pulse-chase experiment (82,93,152,153).

Another relevant protein in the context of these experiments is CENP-B (centromere protein B). CENP-B is a highly conserved 80 kDa protein which localises to centromeres (154). Crucially, it is the only currently known centromeric protein which has been shown to bind to sequence-specific DNA regions; it recognises a 17bp motif named the CENP-B box, which appears within the α-satellite regions of DNA which are prevalent at the centromere, as discussed above (155,156). Unlike other members of the CENP family, CENP-B is maintained at α-satellite regions, rather than being epigenetically recruited to active centromeric loci during neocentromere formation (157). Indeed, the biological function of CENP-B remains disputed; CENP-B is found to be dispensable in mice, with knockout mutants remaining viable, fertile, and displaying normal kinetochore assembly and chromosome segregation (158–160). However, CENP-B has also been shown to bind to the CENP-B box as a homodimer (161) and to induce kinks in DNA conformation (162), suggesting that it may play a role in determining higher-order centromeric chromatin architecture via the formation of intramolecular loops (163). Indeed, CENP-B has shown to be capable of directly interacting with CENP-A and CENP-C, and to reduce chromosome mis-segregation rates, suggesting a function in stabilising and enhancing the fidelity of the otherwise epigenetically defined centromere (95,164). Whilst centromeric CENP-B was for the most part not directly investigated in these experiments, it served as an independent centromeric marker during image analysis to aid in unbiased quantification of CENP-A-SNAP-TMR fluorescence at these foci. This is further described below.

Following transfection, cells were seeded on poly-lysine treated glass coverslips and incubated (37°C, 5% CO_2) to proliferate for 48 hours, after which they were fixed in 4% formaldehyde. CENP-B was stained via immunofluorescence, and generic chromatin was stained using DAPI as a nuclear marker. This is summarised below (Figure 2.3).

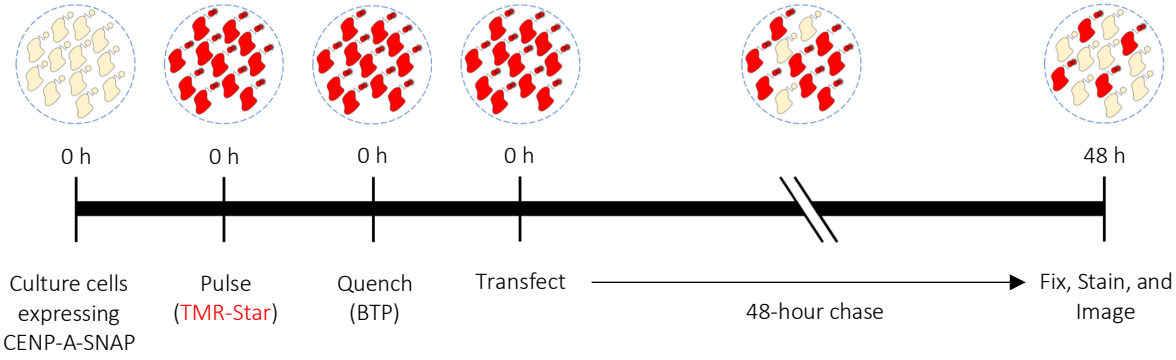


Figure 2.3 – Overview of the pulse-chase protocol

Cells were visualised at 63X magnification using an inverted-light microscope, with 0.2 µm Z-stacks consecutively imaged to capture a full range of in-focus planes for centromeric loci. These images were analysed using an automated 'Centromere Recognition and Quantification' (CRaQ) ImageJ macro. This macro, created by Bodor *et al* (116) allows for unbiased quantification of centromeric fluorescence by detecting centromeric foci in one microscopic channel and using these data as a reference to measure centromeric fluorescence intensity in another channel. Thus, fluorescently tagged CENP-A-SNAP was quantified regardless of its intensity or lack thereof by setting the channel used to visualise CENP-B as a reference. This protocol is rapid, fully automated, and deterministic. It will return the same quantifications for a given data set upon reanalysis; results will not vary by chance. Example images from a pulse-chase protocol are shown below (Figure 2.4).

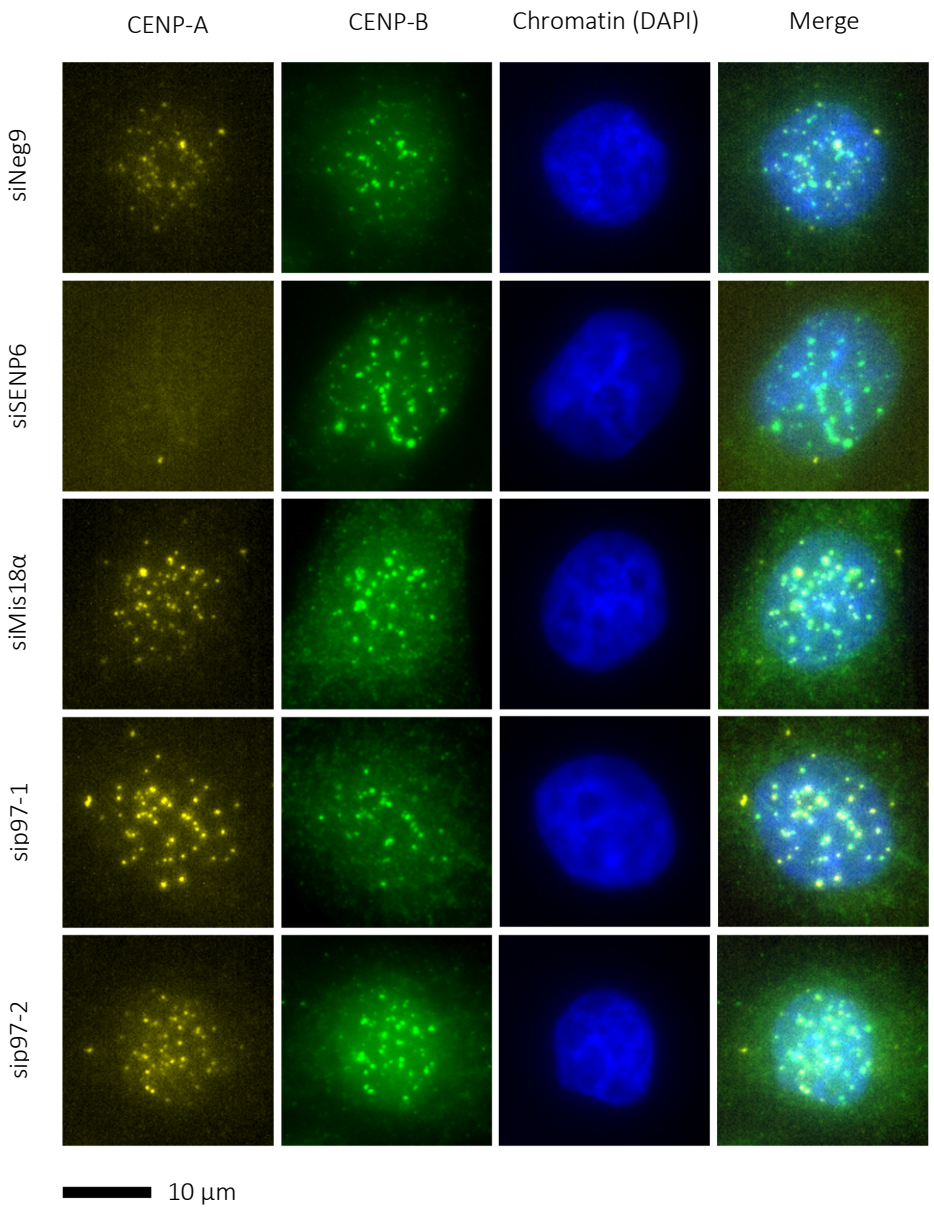


Figure 2.4 – Representative images from a pulse-chase experiment. Images show maximum projections of Z-stacks. Brightness and contrast in CENP-A and CENP-B channels normalised for comparison. CENP-A nucleosomes visualised via 600 nm rhodamine fluorescence of the TMR-Star SNAP-tag substrate. CENP-B was visualised via immunofluorescence imaging at 527 nm. DNA was visualised at 470 nm by DAPI staining. Images enlarged and cropped to highlight CENP-A and CENP-B colocalization in single cells.

Initial examination of Figure 2.4 suggests that there may be an increase in the number – as well as the fluorescence – of centromeric foci following p97 knockdown, and potentially following knockdown of Mis18α. However, as this is data from a pulse-chase experiment, this is unlikely to indicate the formation of neocentromeres; all centromeric foci must have been present prior to knockdown, during the 'pulse' stage of the protocol (Figure 2.3). Therefore, any potential

neocentromeres produced as a result of this knockdown would not be visualised in these experiments.

In order to exemplify the operation of the CRaQ macro, representative regions-of-interest (ROIs) as calculated by CRaQ are shown below for an siNeg9-treated cell in both the CENP-A channel, and the CENP-B channel in which they were calculated (Figure 2.5)

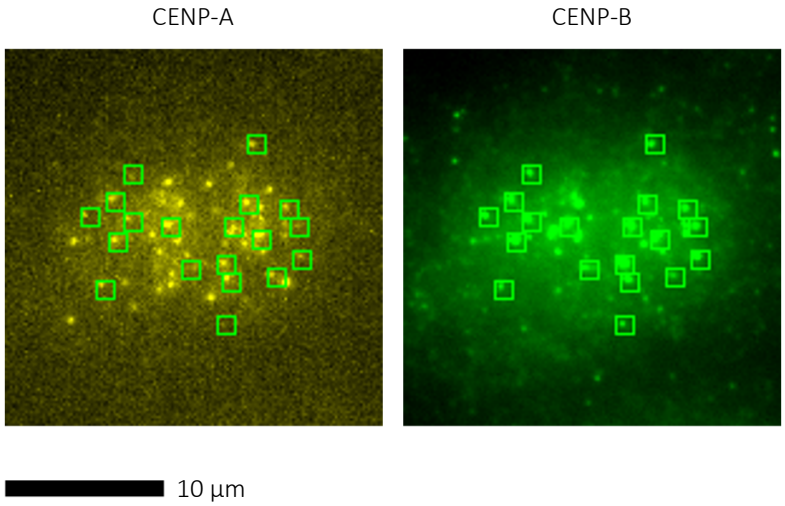


Figure 2.5 – Representative ROIs in a pulse-chase protocol as analysed by CRaQ.

ROIs calculated by analysis of CENP-B fluorescence. These regions are then applied to CENP-A data, and CENP-A fluorescence is quantified. Overlap of centromeric foci across these two channels within the ROIs can be observed

Immediately apparent in Figures 2.4 and 2.5 are foci corresponding to either CENP-A nucleosomes or CENP-B molecules – depending on fluorescence wavelength – as distinct centromeric spots within nuclei. However, while CENP-B fluorescence does not obviously vary, CENP-A foci can be seen to visibly diminish following knockdown of SENP6. This is in full agreement with the screen conducted by Mitra *et al*, who found that SENP6 is a vital factor for the maintenance of centromeric CENP-A. Quantification of a total of 80-140 images per condition using CRaQ is shown (Figure 2.6).

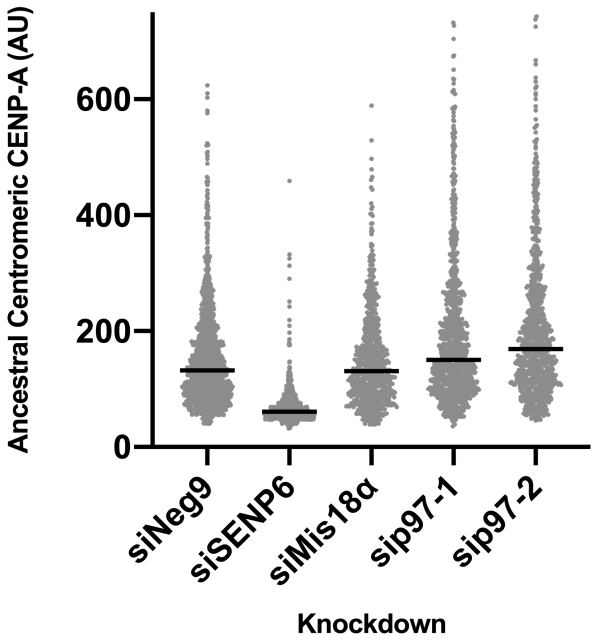


Figure 2.6 – Quantification of ancestral CENP-A levels in a single pulse-chase experiment. Individual points correspond to individual centromeric foci. Median values are overlayed.

While there is significant overlap between these populations under different siRNA conditions in Figure 2.6, this is due to the wide biological variance in the levels of centromere-associated proteins and is expected, in part because of the periodic replicative halving and subsequent reloading of CENP-A nucleosome levels across the cell cycle as discussed previously. Populational changes may nonetheless be reliably tracked over a number of replicates, using the median as an indicator for the population as a whole. Note that the median was chosen so as to avoid over-representation of the long 'tails' characteristic of these data; these are a standard finding and may occur due to differences in biological CENP-A levels as discussed above, as well as potential differences in local TMR-Star diffusion during the pulse, or cases of autofluorescence.

Notably, while increases in CENP-A stability were observed during p97 knockdown across both p97-targeting siRNAs, these increases were not of the magnitude seen by Mitra *et al*, who noted a roughly 2.6-fold increase in apparent CENP-A stability under these same conditions. Instead, in this experiment, a very small increase in the fluorescence of ancestral CENP-A at the centromere was observed. However, this small increase in the fluorescence of centromeric CENP-A-SNAP-TMR was found to be highly reproducible across multiple biological replicates (Figure 2.7)

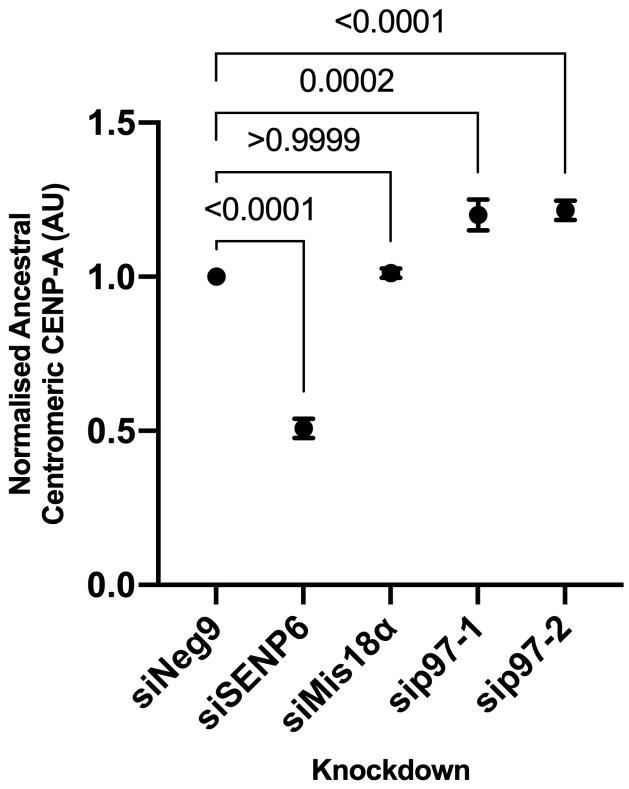


Figure 2.7 – Combined pulse-chase results. Error bars show SEM, P-values calculated relative to siNeg9 (n=8)

Median values from biological replicates (n=8) of these pulse-chase experiments were normalised to siNeg9 within each experiment in order to correct for experimental variation in raw CENP-A-SNAP-TMR fluorescence values between biological replicates. These median values were used to plot the standard error of the mean and calculate P-values relative to the siNeg9 internal control using an ordinary one-way ANOVA and a Bonferroni multiple-comparisons test. The change in ancestral CENP-A-SNAP-TMR fluorescence was found to be relatively small, with an average increase of 20.8% following p97 knockdown compared to negative control. As above, this effect was found to be readily reproducible, with P-values indicating a high degree of confidence. Therefore, while these experiments did broadly confirm the increase in ancestral centromeric CENP-A levels under p97 knockdown conditions observed by Mitra *et al*, they did not note the dramatic increase suggested by data from that screen. Instead, a much subtler shift in these populations was observed.

Knockdown of SENP6 was shown to drastically reduce the level of ancestral CENP-A-SNAP-TMR fluorescence, indicating a destabilisation of CENP-A nucleosomes at the centromere over the 48-hour chase window. This is in agreement with Mitra *et al*. Knockdown of Mis18α was shown to have no effect on CENP-A stability, in agreement with findings by Bodor *et al* (93). These

observations reflect the success of the positive and negative controls and lend confidence that the experimental setup was functioning as intended.

In addition, to confirm that CENP-B serves as an independent measure of centromere location, its levels during these experiments were quantified by CRaQ, using their own foci as a self-reference. This methodology is not ideal; without an external reference, analyses may ignore non or low-fluorescing foci. However, this setup can nonetheless be utilised as a coarse quantification to highlight any substantial populational changes in fluorescence across a large number of cells. As expected, CENP-B fluorescence was not observed to change significantly under any of the knockdown conditions (Figure 2.8), giving confidence in the use of CENP-B as a centromeric reference.

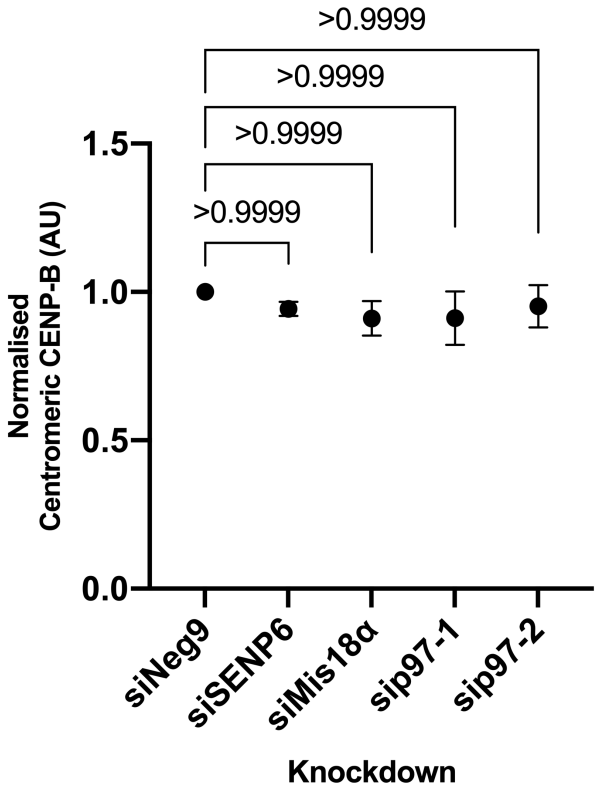


Figure 2.8 – Total CENP-B levels across SENP6, Mis18α, and p97 knockdown conditions. Median values were normalised to siNeg9 within each biological replicate. Confidence intervals were analysed by one-way ANOVA with Bonferroni multiple comparisons analysis. Error bars show standard error of the mean (n=8).

2.1.2 – Confirmation of p97 Knockdown in Pulse-Chase Experiments

In order to confirm that this smaller than expected effect did not simply result from poor knockdown of p97, samples from these same experiments were analysed by Western blot. These samples were transfected concurrently to those grown on coverslips for microscopic fluorescence analysis as above, using the same population of cells and the same transfection reagents. After 48 hours, they were harvested into a pellet simultaneously as those grown on coverslips were fixed (see Figure 2.3). Proteins in this pellet were linearised by heat treatment in sodium dodecyl sulphate (SDS) and exposure to β-mercaptoethanol, and separated by SDS-PAGE before being transferred to a nitrocellulose membrane for immunoblotting. Antibody staining and imaging visualised p97 levels under each siRNA condition, as well as α-tubulin to normalise against general proteins levels in the pellet.

A representative blot is shown below, alongside combined quantification of data from multiple blots from these experiments (Figures 2.9a, 2.9b). These data show that p97 knockdown was indeed successful at reducing cellular levels of p97 by approximately 60%; a satisfactory result given that p97 is extremely abundant, totalling approximately $2.7x10^6$ copies per HeLa cell (140), rendering complete depletion by these means unrealistic. This protocol would therefore otherwise be expected to reproduce the results obtained by Mitra *et al*.

Unexpectedly, knockdown of Mis18α appears to significantly increase cellular levels of p97 by ~37% compared to control. However, as shown in Figures 2.6 and 2.7, any increase in cellular p97 under these conditions does not then have any measurable impact on the stability of CENP-A at the centromere. Whilst certainly interesting, this newly observed phenomenon remains outside the scope of this thesis and is as-yet unexplained.

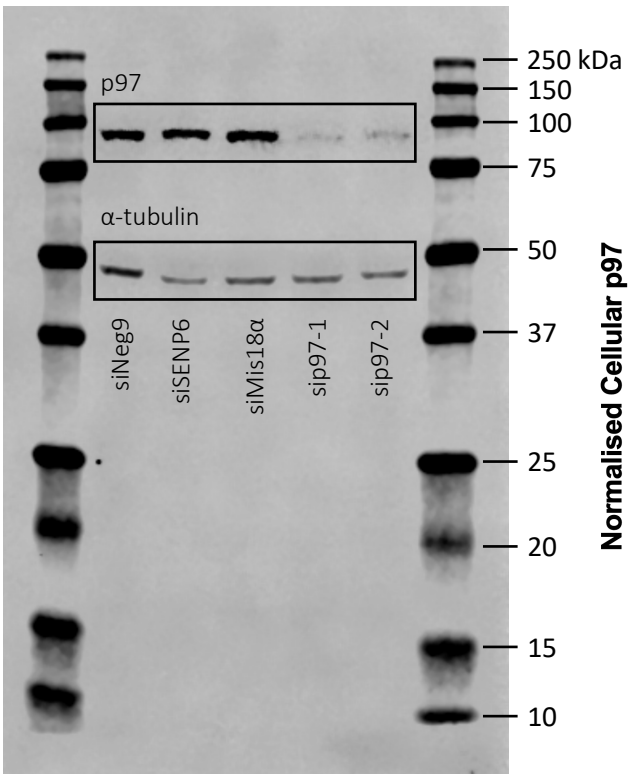


Figure 2.9a – Representative Western blot from a pulse-chase protocol. Transfection with either p97-targeting siRNA can be readily seen to deplete cellular p97 over 48 hours. A 700 nm channel was used to measure α-tubulin levels, and an 800 nm channel for p97; channels are shown merged for visual clarity.

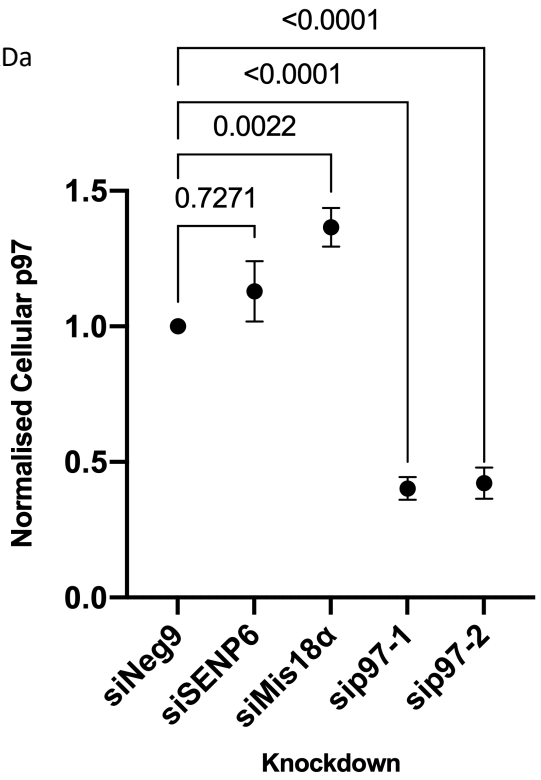


Figure 2.9b – Quantification of p97 knockdown in pulse-chase experiments. Levels of p97 in each sample within a biological replicate were normalised to that of α-tubulin. Different biological replicates were made comparable by normalising each condition to siNeg9, to control for differing cell counts. Error bars represent SEM, and P-values were calculated as in *Fig* 2.7 (n=7).

2.2 – The CENP-A Overloading Hypothesis

One possible explanation for the increase in CENP-A-SNAP-TMR fluorescence during p97 knockdown in a pulse-chase protocol (Figure 2.7) is that there is a measurable quantity of CENP-A-SNAP produced prior to labelling with TMR-Star, but which has not yet been incorporated into chromatin at the time of labelling. Instead, this CENP-A-SNAP may exist solubilised in the cytoplasm and/or nucleoplasm. Therefore, if knockdown of p97 were to lead, by an unknown pathway, to the over-incorporation of these labelled CENP-A-SNAP molecules at the centromere over the 48-hour chase, we would expect to see an increase in centromeric CENP-A-SNAP-TMR fluorescence compared to control. Thus, the increase in ancestral centromeric CENP-A levels during p97 knockdown in the above experiments may not be indicative of decreased CENP-A turnover, but rather of its increased loading at the centromere under these conditions. This is here defined as the CENP-A overloading hypothesis and is shown schematically below (Figure 2.10).

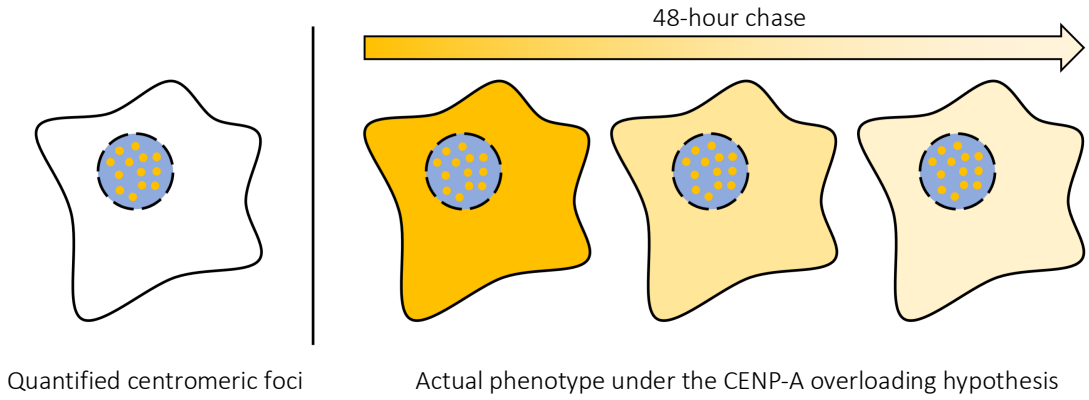


Figure 2.10 – Schematic overview of the CENP-A overloading hypothesis. CENP-A-SNAP-TMR levels, as observed at centromeric foci and analysed by CRaQ, are shown on the left. This is contrasted on the right hand side by annotation of a significant soluble pool of CENP-A-SNAP-TMR (shown in orange), which is conjectured to load at chromatin over subsequent generations. Knockdown of p97 may lead to over incorporation of this pool at the centromere compared to control, granting the results seen in Figure 2.7.

2.2.1 – Modified Pulse-Chase Experiments

To probe this hypothesis, a modified pulse-chase protocol was designed. In these experiments, HeLa cells expressing CENP-A-SNAP were treated with TMR-Star and seeded on coverslips as above. However, they were not simultaneously transfected. Instead, they were left to grow under otherwise normal conditions for 24 hours before transfecting. This allowed all labelled

CENP-A-SNAP which was not yet incorporated into chromatin at the onset of the chase period to load at centromeres prior to depletion of p97. This protocol is shown schematically below (Figure 2.11) Logically, if p97 knockdown causes this hypothesised overloading of fluorescently tagged CENP-A-SNAP at the centromere, then this effect should be at least partially negated during this first 24-hour period during which p97 remains at endogenous levels and so may regulate CENP-A in a physiologically normal manner.

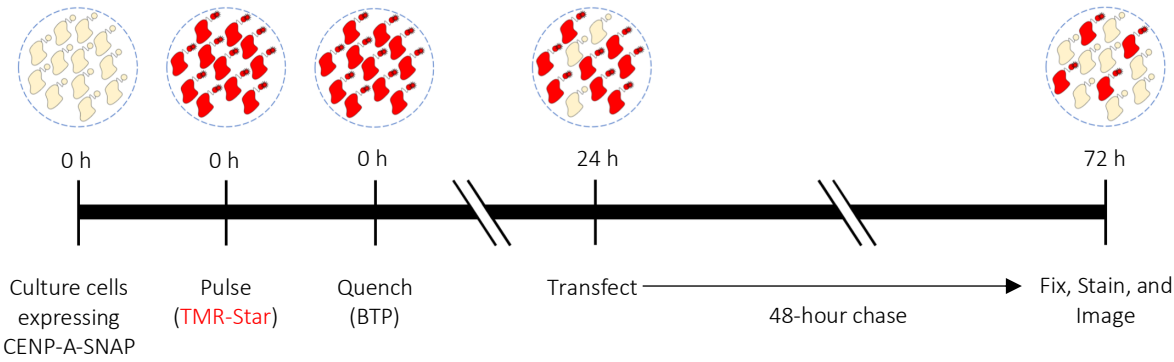


Figure 2.11 – Overview of the modified pulse-chase protocol.

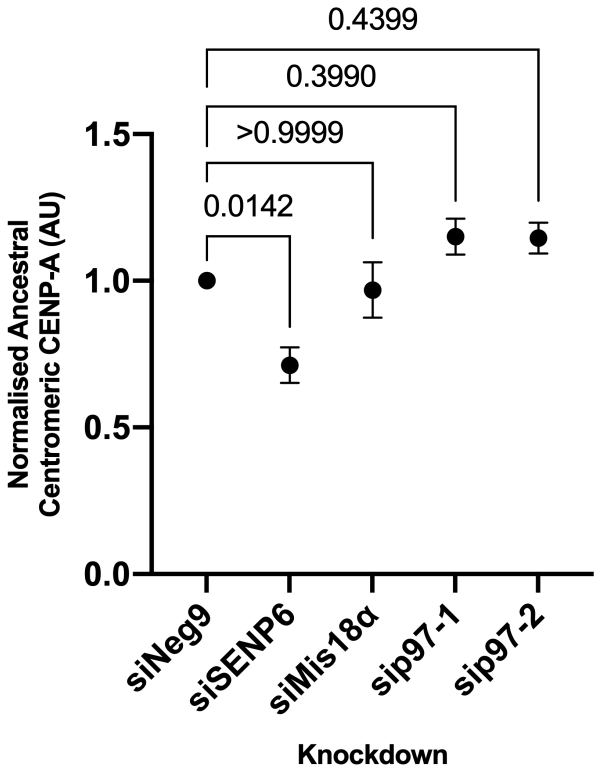


Figure 2.12 – Combined modified pulse-chase results. Error bars show SEM, P-values calculated relative to siNeg9 (n=4)

However, CRaQ analysis of images obtained under this protocol did not show substantial negation of the apparent increased stability of CENP-A-SNAP at the centromere (*Figure 2.12*).

A characteristic small increase in the fluorescence levels of ancestral centromeric CENP-A is still observed following p97 knockdown compared to siNeg9 control.

Admittedly, P-values calculated by one-way ANOVA (n=4) no longer reach the 95% confidence interval to fully authenticate this increase. This is largely due to decreased TMR-Star signal in this experiment. As cells were left to cycle for 72 hours in total (rather than 48 hours) they are expected to have undergone roughly one extra division. Therefore, ancestral CENP-A nucleosomes were diluted amongst daughter cells by one extra DNA replication cycle (as per Figures 1.4 and 1.5b) and CENP-A-SNAP-TMR signal was decreased by half relative to a standard pulse-chase setup. This resulted in a poorer signal:background ratio and so increased potential error in CRaQ analysis.

2.2.2 – Quench-Chase-Pulse Experiments

In order to address this problem and investigate the CENP-A overloading hypothesis from a different angle, the quench-chase-pulse protocol was employed as an alternate methodology. As discussed previously, this protocol allows quantification of the effects of knockdown on the loading of CENP-A nucleosomes at the centromere during the 'chase' period (Figure 2.13)

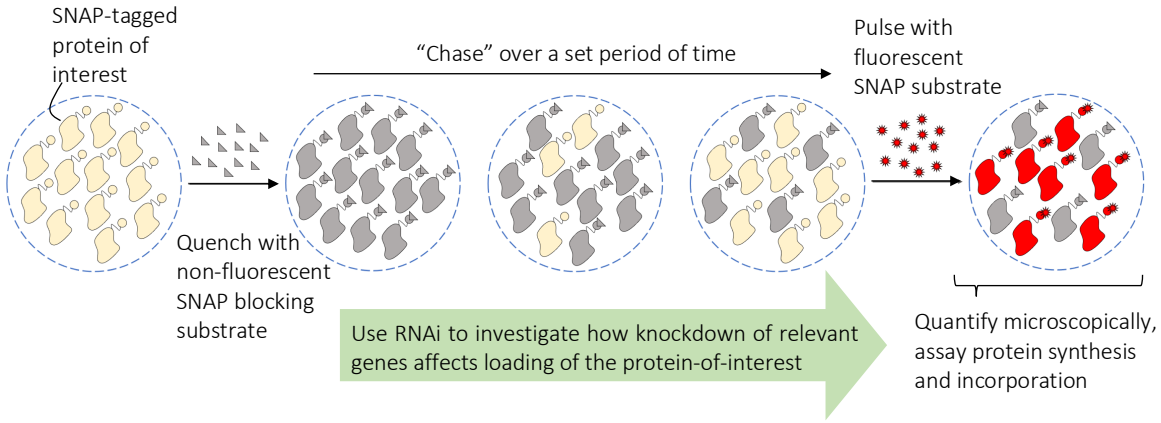


Figure 2.13 – Interpretation of a quench-chase-pulse experiment tied to RNAi. Fluorescence quantification at the conclusion of the experiment gives information regarding the quantities and subcellular localisation of SNAP-tagged protein of interest synthesised during the chase period. Within context, this grants an assay for the loading of CENP-A-SNAP nucleosomes at centromeric chromatin.

HeLa cells expressing CENP-A-SNAP were 'quenched' with a non-fluorescent alkylguanine based SNAP substrate. This substrate occupies the binding sites of CENP-A-SNAP molecules present in

the cell at this point in the protocol but will not then be observable under the microscope, thus discounting these species from analysis. Cells were seeded on coverslips and simultaneously transfected with siNeg9, siSENP6, siMis18α, and two p97-targeting siRNAs using a reverse-transfection protocol (see Section 6.2) and incubated at 37°C for a 48-hour 'chase' window. During this time, new CENP-A-SNAP is synthesised by cells and incorporated in nucleosomes loaded at centromeric chromatin as they passage through G1. Any CENP-A-SNAP peptides synthesised during this period will not have been quenched with non-fluorescent SNAP substrate, so can then be visualised by a TMR-Star pulse at the conclusion of the chase period.

Cells were fixed and stained to mark CENP-B by immunofluorescence as a centromeric reference. Chromatin was stained with DAPI. This protocol is summarised below (Figure 2.14) alongside representative images (Figure 2.15).

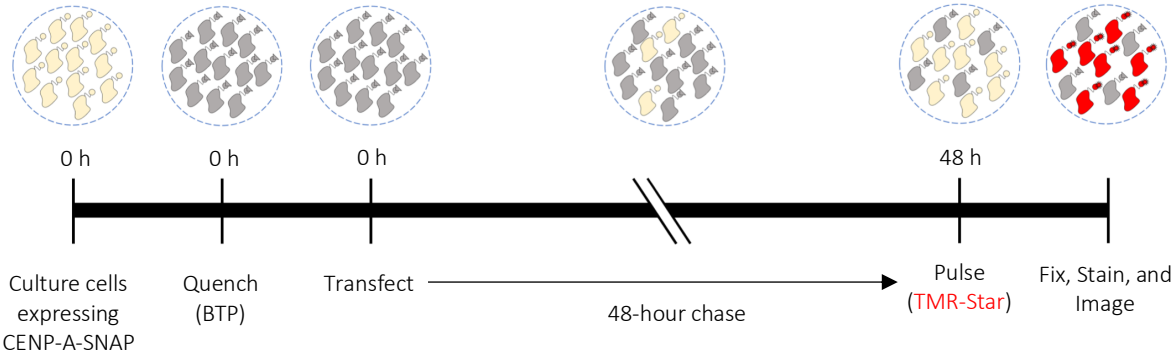


Figure 2.14 – Overview of the quench-chase-pulse protocol.

Images were quantified in ImageJ using CRaQ. Multiple replicates yielded data shown below (Figure 2.16). Median values were again normalised to siNeg9 within each biological replicate. P-values were then calculated from these normalised data using an ordinary one-way ANOVA, with Bonferroni statistical hypothesis tests to correct for multiple comparisons.

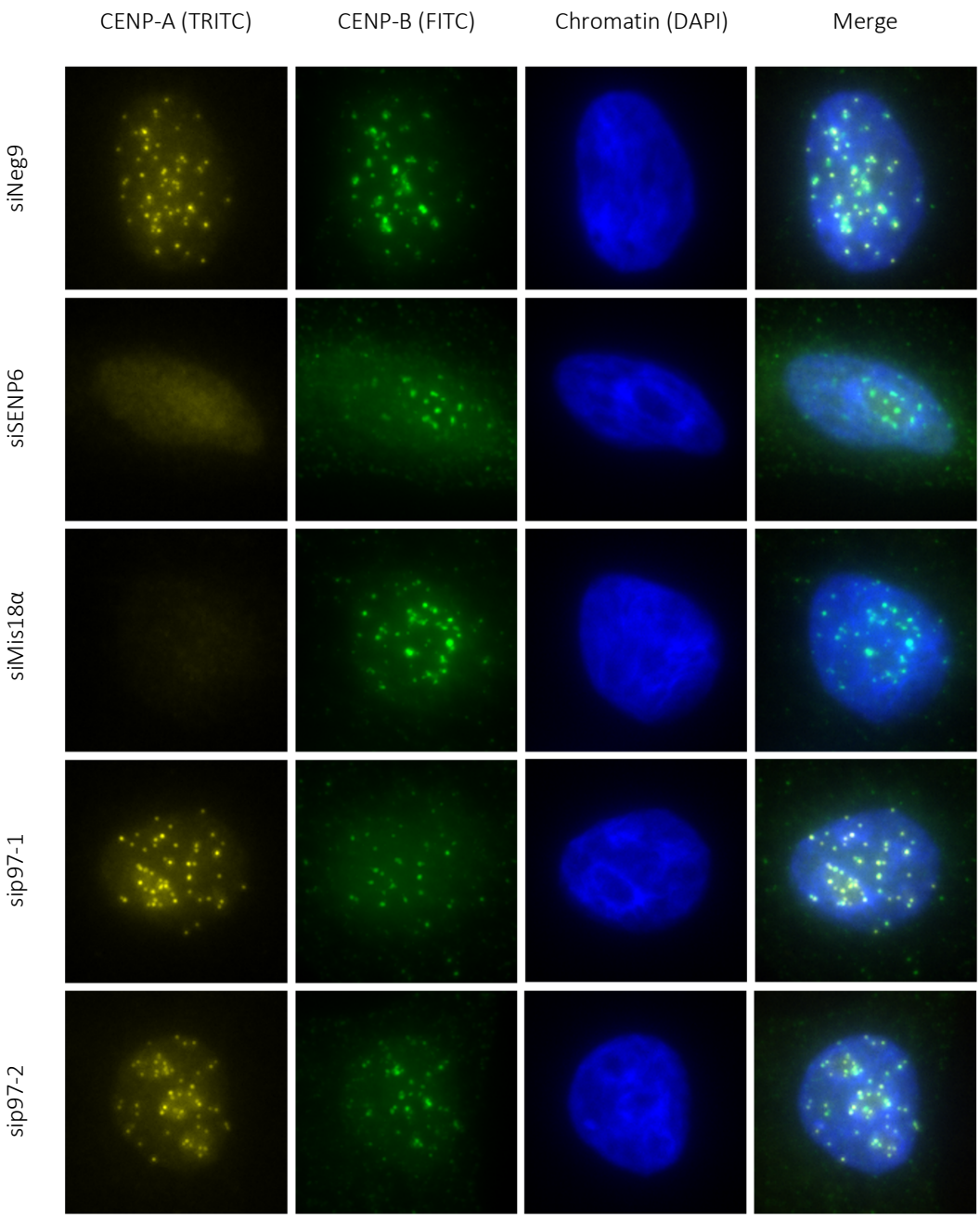


Figure 2.15 – Representative images from a quench-chase-pulse experiment. Co-localisation of CENP-A and CENP-B foci can be observed. Note that whilst knockdown Mis18α appears to remove CENP-A/TRITC signal entirely, this is a scaling artifact and not reflected in the raw data.

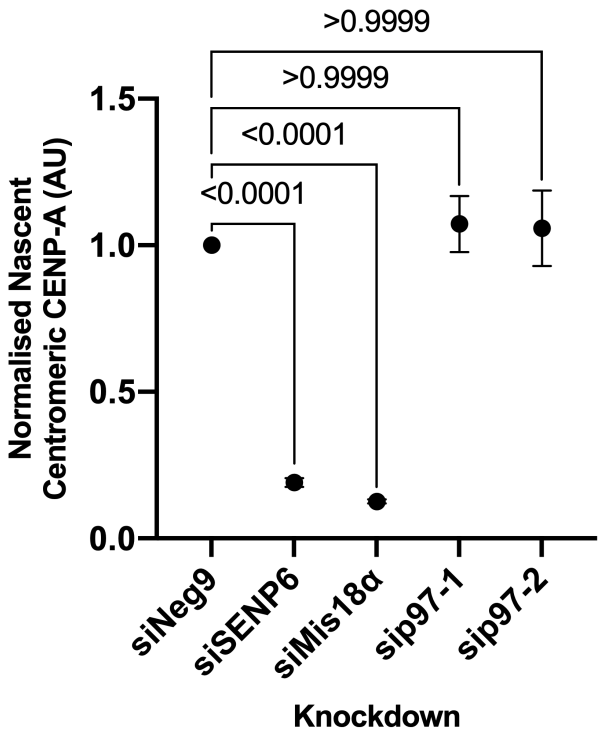


Figure 2.16 – Combined quench-chase-pulse results. Error bars show SEM, P-values calculated relative to siNeg9 (n=4)

Under this setup, p97 knockdown was shown to have no effect on the loading of newly synthesised CENP-A at the centromere, with a high degree of reproducibility across biological replicates. These data, in combination with those of the modified-pulse-chase protocol, effectively refute the CENP-A overloading hypothesis; p97 knockdown has not been found to impact the loading of CENP-A nucleosomes at centromeric chromatin

Notably, in contrast to pulse-chase studies, knockdown of Mis18α was indeed shown to drastically reduce the loading of newly synthesised CENP-A at the centromere. This is in full agreement with literature (82,93) and grants further confidence in the reliability of this protocol, and in its utility in specifically highlighting the effects of perturbation of the cellular environment on CENP-A loading.

2.2.3 – Confirmation of p97 Knockdown in Quench-Chase-Pulse Experiments

In order to confirm that this lack of effect following the treatment of cells with p97-targeting siRNAs did not simply result from unsuccessful p97 knockdown, levels of cellular p97 were quantified by Western blot. These samples were prepared in conjunction with each biological replicate of the quench-chase-pulse protocol, in the same manner as described in Section 2.1.2 above.

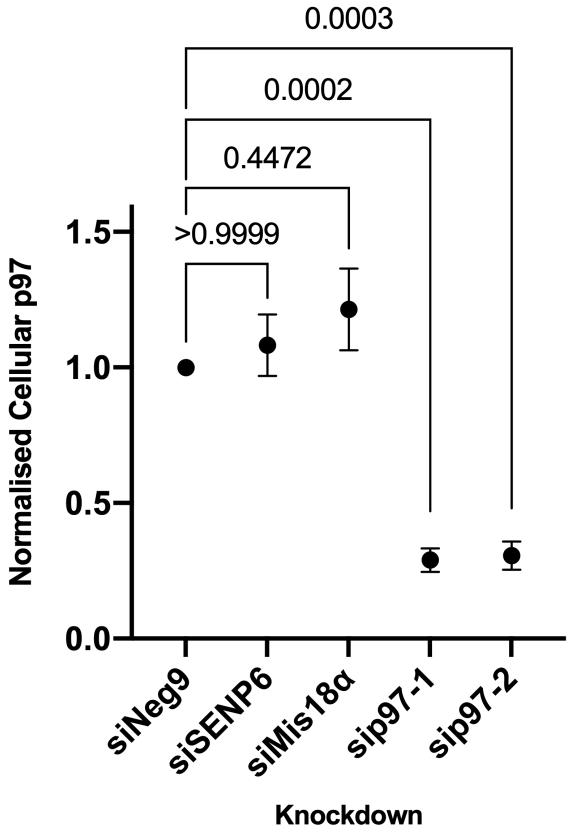


Figure 2.17 – Quantification of p97 knockdown across quench-chase-pulse replicates. Levels of p97 in each sample within a biological replicate were normalised to that of α-tubulin. Comparability between biological replicates was ensured by normalising each condition to siNeg9, to control for differing cell counts. Error bars represent SEM, and P-values were calculated by ordinary one-way ANOVA (n=4).

Combined, normalised results show satisfactory, reproducible depletion of p97 by ~70% (Figure 2.17), lending confidence to findings that p97 does not regulate the loading of CENP-A at the centromere

2.3 – Discussion

Knockdown of p97 has been demonstrated to increase the fluorescence of ancestrally inherited CENP-A-SNAP nucleosomes at the centromere under a pulse-chase protocol, although not to the magnitude suggested by Mitra *et al*. Interpretation of this result remains uncertain. Pulse-chase protocols typically probe for the turnover – and by extension the stability – of proteins of interest within a cell. However, interpreting these results as evidence of increased CENP-A stability at the centromere is in disagreement with the findings of Jansen et al (91), as it implies that centromeric CENP-A nucleosomes must be turned over to some extent under normal conditions.

An alternative hypothesis – that these data instead represent the increased loading of CENP-A nucleosomes at centromeric chromatin – also failed to withstand investigation. A modified version of the pulse-chase protocol showed that this effect is broadly retained even if cells are left to cycle under unperturbed conditions for 24 hours prior to knockdown, allowing incorporation of any residual soluble CENP-A. Further, quench-chase-pulse experiments – which act as reliable and specific probes for centromeric CENP-A loading – showed that p97 knockdown has no effect on this assembly.

Chapter 3 – Investigating the Role of p97 in Regulation of the Cell Cycle

3.1 – The Cell Cycle Delay Hypothesis

In an attempt to reconcile the findings above with those of Jansen *et al* (91), it was conjectured that the effects of the knockdown of p97 on CENP-A maintenance may not be due to the direct action of p97 at the centromere. Instead, p97 RNAi may be hypothesised to inhibit or slow the passage of the cell cycle though one or multiple checkpoints. This would result in p97-deficient populations of cells undergoing fewer completions of the cell cycle during the chase timeframe compared to control. As a result, these p97-deficient cells would undergo DNA replication fewer times on average and would therefore dilute their ancestral CENP-A nucleosomal pools by a lower average amount (see Section 1.3.4). This would result in increased signal of fluorescently tagged ancestral CENP-A-SNAP nucleosomes during a pulse-chase protocol as observed above and illustrated below (Figure 3.1). This is here defined as the cell cycle delay hypothesis.

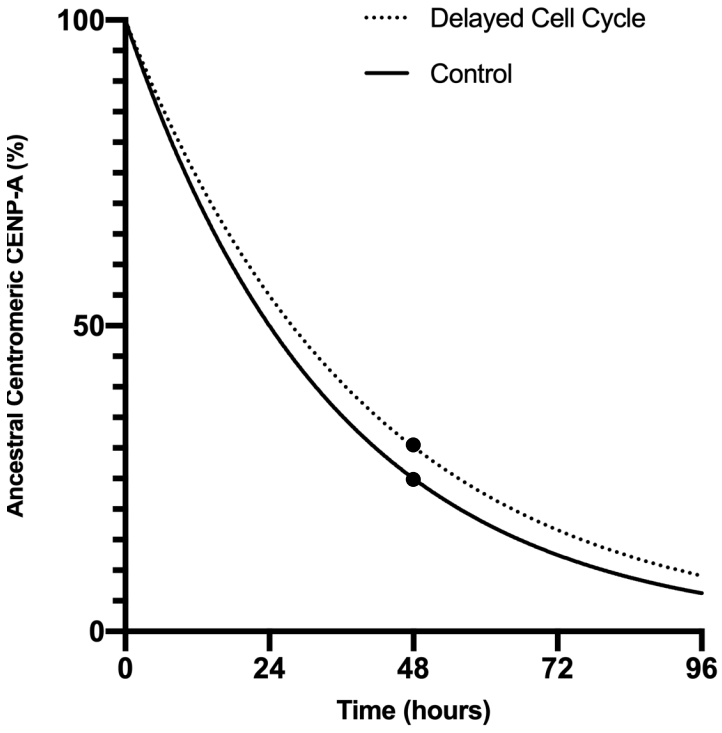


Figure 3.1 – Model of reduced decay of ancestral CENP-A at the centromere owing to slowing of the cell cycle.

In this model, the control population progresses through the cell cycle at a normal rate and so exhibits 50% decay of ancestral centromeric CENP-A every 24 hours; the approximate duration of a complete cycle in HeLa cells. That is to say, ancestral CENP-A levels (*A*) decay with time (*t)* (in hours) according to $A = \frac{100}{2^{\left(\frac{t}{24}\right)}}$ granting a standard exponential decay curve. In contrast, ancestral CENP-A levels would be expected to decay at a slower rate in a population experiencing a slowed cell cycle. This is here modelled as $A = \frac{100}{1.82^{\left(\frac{t}{24}\right)}}$ and corresponds to a 15.7% increase in the average time taken to passage through the cell cycle After 48 hours this would grant an increase in CENP-A fluorescence of 20.8%, in agreement with the average values observed in pulse-chase experiments (Figure 2.7).

3.2 – Use of Flow Cytometry to Investigate the Effects of p97 Knockdown in Cycling Populations

In order to investigate this hypothesis, flow cytometry techniques were used for DNA quantitation in order to analyse changes across the cell cycle that may be caused by the depletion of p97. As discussed above (Section 1.1) the amount of DNA present inside a cell varies as it progresses through the cell cycle. In brief, daughter cells exit mitosis with a single copy of their genome. The quantity of DNA will increase through S-phase during replication and will be doubled by G2/M relative to G1, as each chromosome has been successfully copied for later segregation. Therefore, the number of cells in each stage of this cycle within a population may be analysed by the use of a fluorescent DNA-binding dye. Cells in G2/M will have twice the quantity of DNA as those in G1; they will therefore bind twice as much dye and fluoresce twice as brightly at corresponding wavelengths. Cells in S-phase will be observed in continuum between these extremes (165).

HeLa cells expressing CENP-A-SNAP were transfected with siNeg9 and sip97-1/2 RNAs and grown for 48 hours. Note that while this protocol does not involve direct use of the SNAP-tag, it was important to investigate p97 dynamics in the same genetic environment as that in which the results discussed in Chapter 2 were obtained. Following this 48-hour transfection, cells were harvested, and a sample taken for analysis by Western blot to verify p97 knockdown. The remaining majority of the population was fixed dropwise in cold 70% ethanol, washed in PBS, and treated with Ribonuclease I. This treatment removed any RNA species present in the samples prior to fluorescence staining of the DNA with 50 $\mu g\ mL^{-1}$ propidium iodide.

Stained cells were then analysed using flow cytometry. This technology allows extremely rapid analysis of thousands of individual cells, and operates by passing a suspension of cells one-by-one through a series of laser beams. The forward and side-scattering of light from these beams as each cell passes across them may be quantified and used to stratify the population. Forward-scattering values scale proportionally to cell size, and side-scattering with internal cell complexity. Emission

fluorescence will occur provided that the correct fluorophores are utilised (such as propidium iodide); this may then be linked to wide variety of cellular parameters, depending on the protocol in question. Cells are analysed individually, and so each generates unique data which may be pooled for insight into broader populational changes and dynamics (165,166)

HeLa CENP-A-SNAP populations subjected to RNAi and analysed in this manner were hierarchically gated to select for cells whose scattering parameters were within normal range, in order to exclude dead cells and detritus from subsequent quantification. This healthy population was further gated to discount doublet or cluster events, wherein multiple cells may clump together and so pass through the laser array simultaneously; this would otherwise skew the data.

Data from the remaining successful candidates in each sample was plotted as a histogram. This enabled the clear distinction between cells in G1, S, and G2/M phases (Figure 3.2, top). Peaks corresponding to G1 and G2/M populations were curve-fitted to Gaussian distributions via nonlinear least-squares regression (Figure 3.2, bottom). These curves were then integrated to measure the cell count within each. S-phase populations appear in a continuous spread between the G1/G2 extremes in this analysis and so do not conform well to a bell curve. Instead, they were quantified by subtracting the integrals above from the cell count of the total population.

Biological replicates were run and analysed as above. Differences in the percentage of the population in different stages of the cell cycle were observed, and confidence calculated using multiple comparisons via two-way ANOVA (Figure 3.3).

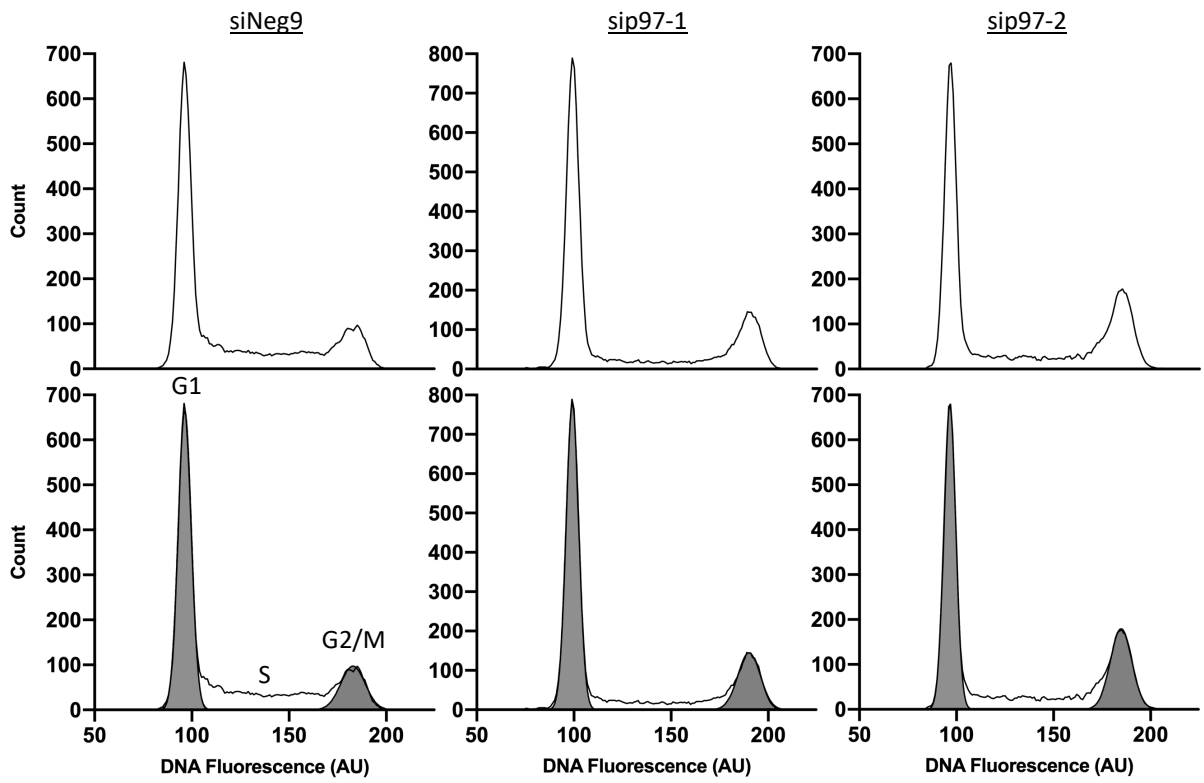


Figure 3.2 – Representative histograms showing cell counts across different stages of the cell cycle under control and p97-deficient conditions. Cells in G1 are readily observed as a large initial spike, with cells in G2/M appearing as a second spike exhibiting roughly twice the relative DNA-stained fluorescence. Cells in S-phase are found in a spectrum between these two states. Gaussian distributions fitted to these data are shown in the second row.

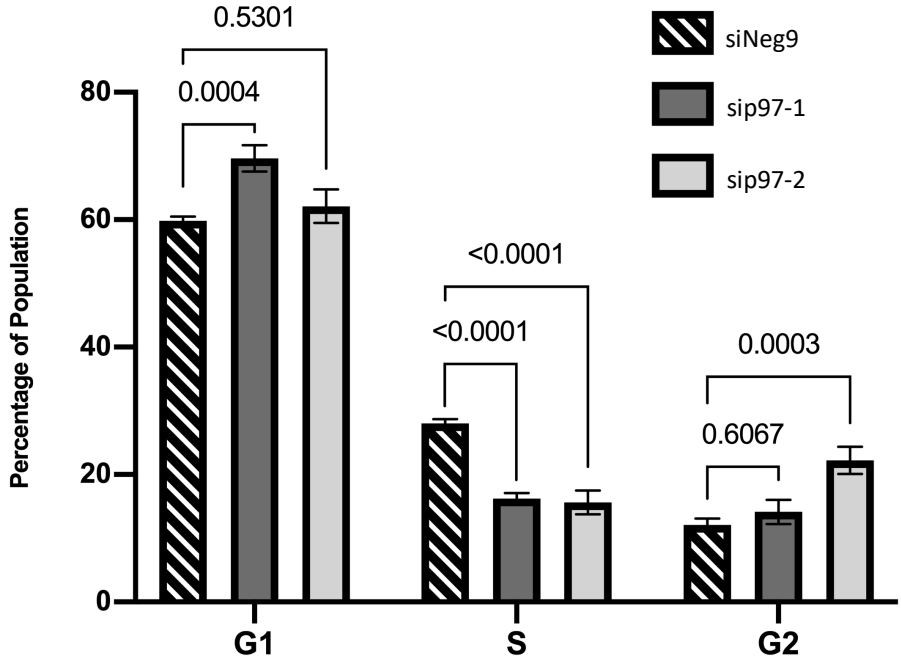


Figure 3.3 – Results of p97 knockdown upon the relative populations of different stages of the cell cycle. Populations were quantified by integration of Gaussian distributions from histograms of propidium iodide fluorescence as above and converted to percentages of the total sample population. Confidence values were calculated by ordinary two-way ANOVA. Error bars show standard error of the mean (n=5).

Clear differences in the percentage of the population in the different stages of the cell cycle were observed following p97 depletion compared to control. In particular, treatment with both available p97-targeting siRNAs resulted in a substantial decrease in the percentage of cells in S-phase, by 12.3 percentage points on average. This difference was offset by statistically significant increases in the G1 population (following use of sip97-1) and the G2/M population (following use of sip97-2). It is not currently understood why use of different siRNAs – both targeting p97 – resulted in these different phenotypes.

These results are in broad agreement with the wide body of literature that has previously noted a role for p97 in regulation of the cell cycle. It has already been noted that p97 acts to extract Aurora B kinase from chromatin during mitosis (Section 1.4.3) (146,147). In addition, p97 has been shown to have a direct role in the enforcement of the G2/M checkpoint by binding ubiquitylated Cdc25A, a phosphatase enzyme which is key for cell cycle regulation. This leads to the eventual degradation of Cdc25A at the proteasome, and is a component of a pathway which has evolved to prevent cells from entering mitosis with damaged DNA (167,168). Further, p97 has also been shown to promote transition though the G1/S boundary in budding yeast by facilitating the degradation of Far1p, a G1-specific CDK (cyclin dependent kinase) inhibitor which otherwise prevents passage into S-phase (169). Indeed, given that p97 is alternatively known in budding yeast as ‘Cdc48’ (cell division control protein 48) it comes as no surprise that its depletion can be shown to lead to significant disturbances in the cell cycle.

3.3 – Thymidine Arrest Experiments

Having confirmed that p97 knockdown does indeed result in perturbations of the HeLa cell cycle, it was important to investigate whether these perturbations were responsible for the increases in ancestral CENP-A-SNAP fluorescence under a pulse-chase setup (as discussed in Section 3.1). To accomplish this, an S-phase block was used to inhibit passage through the cell cycle, regardless of

knockdown conditions. Deoxythymidine (commonly referred to as thymidine) is a deoxynucleoside. It is a DNA base and therefore a crucial component of genetic material. However, when added in great excess, thymidine instead causes the inhibition of DNA synthesis, blocking the passage of cells through S-phase (170–172). This occurs because excess cellular quantities of thymidine inhibit the production of deoxycytidine, another DNA base. This prevents the cell from entering S-phase (173).

If the cell cycle delay hypothesis is correct and observed increases in ancestral CENP-A-SNAP fluorescence during p97 knockdown in a pulse-chase protocol stem from the slowing of progress through the cell cycle, then these increases would be negated by exposing all samples to a thymidine block. This is because that block would cancel out any differences in cycle passage speed between the siNeg9 and sip97 conditions, as cycling would simply be prevented regardless of any other effects. Therefore, the cell cycle delay hypothesis was directly tested by running further pulse-chase studies with the inclusion of a continuous thymidine arrest, in order to investigate whether these characteristic increases in TMR-Star fluorescence were no longer observed in S-phase arrested populations.

HeLa CENP-A-SNAP cells were grown, pulsed with TMR-Star, transfected (siNeg9, siSENP6, siMis18α, sip97-1/2) and left to cycle for 48 hours as in Section 2.1.1 above. In addition, 2mM thymidine was added to media concurrently with transfection, and retained throughout the chase period. This is summarised below (Figure 3.4).

Following the chase, cells were processed and imaged identically as per a standard pulse-chase protocol (Section 2.1.1). Centromeric fluorescence was quantified using CRaQ, using CENP-B fluorescence in the 527 nm channel as a reference. Results are shown below (Figure 3.5)

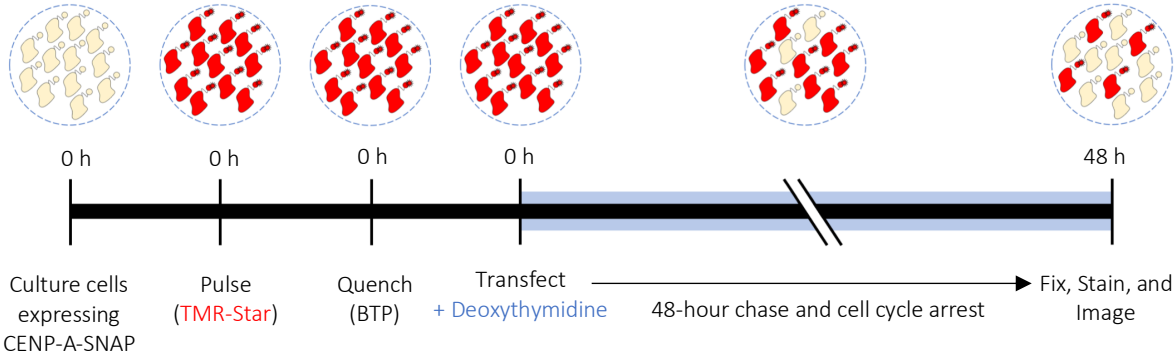


Figure 3.4 – Overview of a pulse-chase protocol incorporating S-phase arrest using thymidine during the chase period.

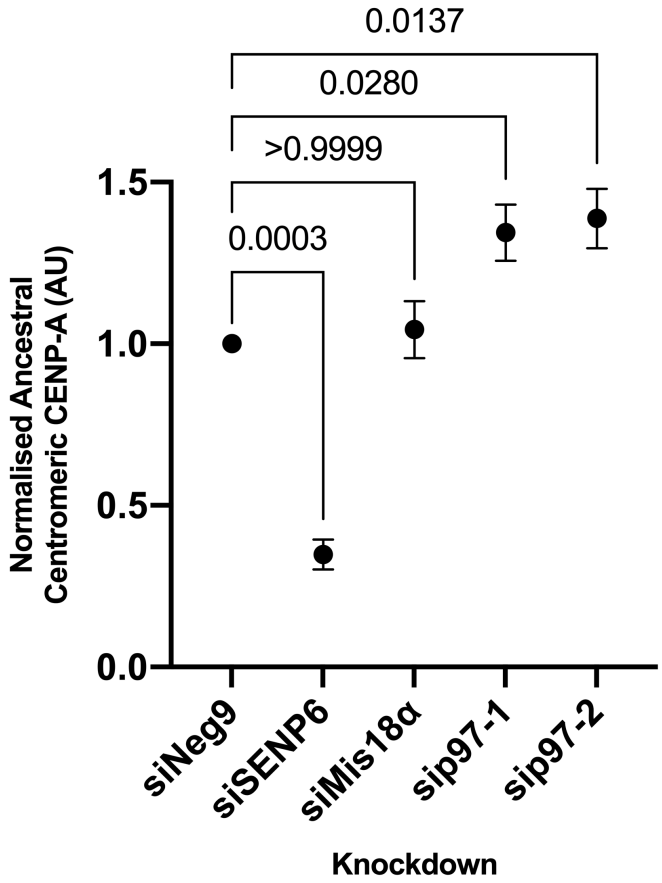


Figure 3.5 – Quantified and combined data from pulse-chase experiments alongside thymidine arrest.

Error bars show the standard error of the mean. Reproducibility is indicated by P-values calculated by ordinary one-way ANOVA using Bonferroni multiple comparisons analysis (n=3). Median fluorescence values for siSENP6, siMis18α, sip97-1/2 were quantified by CRaQ and normalised to those of siNeg9 within their respective biological replicates for comparison.

Surprisingly, negation of the cell cycle did not suppress the effect of p97 knockdown on ancestral centromeric CENP-A-SNAP fluorescence. Use of both p97-targeting siRNAs resulted once again in a slight yet significant increase in the apparent stability of CENP-A nucleosomes at the centromere. This is strong evidence that, while p97 knockdown may disrupt the HeLa cell cycle, these disruptions are not the cause of the results of pulse-chase protocols discussed in Chapter 2.

These findings are not necessarily inconsistent; p97 knockdown may conceivably change the relative percentage of cells in each stage of the cell cycle without causing any net slowing of passage through the cycle as a whole. Provided that the average time taken to progress through the complete cycle remains at or very close to 24 hours, p97 knockdown could cause disorder amongst the relative populations of each stage (G1, S, G2, M) compared to control without impacting the overall generational turnover rate of centromeric CENP-A nucleosomes.

3.3.1 – Analysis of Cell Counts to Confirm Successful Arrest

In order to validate these results, it was necessary to confirm that the thymidine block had occurred successfully, and that these observations were not simply the result of poor drug delivery or incomplete arrest. Cell numbers in the thymidine-arrested pulse-chase experiments above were counted for comparison to those of standard pulse-chase experiments, which were run simultaneously without the addition of 2mM thymidine. These data are shown below (Figure 3.6).

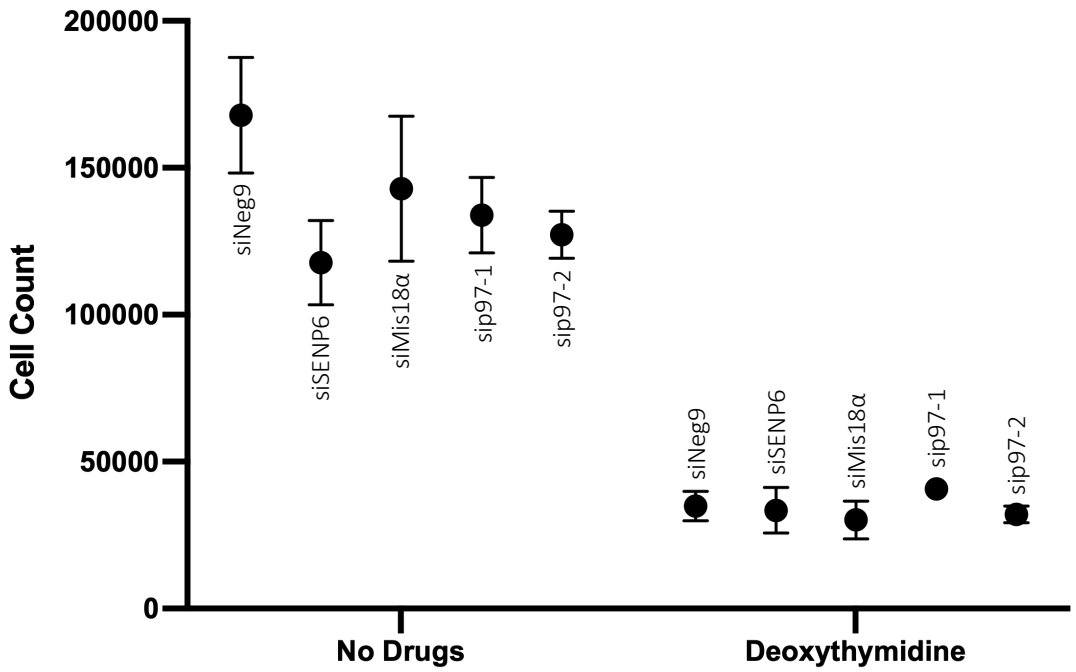


Figure 3.6 – Cell counts after a 48-hour chase. Quantified after both a standard pulse-chase setup and a pulse-chase coupled to deoxythymidine S-phase arrest. Error bars show standard error of the mean (n=3). In the interests of readability, P-values are not plotted. However, multiple comparison analysis via two-way ANOVA yielded P<0.001 for all deoxythymidine-positive knockdown conditions versus their respective non-arrested analogues.

Note that data from the non-arrested control pulse-chase experiments was incorporated into that presented in Figure 2.7 above. Addition of 2mM thymidine clearly led to a lower cell count after 48 hours. Notably, population size was decreased by an average factor of 4.06 across the knockdown conditions. This is remarkably consistent with the factor of 4 that would be expected for HeLa cells prevented from dividing twice, resulting from the inhibition of passage through two cell cycles lasting 24 hours each. This suggests that the arrest was indeed successful.

3.3.2 – Use of EdU Staining to Confirm Successful Arrest

As further evidence that use of 2mM thymidine prevented the passage of HeLa CENP-A-SNAP cells into mitosis, a protocol using 5-Ethynyl-2'-deoxyuridine (EdU) as a DNA marker was utilised to highlight cells that were actively synthesising DNA, and so directly measure their ability to proliferate under these conditions. EdU is a modified thymidine analogue; when added to cells it will incorporate into newly synthesising DNA (174). EdU contains a terminal alkyne group, which may undergo a click reaction with a fluorophore bound azide via a copper (I) catalysed Huisgen [3+2] cycloaddition (Figure 3.7) (175,176). This fluorophore can then be visualised by microscopy, allowing observation of whether a cell was undergoing active DNA synthesis when EdU was added.

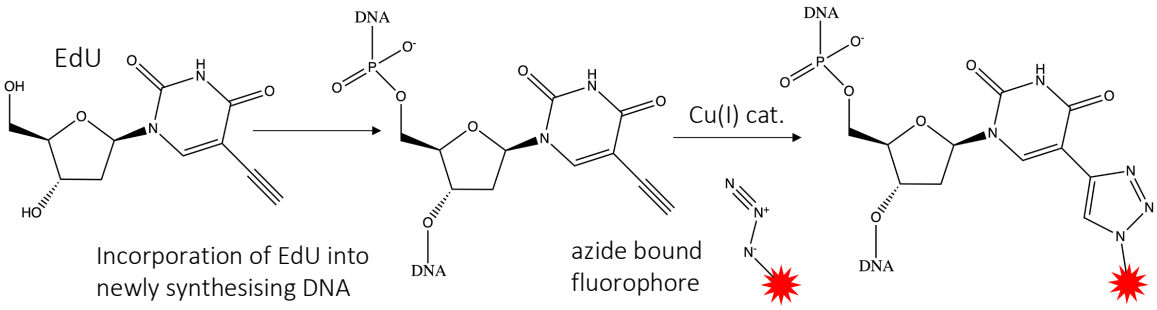


Figure 3.7 – Overview of the incorporation of EdU at DNA and its staining via click chemistry

This technique has advantages over traditional BrdU-coupled antibody staining protocols, which were previously developed for quantification of DNA synthesis (177). Antibodies are no longer required under an EdU protocol, and so the reactive species involved are significantly smaller and

able to more efficiently permeate through to chromatin. This removes the need for denaturation of the DNA with nucleases, heat, and acid, and grants a rapid, sensitive and reproducible assay (178).

HeLa CENP-A-SNAP cells were seeded on poly-lysine coated coverslips and grown for 48 hours with and without 2 mM thymidine. Whilst the SNAP-tag was again not directly utilised in this protocol, it remained important to use the same cell line as the experiments above, in order to ensure that differences in genetic environment did not alter observations. Upon completion of this period, cells were treated with 10 mM EdU for 10 minutes and fixed in 4% formaldehyde. Fixed cells were then stained with the EdU compatible azide-bound fluorophore as above, and with DAPI to act as a nuclear marker regardless of DNA-synthesis state. They were then visualised at 63X magnification using inverted light microscopy. Representative images are shown below (Figure 3.8).

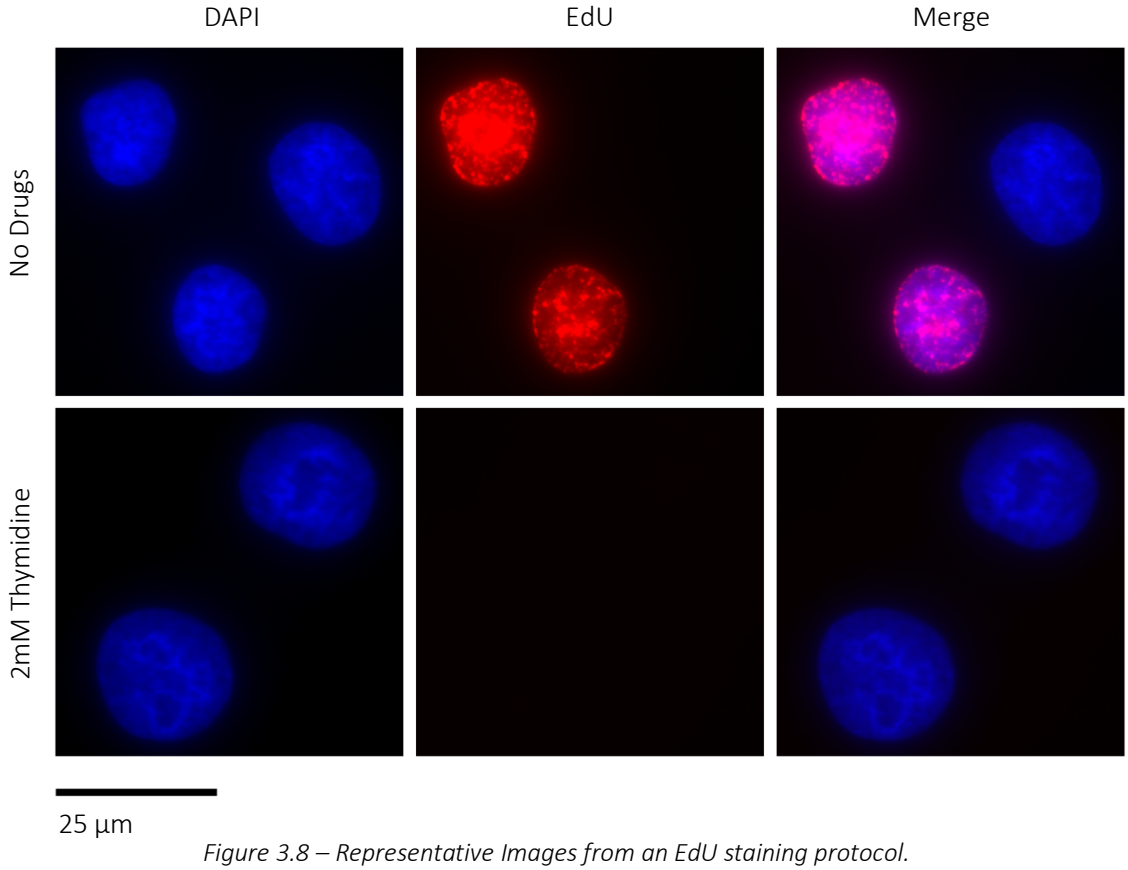


Figure 3.8 – Representative Images from an EdU staining protocol.

Nuclei are clearly visible under all conditions. However, EdU incorporation was significantly reduced following treatment with thymidine, indicating a lack of DNA synthesis, as expected. Note that only a subset of nuclei were EdU-positive in the unperturbed control; this is again fully as expected given that only a subset of cells will be in S-phase during the EdU incorporation timeframe.

Images were quantified using an ImageJ macro which used DAPI as a nucleic reference and then quantified median EdU fluorescence across the nucleus of each cell. These data are shown below (Figure 3.9)

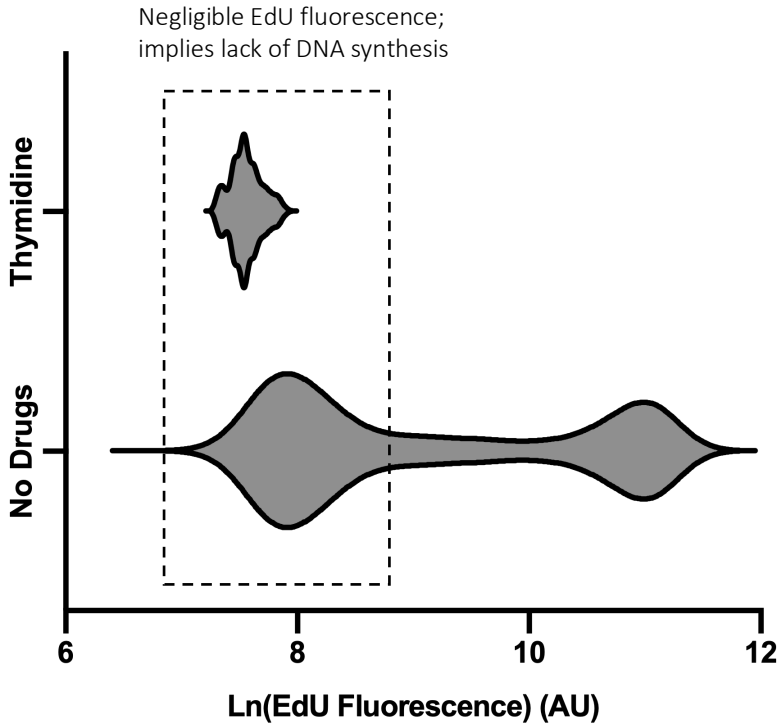


Figure 3.9 – Violin plot of EdU fluorescence following 2 mM thymidine treatment, versus an unperturbed control.

EdU fluorescence is presented as a natural logarithm for ease of interpretation. Violin plots represent the relative probability across EdU fluorescence states for cells in the population.

Untreated control populations displayed a wide range of EdU fluorescence values, corresponding to a multitude of synthesis states. This implies that these cells were randomly cycling in a normal manner, as expected. Conversely, treatment for 48 hours with 2 mM thymidine prevented the observation of any significant EdU fluorescence. This strongly implies that DNA synthesis was successfully prevented, and that the cell cycle was indeed arrested by this protocol.

3.4 – Discussion

Combined, the experiments above serve to dispute the cell cycle delay hypothesis. In agreement with current literature, p97 knockdown was shown using flow cytometry to have significant influence on the HeLa CENP-A-SNAP cell cycle. In particular, a decrease in the S-phase population was noted, coupled to either an increase in the G1 population or the G2/M population depending on which specific p97-targeting siRNA was used. However, these perturbations cannot be responsible for the characteristic increases in ancestral CENP-A-SNAP fluorescence observed in pulse-chase experiments. Repetition of such protocols with the inclusion of a 48-hour S-phase arrest concurrently with the chase period using 2 mM thymidine did not negate this observation. Efficacy of the arrest was demonstrated using cell counts, and by EdU staining to directly detect DNA synthesis. Thus, while p97 depletion may well cause disturbances in the passage of the cell cycle, these disturbances are not solely responsible for the increase in apparent CENP-A stability that simultaneously occurs.

Chapter 4 – Investigating the Direct Action of p97 at Centromeric Chromatin

4.1 – Hypothesising an Increase in CENP-A Stability

Having demonstrated that p97 depletion does not affect the loading of nascent CENP-A nucleosomes, and that any cell-cycle disturbances resulting from this knockdown are not responsible for simultaneous increases in CENP-A-SNAP-TMR fluorescence observed at the centromere, it was hypothesised that p97 depletion may legitimately improve the stability of chromatin-bound CENP-A nucleosomes. That is to say; p97 may be conjectured to play a role in turning over centromeric CENP-A nucleosomes, such that they are maintained to a higher degree when p97 is depleted. This hypothesis is not in agreement with Jansen *et al,* whose data suggested that CENP-A nucleosomes are already maximally stable once loaded onto centromeric chromatin. However, given the small magnitude of the effect observed – especially in comparison to that noted by Mitra *et al* – it was hypothesised that p97 knockdown may only result in a very slight increase in the stability of these species, and that this effect may take time to reach a level which is observable using current methods. Therefore, it is plausible that low levels of physiological non-replication-based turnover of CENP-A nucleosomes at the centromere may occur but have escaped detection due to experimental variance in the original experiments conducted by Jansen *et al*, preventing the observation of this effect until now.

4.1.1 – p97 Acting as an Antagonist to SENP6

As discussed above, the study by Mitra *et al* highlighted a wide variety of genes whose knockdown was found to destabilise CENP-A nucleosomes at the centromere. That is to say; these factors were shown to be involved in the maintenance of chromatin-bound CENP-A nucleosomes, and so are jointly responsible for the very low levels of endogenous turnover observed. One such key factor highlighted by this screen was SENP6, which was found to be indispensable for the maintenance of CENP-A at the centromere (112). This observation has also been consistently borne out throughout this thesis. SENP6 RNAi was confirmed to lead to dramatic destabilisation

of centromeric CENP-A-SNAP under pulse-chase protocols (Figures 2.6, 2.7) and modified pulse-chase protocols (Figure 2.12). SENP6 depletion was also confirmed to drastically hinder the loading of newly synthesised CENP-A-SNAP under a quench-chase-pulse protocol (Figure 2.16).

In order to provide a mechanistic basis for the hypothesis that p97 is responsible for low-level physiological turnover of CENP-A nucleosomes, it was conjectured that p97 and SENP6 may play roles antagonistic to one another. As noted above, p97 is a SUMO segregase, which acts to extract SUMOylated substrates from larger protein assemblies (141,148). Conversely, SENP6 is a SUMO protease; it cleaves SUMO chains from its substrates, whilst otherwise leaving them unmodified (120–122). It is therefore conceivable that p97 and SENP6 jointly regulate chromatin-bound CENP-A nucleosomes with opposing activities; p97 may extract SUMOylated centromeric species from the chromatin, whilst SENP6 attempts to cleave these polySUMO chains which otherwise act as a marker for removal by p97.

Given that CENP-A nucleosomes are extremely (if perhaps not absolutely) stable under physiological conditions, it may be assumed that the deSUMOylating action of SENP6 is the dominant force at the centromere under most circumstances. However, knockdown of SENP6 may shift this balance, allowing p97 increased license to remove centromeric proteins from the chromatin. This would yield the results of SENP6 RNAi observed by Mitra *et al and* confirmed in this work.

If p97 and SENP6 coregulate chromatin-bound CENP-A by acting antagonistically, then we would expect their simultaneous depletion to rescue the effects observed above. That is to say; if neither was available to act upon chromatin, then we would expect no net effect on CENP-A stability if they each serve to counter the actions of the other.

4.1.2 – The Auxin Inducible Degron

In order to investigate this hypothesis, rescue experiments were run using a line of HeLa cells expressing an auxin inducible degron (AID) tagged to SENP6. This technology, initially developed by Nishimura *et al* (179) utilises a degradation system found naturally in plant cells. It relies upon the Auxin family of hormones, which regulate a wide variety of growth and development processes in plants (180). Notably, in *Arabidopsis thaliana,* indole-3-acetic acid (IAA) (Figure 4.1), a member of the auxin family, has been shown to target the E3 ubiquitin ligase SCF-TIR1 (181,182) and promote its interaction with a variety of transcription factor substrates (183). This leads to the polyubiquitination of those substrates, and their downstream proteasomal degradation (179). Whilst the ubiquitin system is highly conserved amongst eukaryotes (25), the auxin-specific branch of this pathway is unique to plants (184).

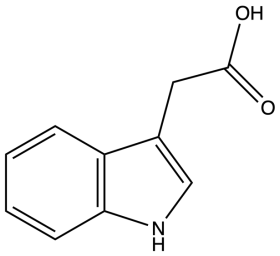


Figure 4.1 - Structure of indole-3-acetic acid

This was noted by Nishimura *et al,* who were successful in introducing SCF-TIR1 to non-plant cells. Therefore, by also genetically fusing a substrate of SCF-TIR1 to proteins of interest, they were able to use IAA in solution to induce the rapid and reversible degradation of those fusion proteins. This substrate, known in *Arabidopsis* as IAA17, was termed the auxin inducible degron (AID). Note that further refinement of this setup by Nishimura *et al* resulted in use of an *Oryza sativa* TIR1 ("transport inhibitor response 1"; the auxin-receptor component of SCF-TIR1) mutant for enhanced temperature tolerance. This *OsTIR1* mutant forms SCF-TIR1 in the cell by complexing with other evolutionarily conserved components of the ubiquitin degradation pathway (179). Holland *et al* followed up on this work and showed that these AID-fusion proteins are capable of reproducing the functionality of their endogenous analogues in mammalian cells, and that they may be rapidly degraded at all stages of the cell cycle using the system described above (185). This is shown schematically below (Figure 4.2).

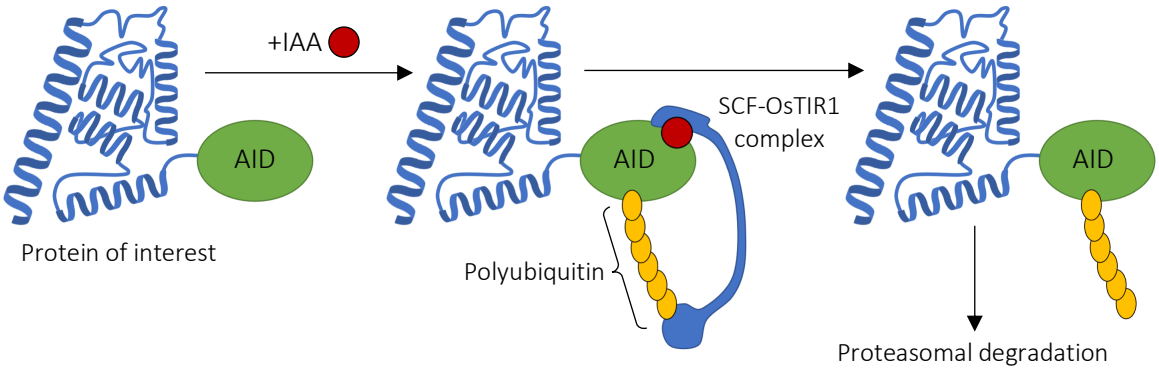


Figure 4.2 – Schematic overview of the AID degradation system. Consult Nishimura *et al* for full specifics on the nature of the SCF-OsTIR1 complex (179).

AID technology has been successfully used previously in order to specifically deplete CENP-A and CENP-B and to investigate their physiological roles (164,186). Further, Mitra *et al* developed upon the HeLa CENP-A-SNAP line and augmented it with OsTIR1 alongside an endogenously tagged SENP6-AID-EGFP construct targeting all SENP6 alleles. The additional tagging of SENP6 with GFP (green fluorescent protein) alongside the AID allows for rapid and cell-specific confirmation of SENP6-AID-GFP depletion by measuring GFP fluorescence levels. They showed that, in this line, addition of IAA fully depleted nuclear SENP6 within 3 hours. This then resulted in evident loss of centromeric CENP-A within 6 hours, at all stages of the cell cycle (112). For simplicity, this cell line will be referred to in this work as HeLa SENP6-AID.

4.1.3 – SENP6-AID Rescue Experiments using p97 RNAi

To investigate the hypothesis that p97 and SENP6 act antagonistically to one another, p97 RNAi over an extended period of time in HeLa SENP6-AID cells was followed by treatment with 1 mM IAA, in order to determine whether this rescued the effects of SENP6 depletion on CENP-A stability. Cells were transfected using siNeg9 as a non-gene-targeting scrambled control and two siRNAs targeting p97 before seeding on poly-lysine coated glass coverslips. They were incubated (37°C, 5% CO_2) for 65 hours, before induction with 1 mM IAA for a further 7 hours to fully deplete

SENP6. Cells were then fixed in 4% formaldehyde, stained via immunofluorescence/DAPI and imaged as described above in Chapter 2 (see also Section 6.6). The general experimental scheme is outlined below (Figure 4.3) alongside representative images (Figure 4.4)

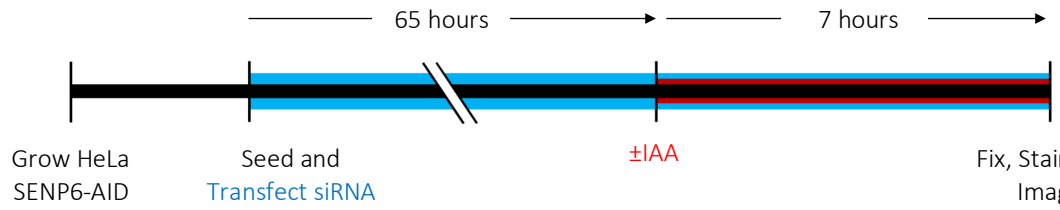


Figure 4.3 – Overview of a protocol combining SENP6-AID depletion with p97 knockdown over 72 hours. Knockdown is indicated in blue, and depletion of SENP6 in red. Note that, whilst siRNA species are only present for the first 65 hours, p97 RNAi is assumed to continue for the final 7 hours.

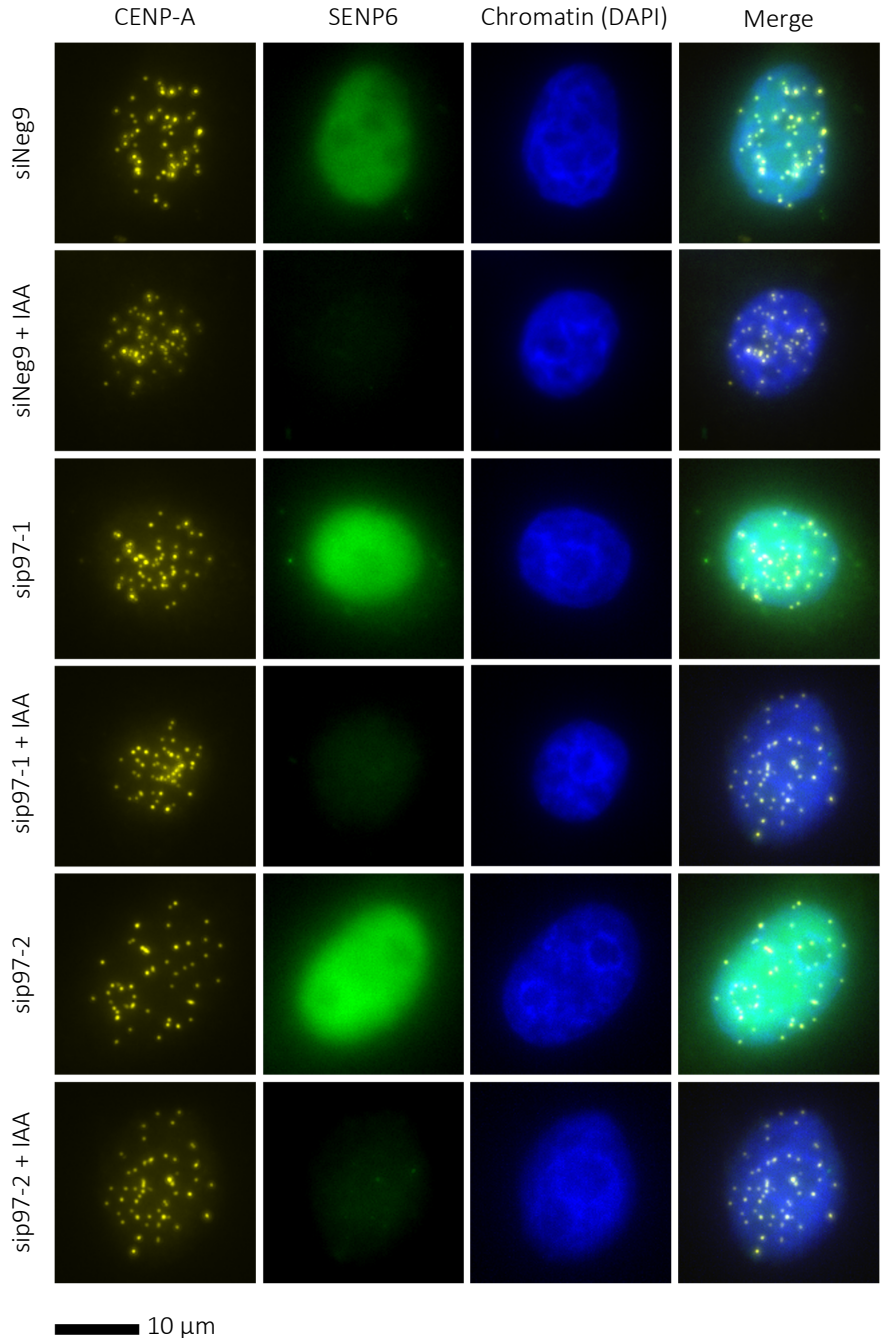


Figure 4.4 – Representative Images from SENP6-AID depletion tied to p97 knockdown.

Brightness and contrast of CENP-A and SENP6 channels are shown normalised for comparison. Addition of IAA can be readily seen to deplete SENP6 signal. The effects of this on CENP-A were quantified by CRaQ, as discussed below.

Whilst this cell line does contain CENP-A-SNAP, the SNAP-tag was not directly used in these experiments. Preliminary experiments combining siRNA transfection with auxin addition as well as SNAP pulse-chase labelling proved detrimental to cell viability. To circumvent this problem, SNAP-labelling was omitted, and CENP-A levels were instead assayed by immunofluorescence. Therefore, results of these experiments should not be directly interpreted in terms of CENP-A stability, but rather in terms of the maintenance of steady-state CENP-A levels. DAPI was again used to stain chromatin. In addition, note that CENP-B was not used as a centromeric marker for CRaQ during analysis of these experiments. SENP6-AID-GFP fluoresces at 527 nm, occupying a channel at which our available antibodies for CENP-B provide a good signal. However, it was noted that the 600 nm signal in a separate channel from centromeric CENP-A remained readily discernible above background levels under all conditions in this protocol. As expected, CENP-A levels were visually diminished following 7-hour IAA-induced depletion of SENP6. However, these foci were still easily distinguished owing to an excellent signal:noise ratio at the 600 nm channel. Therefore, CENP-A fluorescence was suitable for use as a self-reference in CRaQ analysis. ROIs were scrutinised in order to confirm that the algorithm had correctly identified centromeric foci; representative images with ROIs overlayed are shown (Figure 4.5).

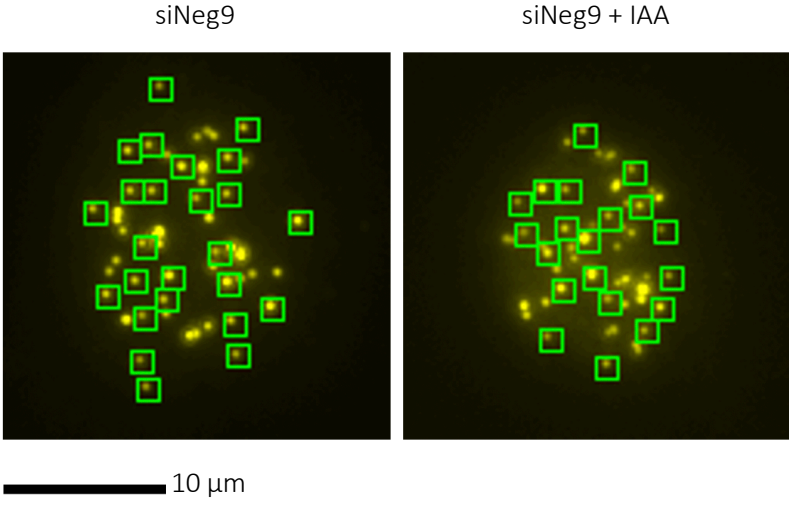


Figure 4.5 – CRaQ ROIs identifying CENP-A fluorescent foci. Images show single cells from control and IAA positive conditions. Brightness and contrast scaled individually in each image to enhance clarity of centromeric foci. ROIs can be seen to correspond well to individual centromeres in both cases.

The cumulated results of CRaQ analysis of images from this protocol are shown below (Figure 4.6).

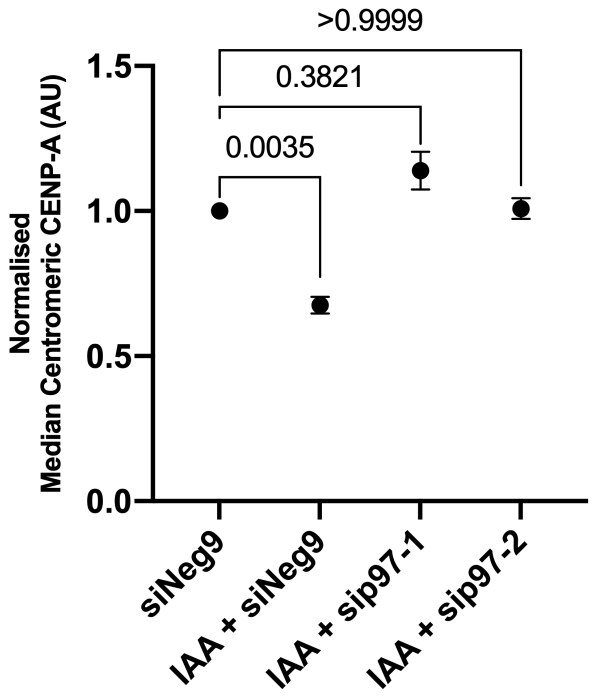


Figure 4.6 – Results of SENP6-AID depletion coincident with p97 RNAi. Median values normalised to siNeg9 within each biological replicate. Error bars show standard error of the mean; P-values calculated using one-way ANOVA and Bonferroni multiple comparisons analysis (n=3).

As expected, control transfection with siNeg9 alongside addition of 1 mM IAA to deplete SENP6 led to a statistically significant reduction in CENP-A at the centromere by ~33% after 7 hours. Remarkably, transfection with either p97-targeting siRNA was able to fully rescue this effect; no statistically significant changes in total centromeric CENP-A levels were observed upon simultaneous depletion of p97 and SENP6. This is strong evidence in favour of the hypothesis that these species coregulate centromeric CENP-A by working antagonistically.

As a control, cells were also subjected to p97 knockdown alone, to ensure that any rescue observed was not simply a superposition of two unrelated effects. These experiments were conducted within the same biological replicates as those in Figure 4.6 above but are presented separately to facilitate interpretation and discussion (Figure 4.7).

Neither of the two p97-targeting siRNAs resulted in changes in total centromeric CENP-A levels clearing a 95% confidence interval. Admittedly, sip97-1 may have caused a small, uncertain, increase in centromeric CENP-A and potentially contributed towards a similarly small relative

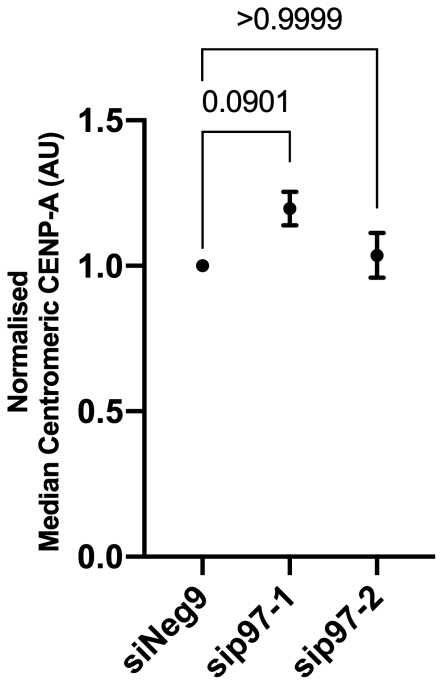


Figure 4.7 – Results of p97 RNAi on SENP6-AID cells. Data collected, presented, and analysed alongside that of Figure 4.6 above.

increase observed in Figure 4.6. This is further discussed and investigated below. In contrast, sip97-2 caused no such change in Figure 4.7, yet still resulted in complete rescue of the effects of SENP6 depletion upon centromeric CENP-A. This increases confidence that the observations above constitute a 'true' rescue.

To ensure that p97 RNAi was not simply interfering with the AID system and preventing the depletion of SENP6, levels of SENP6 in each cell were measured by microscopically observing GFP fluorescence. These levels were quantified using an ImageJ macro analogous to CRaQ. However, whereas CRaQ is designed to detect centromeric foci, this modified algorithm instead calculated the median nucleic SENP6-AID-GFP fluorescence in maximum projections of Z-stack images, using a DAPI mask as a nuclear reference. Results are shown below, separated again to facilitate interpretation and discussion (Figures 4.8a, 4.8b).

These data clearly indicate that p97 RNAi did not interfere with SENP6-AID degradation; loss of GFP fluorescence was observed in all IAA positive samples (Figure 4.8a). This is a key control and shows that this rescue indeed occurs due to the depletion of both proteins simultaneously. An unexpected result was again observed following transfection with sip97-1, wherein a statistically significant decrease in SENP6 was also seen (Figure 4.8b). This observation was not mirrored when using sip97-2; nucleic SENP6 levels were here found to show no difference compared to control. This is a currently unexplained phenomenon, which invites further investigation. In particular, it does suggest the possible existence of a regulatory feedback loop between p97 and SENP6

themselves, in addition to their antagonistic regulation of CENP-A nucleosomes. However, significantly more research would be required in order to establish this, and the observation otherwise lies outside of the scope of this thesis.

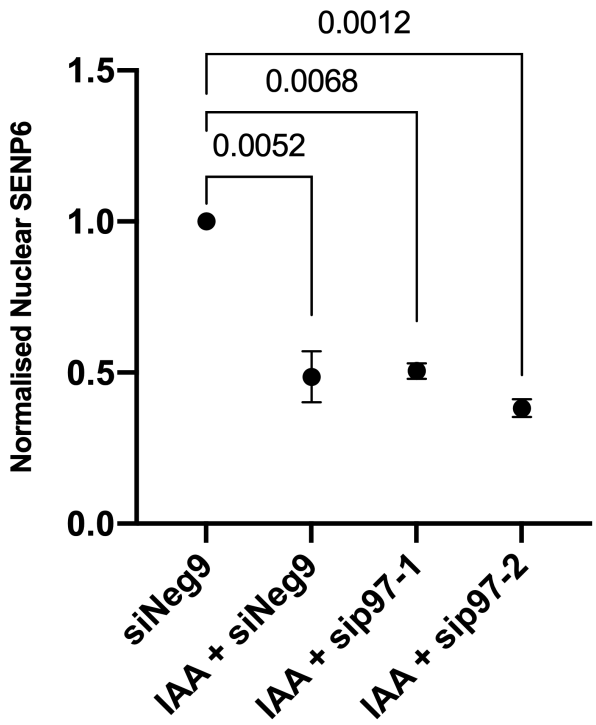


Figure 4.8a – Quantification of SENP6 levels in IAA positive samples compared to control.

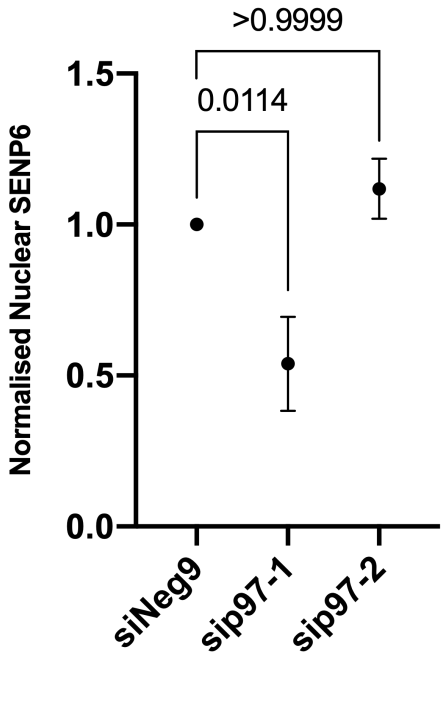


Figure 4.8b – Quantification of SENP6 levels during p97 knockdown alone.

4.1.4 – SENP6-AID Rescue Experiments using Pharmacological p97 Inhibition

Whilst considering explanations for the incongruous results obtained from the use of one specific p97-targeting siRNA shown in Figures 4.7 and 4.8b above, it was noted that the HeLa SENP6-AID cells experience harsh treatment during long-term depletion of p97. As discussed previously, p97 is a core housekeeping protein which is responsible for a wide range of functions (Section 1.4.3). Consistently, increased cell death is observed during extended p97 knockdown, as a wide variety of vital systems may be affected. Therefore, these incongruous observations may stem from decreased fitness of the population and pleiotropic effects of p97 loss.

In order to further investigate the rescue of the effects of SENP6-AID depletion on CENP-A through simultaneous p97 depletion, a fast-acting p97-specific inhibitor was used instead of long-term RNAi. NMS-873 (Figure 4.9) is a potent, selective allosteric inhibitor of p97 (187) and was used in conjunction with IAA-induced degradation of SENP6 to test whether the rescue of CENP-A removal from the centromere could be replicated without the requirement to subject cells to extended p97 depletion.

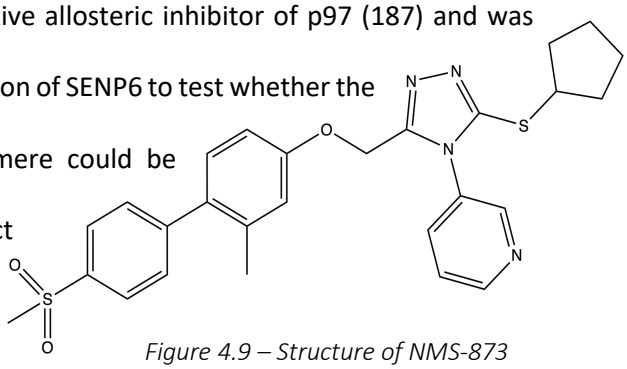


Figure 4.9 – Structure of NMS-873

HeLa SENP6-AID cells were seeded on poly-lysine coated glass coverslips, and incubated for 41 hours (37°C, 5% CO_2) in media in order for cells to adhere and proliferate in a healthy manner. They were then re-incubated in media containing a mixture of drugs for a further 7 hours before fixing in 4% formaldehyde. This mixture contained either 1 mM IAA, 1mM NMS-873, or both simultaneously. A drug-free control was also performed. The general experimental scheme is outlined below (Figure 4.10).

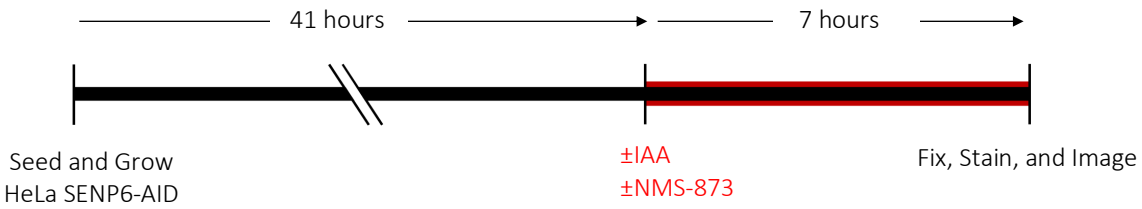


Figure 4.10 – Overview of a protocol combining SENP6-AID depletion with p97 inhibition using NMS-873. The timeframe of drug addition is indicated in red

Coverslips were stained by immunofluorescence and imaged identically to RNAi experiments described in Section 4.1.3 above. This was followed by CRaQ analysis, again measuring CENP-A levels using a self-reference as discussed previously. Results are shown below (Figure 4.11).

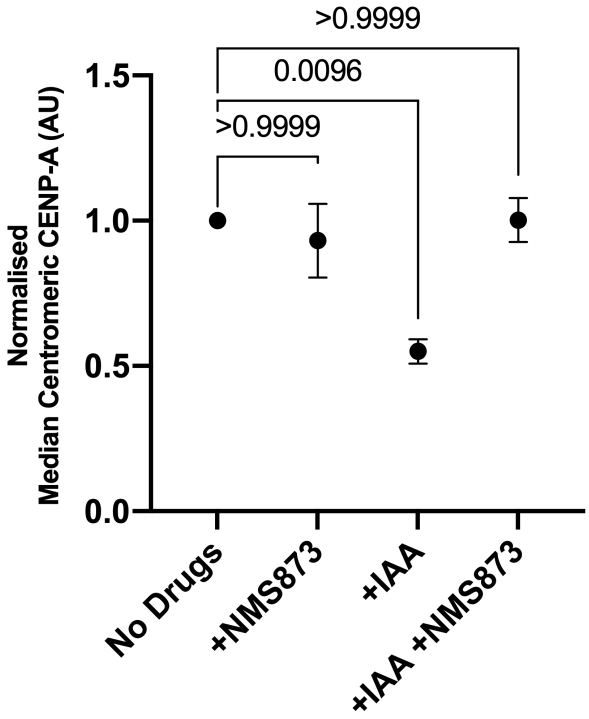


Figure 4.11 – Effects of simultaneous SENP6-AID depletion and p97 inhibition on centromeric CENP-A.

Median centromeric CENP-A fluorescence normalised to that of the drug-free control within each biological replicate. Error bars show standard error of the mean. P-values calculated by one-way ANOVA using Bonferroni multiple comparisons analysis (n=3).

Incubation with 1 mM NMS-873 had no measurable effect on CENP-A levels at the centromere, in contrast to the slightly anomalous result shown in Figure 4.7. Treatment with 1 mM IAA alone resulted in depletion of centromeric CENP-A, as expected. Further, addition of IAA and NMS-873 simultaneously resulted in complete rescue of this effect, returning CENP-A levels to the control baseline with a very high degree of confidence.

Nuclear SENP6 levels were again quantified by GFP fluorescence, in order to confirm that incubation with NMS-873 was not simply inhibiting the auxin pathway (Figure 4.12).

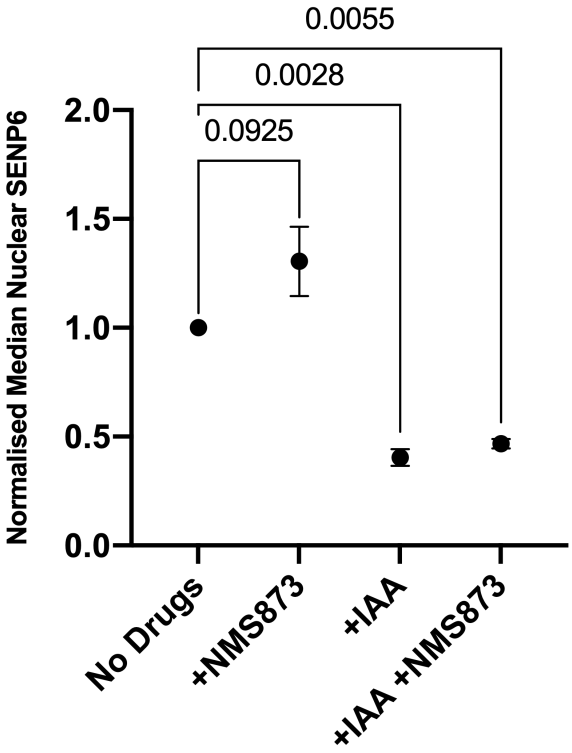


Figure 4.12 – Effects of simultaneous SENP6-AID depletion and p97 inhibition on nuclear SENP6.

Median nuclear SENP6 levels were measured by GFP-fluorescence on a per cell basis and normalised to the drug-free control within each biological replicate. Error bars show standard error of the mean. P-values calculated by one-way ANOVA using Bonferroni multiple comparisons analysis (n=3).

Addition of IAA resulted in loss of SENP6 from the nucleus, regardless of whether NMS-873 was added simultaneously. Interestingly, a small increase in nucleic SENP6 levels was tentatively observed upon incubation with NMS-873 alone, although this observation did not clear a 95% confidence interval. This also runs contrary to the depletion of nucleic SENP6 commented upon in Figure 4.8b. Whilst these observations are worth following up on and may again imply some level of feedback-induced regulation of the two species, they remain uncertain and outside the scope of this thesis.

4.1.5 – Discussion of SEN6-AID Rescue Experiments

Collectively, the above experiments constitute strong evidence in favour of the hypothesis that SENP6 and p97 co-regulate the levels of CENP-A nucleosomes at the centromere by acting antagonistically. Figure 4.6 demonstrates that the knockdown of p97 over a total of 72 hours is capable of eliminating the effects of SENP6-AID depletion on CENP-A. Figure 4.11 reinforces this by showing that short-term inhibition of p97 is equally capable of producing this result. This is a very exciting finding, and provides a level of mechanistic elucidation of the results of Mitra *et al*, who first identified SENP6 as a crucial maintenance factor for centromeric CENP-A (112). Collectively, the data presented here demonstrate that the depletion of CENP-A from centromeric foci during SENP6 depletion relies upon the action of p97. This is further discussed in Chapter 5.

4.2 – Investigating the Direct Action of p97 on CENP-A Nucleosomes

Whilst the results above show that the actions of p97 may have a destabilising effect on CENP-A nucleosomes at the centromere, it is not yet clear by what mechanism this destabilisation is triggered. The simplest hypothesis would be that p97 directly extracts SUMOylated CENP-A from chromatin, and that SENP6 acts by deSUMOylating CENP-A, such that it is no longer a target for p97. However, whilst searching for SUMOylated centromeric species, Mitra *et al* found no evidence for the SUMOylation of CENP-A. This suggests that CENP-A may not be a direct target of

p97, and that it instead resides downstream of another species which is directly regulated by p97/SENP6 branch of the SUMO pathway. One possible contender for this upstream species is CENP-C, a component of the CCAN (Figure 1.3) (188) which is required for assembly of the centromere and kinetochore (189–191) and maintenance of CENP-A nucleosomes at the centromere (192) (Figure 2.2). That is to say; depletion of CENP-C was found to destabilise CENP-A nucleosomes at the centromere. Strikingly, CENP-C was also one of two centromeric species (alongside CENP-I) for which Mitra *et al* found evidence of SUMOylation (112). This suggests that CENP-C is the centromeric target of p97/SENP6 regulation by the SUMO pathway, and that its removal from the centromere causes changes in the CCAN architecture which lead to the destabilisation of CENP-A nucleosomes.

4.2.1 – CENP-A-AID Rescue Experiments using p97 RNAi

Whilst this thesis focuses on p97 acting as a SUMO segregase, it is commonly also known to act upon ubiquitinated substrates (discussed in Section 1.4.3). Therefore, if CENP-A is a direct substrate of p97, we might expect p97 depletion to offer some rescue of the degradation of ubiquitinated CENP-A during an AID protocol.

To test this idea, DLD1 (colorectal adenocarcinoma) cells expressing CENP-A-AID-EYFP (tagged at one allele, while the other was inactivated) alongside OsTIR1 were adopted, following their recent production by Hoffmann *et al*. This line allows for the rapid depletion of CENP-A within 50 minutes following the addition of IAA, by the same principles outlined above (Section 4.1.2) (186) and will henceforth be referred to as DLD1 CENP-A-AID for simplicity.

Experiments analogous to those discussed in Section 4.1.3 were performed to probe for direct action of p97 upon ubiquitinated centromeric CENP-A. In brief, DLD1 CENP-A-AID cells were simultaneously seeded on coverslips and transfected with siNeg9 and two siRNAs targeting p97.

They were then left for a period of 71 hours, during which p97 was depleted. Following this, samples from each siRNA condition were incubated for one further hour either with 1 mM IAA, or with a drug-free control. Coverslips were then stained; CENP-A levels were assessed by imaging the auto-fluorescent EYFP tag at 527 nm, and CENP-B was stained for use as a centromeric reference in CRaQ analysis. Chromatin was stained using DAPI. This experimental structure is outlined below (Figure 4.13) alongside quantified results (Figure 4.14) and representative images (Figure 4.15).

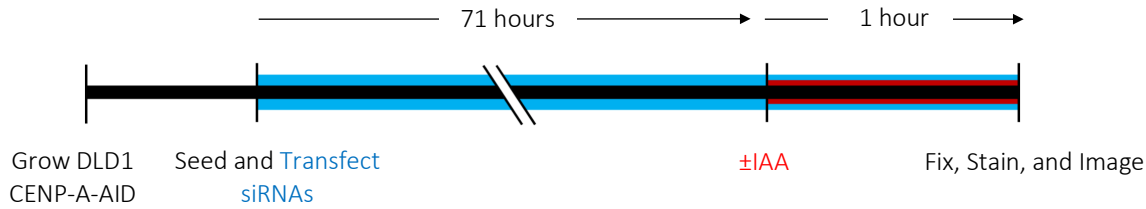


Figure 4.13 – Overview of a protocol combining CENP-A-AID depletion with p97 knockdown over 72 hours. Knockdown is indicated in blue, and depletion of CENP-A for the final hour in red. Whilst siRNA species are only present for the first 71 hours, p97 RNAi is assumed to continue for the final hour.

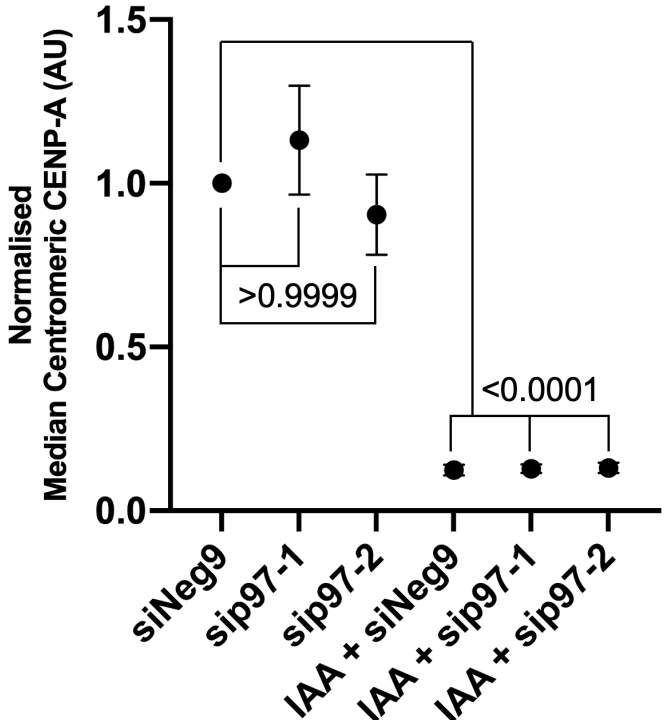


Figure 4.14 – Results of CENP-A-AID depletion coincident with p97 RNAi.

Median values were normalised to siNeg9 within each biological replicate. Error bars show standard error of the mean. P-values were calculated via ordinary one-way ANOVA with Bonferroni multiple comparisons analysis (n=3); all data granted either P>0.9999 or P<0.0001 depending on auxin condition; these are plotted collectively for clarity.

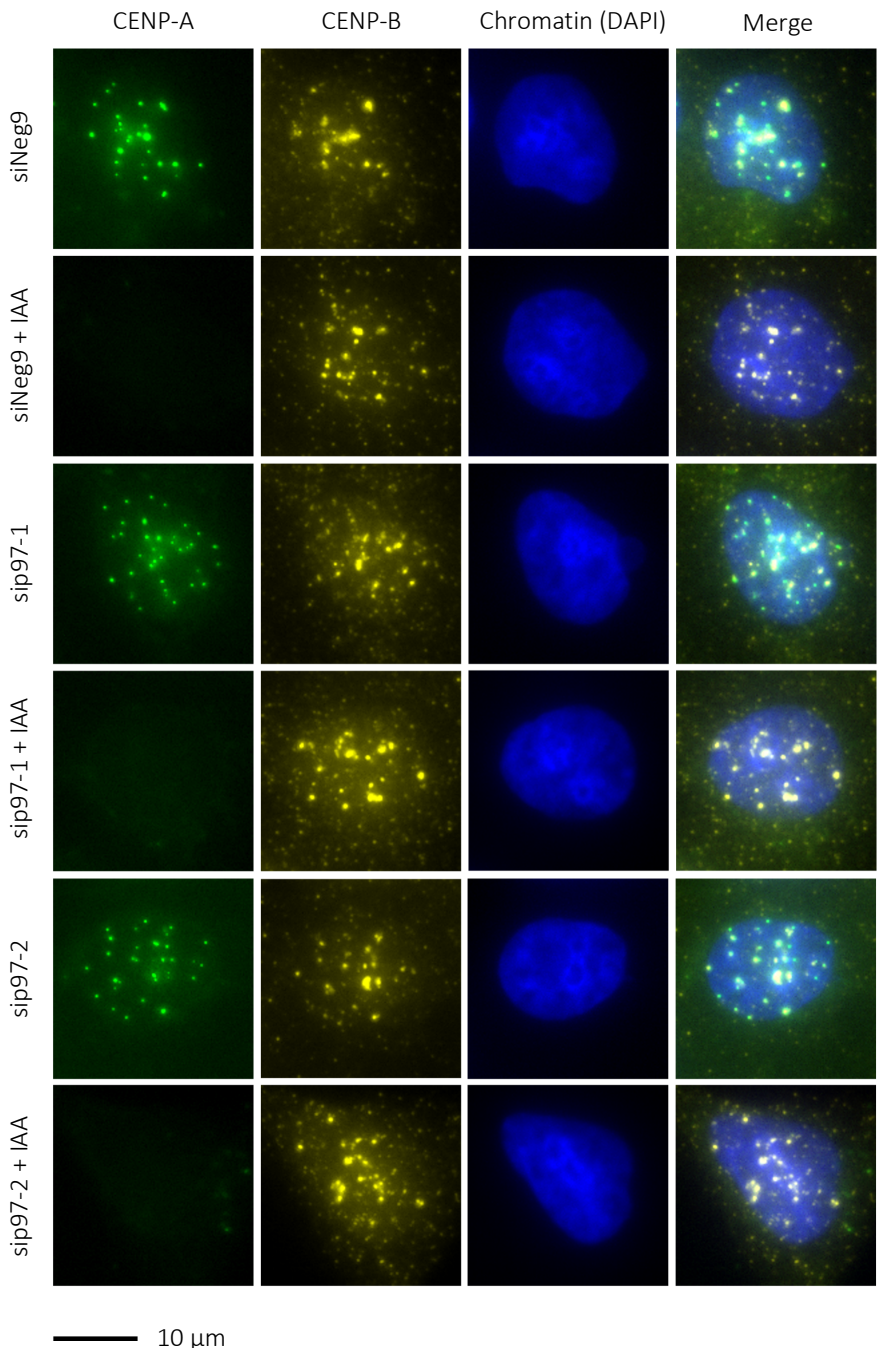


Figure 4.15 - Representative images from a protocol combining CENP-A-AID depletion with p97 knockdown.

Brightness and contrast of CENP-A and CENP-B channels are shown normalised for comparison.

Addition of IAA for 1 hour can be seen to remove virtually all centromeric CENP-A signal whilst leaving CENP-B unaffected.

As shown in Figures 4.14 and 4.15 above, p97 depletion via RNAi was not found to prevent the removal of ubiquitinated CENP-A from the centromere. This suggests that p97 does not act directly upon ubiquitinated CENP-A. Therefore, the role of p97 in regulating the stability of CENP-A nucleosomes specifically involves the SUMO pathway.

4.2.2 – CENP-A Rescue Experiments using Pharmacological p97 Inhibition

In order to confirm the results discussed in Section 4.2.1 above, analogous experiments were run using NMS-873 to acutely inhibit p97. This granted confidence that the lack of CENP-A-AID rescue observed was not simply due to poor depletion, or a result of other pleiotropic effects following 72 hours of p97 knockdown. These experiments proceeded analogously to those discussed in Section 4.1.4. In brief; DLD1 CENP-A-AID cells were seeded on coverslips and incubated (37°C, 5% CO_2) for 47 hours in order to proliferate and establish a healthy population. Cells were then incubated for a further hour with either 1 mM IAA, 1 mM NMS-873, or both. A drug-free negative control was also run. Coverslips were fixed and stained as in Section 4.2.1. This protocol is summarised below (Figure 4.16) alongside quantified results (Figure 4.17).

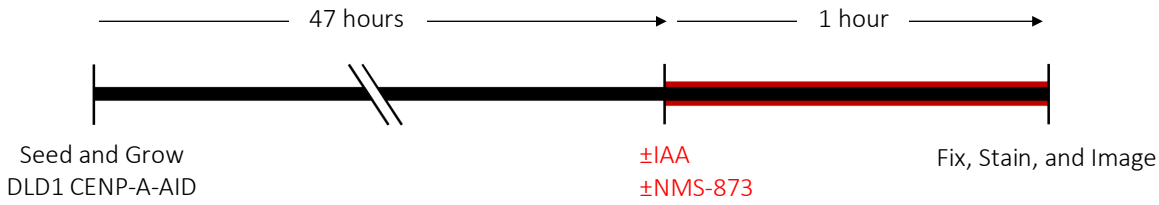


Figure 4.16 - Overview of a protocol combining CENP-A-AID depletion with p97 inhibition using NMS-873. The timeframe of drug treatment is indicated in red

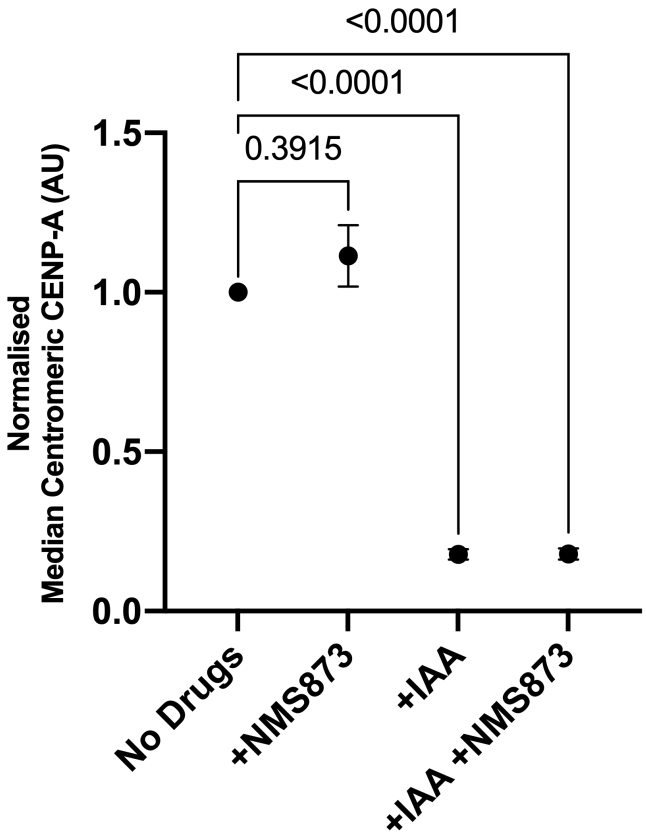


Figure 4.17 – Results of CENP-A-AID depletion coincident with p97 inhibition using NMS-873.

Median CENP-A intensities normalised to that of the drug-free control within each biological replicate. Error bars show standard error of the mean. P-values calculated by ordinary one-way ANOVA using Bonferroni multiple comparisons analysis (n=4).

These results clearly show that simultaneous treatment with NMS-873 was unable to rescue CENP-A depletion upon its ubiquitination by the auxin degron. In order to confirm that this was not simply due to slow kinetics of drug action of NMS-873, a further set of experiments was conducted, wherein NMS-873 positive samples were pre-incubated for 1 hour with this inhibitor in addition to NMS-873 treatment alongside IAA for a further hour. This yielded very similar results (Figure 4.18).

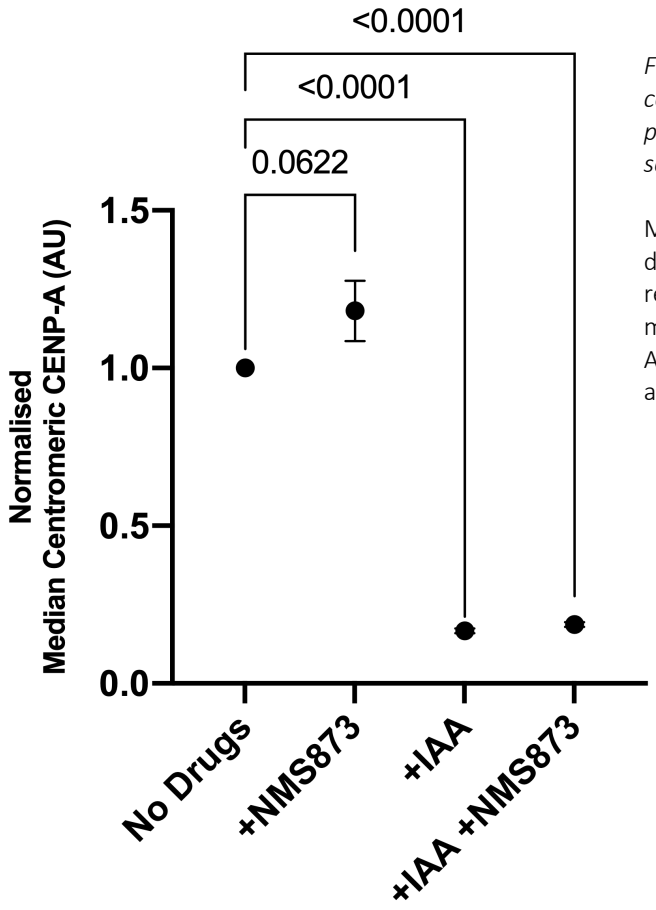


Figure 4.18 – Results of CENP-A-AID depletion coincident with p97 inhibition including a 1-hour pre-incubation step for NMS-873 positive samples.

Median CENP-A intensities normalised to the drug-free control within each biological replicate. Error bars show standard error of the mean. P-values calculated by ordinary one-way ANOVA using Bonferroni multiple comparisons analysis (n=4).

4.3 – Discussion

The above data from CENP-A-AID experiments collectively suggest that p97 is not involved in the direct interaction with CENP-A bound to centromeric chromatin. Neither RNAi-based depletion, nor pharmacological inhibition of p97 was capable of preventing the removal of ubiquitinated

CENP-A from the centromere. This suggests that another currently unknown mechanism is responsible for the removal of CENP-A once ubiquitinated.

In contrast, p97 knockdown or inhibition was found to result in a total rescue of CENP-A levels following auxin-induced depletion of SENP6. This is a remarkable finding and suggests that p97 and SENP6 act antagonistically to one another in order to regulate core CCAN components. Whilst SENP6 depletion may cause the removal of CENP-A from the centromere, this removal is dependent upon the action of p97. Together, these results show that the regulation of CCAN components by p97/SENP6 is selectively dependent on the SUMO pathway; the ubiquitination of CENP-A does not constitute an appropriate signal for p97 recruitment.

Chapter 5 – Discussion and Conclusions

This thesis delivers insights into the role of the segregase enzyme p97 in the regulation of centromeric chromatin. This began by confirming the results obtained in a high throughput screen conducted by Mitra *et al*, who found that knockdown of p97 by RNAi leads to an increase in CENP-A-SNAP-TMR fluorescence at centromeric foci under a pulse-chase protocol compared to control. There are three logical explanations for this observation. Firstly, that depletion of p97 may lead to an overloading of CENP-A nucleosomes at the centromere. However, quench-chase-pulse experiments, which probe directly for the loading of CENP-A, found no evidence that p97 RNAi has any effect on the incorporation of CENP-A nucleosomes at centromeric chromatin. This observation is backed up by results from pulse-chase experiments in which all soluble TMR-Star bound CENP-A-SNAP was allowed to incorporate into chromatin prior to p97 depletion. Even under these conditions, the same increase in CENP-A-SNAP-TMR fluorescence at the centromere was observed. Collectively, these data give confidence that the loading of nascent CENP-A nucleosomes remains unaffected by cellular p97 levels.

Secondly, it was suggested that these observed increases owe simply to a slowing of passage through the cell cycle. Again, this idea did not withstand scrutiny. Whilst p97 knockdown did indeed lead to disturbances in the relative distributions of cells across different stages of the cell cycle, these disturbances were found not to be responsible for the increase in CENP-A-SNAP-TMR fluorescence discussed above. Addition of excess thymidine in order to arrest DNA synthesis and prevent progression through the cell cycle did not suppress these increases in fluorescence. Therefore, changes to cell cycle dynamics are not responsible for our initial observations.

After excluding the more trivial explanations outlined above, it was hypothesised that the effects of p97 knockdown on CENP-A-SNAP-TMR fluorescence during a pulse-chase protocol may represent a genuine stabilisation of CENP-A nucleosomes at centromeric chromatin under these

conditions. This is an unexpected result, as it is not in agreement with longstanding theory that CENP-A nucleosomes are maximally stable once incorporated into chromatin; a premise originally put forward by Jansen *et al* in their 2007 paper (91). Collectively, these data constitute the first confirmation of a mechanism which acts endogenously in human cells to destabilise CENP-A nucleosomes after they have been incorporated into chromatin.

It is notable that this effect has not been observed on the scale suggested by Mitra *et al* during their high-throughput screen. The discrepancies in these findings remain unexplained. However, Mitra *et al* conducted their screen via a methodology that differed in several ways from the approaches used throughout this study. Due to the high-volume nature of their research, Mitra *et al* used a solid-phase RNAi microarray transfection protocol, whereby transfection reagents were spot-printed onto slides which were later seeded with HeLa CENP-A-SNAP cells to initiate knockdown. In addition, cells were analysed at a lower magnification (20X as opposed to 63X) and a single plane image was taken for each siRNA spot, offering a rough measurement of CENP-A levels. Instead, in this study, Z-stacks were imaged and quantified, thus allowing the assessment of many more datapoints and ensuring that all centromeres were imaged in their focal plane. Further, images taken during the high-throughput screen were not quantified by CRaQ; Mitra *et al* instead used a rapid analysis CellProfiler pipeline (112,193) which integrated centromeric CENP-A-SNAP fluorescence data atop a DAPI mask and calculated a mean value for each cell, as opposed to quantifying individual centromeres. This method also did not include use of a centromeric reference. Together, these differences of approach between this study and the screen conducted by Mitra *et al* may account for discrepancies in the observed magnitude of the effects of p97 knockdown.

Following up on observations that depletion of SENP6, a SUMO protease, leads to the loss of CENP-A from the centromere, it was found that the simultaneous depletion or pharmacological

inhibition of p97 was capable of fully rescuing this effect. Therefore, the removal of CENP-A during a SENP6-depleted phenotype requires the presence of p97. This suggests that p97 and SENP6 act antagonistically in order to regulate components of centromeric chromatin. Given their previously established modes of action, it is hypothesised that p97 extracts SUMOylated CCAN substrates away from chromatin, whilst SENP6 cleaves the SUMO chains which allow p97 to do this, thereby stabilising the centromere complex.

The exact target(s) of this newly found p97/SENP6 branch of the SUMO network remain uncertain. Degradation of CENP-A via artificial ubiquitination using a transgenic auxin system was not found to rely upon p97. This lack of dependence implies that CENP-A may not be a direct substrate of p97. However, this remains to be confirmed as CENP-A may plausibly be a target of p97 via the SUMO pathway, but not via ubiquitination. An alternative candidate that may be responsible for the removal of ubiquitinated CENP-A is the 19S subunit of the 26S proteasome, a non-proteolytic 'regulatory particle' which is capable of recognising and unfolding ubiquitinated proteins, and which has previously been implicated in the regulation of heterochromatin in fission yeast (194).

As suggested above, it may alternatively be hypothesised that the p97/SENP6 pathway directly targets other core components of the CCAN. CENP-C, unlike CENP-A, has been observed in a state of SUMOylation. Its removal from the centromere is known to destabilise the rest of the CCAN, including CENP-A. Indeed, CENP-C is a close binding partner of CENP-A (as indicated in Figure 1.3) and was found by Mitra *et al* to be removed from the centromere during SENP6 depletion (112). Therefore, if p97 were to directly target CENP-C for removal from the CCAN, then CENP-A nucleosomes may be extracted simultaneously whilst bound to CENP-C. The binding of CENP-C has also been shown to modify the conformation of CENP-A nucleosomes such that they more closely resemble their canonical H3 counterparts (95,192). Therefore, another possible mechanism that may underly these observations is that loss of CENP-C by p97-mediated

segregation leads to conformational changes within the CENP-A nucleosome which result in its destabilisation at the chromatin. This destabilisation may simply be an inherent consequence of changes in nucleosome architecture. Alternatively, loss of CENP-A may require additional factors such as the disruptive events of transcription or replication (as discussed in Section 1.3.4), but these are not yet fully mechanistically understood. This hypothesis parallels well with results recently reported by Nechemia-Arbely *et al*, who found evidence that DNA replication acts as error correction mechanism for centromeric location by removing CENP-A ectopically loaded at non-centromeric sites (94). Assuming that constituents of the CCAN are involved, we may also hypothesise that loss of CCAN components by p97-mediated segregation could impede these conservatory systems, thus preventing the stable transmission of CENP-A nucleosomes during such processes and resulting in their loss from the centromere over time. These hypotheses mirror recent research carried out in *Saccharomyces* by Suhandynata *et al*, who noted that Ulp2 (the yeast analogue of SENP6) directly targets CCAN components to prevent their hyper-SUMOylation (195).

From an evolutionary perspective, it is perhaps expected that the cell has developed homeostatic pathways through which it can destabilise CENP-A nucleosomes at the chromatin. SUMOylation of the CCAN and subsequent removal of key proteins by p97 may fulfil two non-mutually exclusive biological requirements. Firstly, this pathway may serve as a regulator of centromere size and location, preventing the uncontrolled spread of CENP-A nucleosomes and CCAN architecture into formerly non-centromeric regions. Should CENP-A nucleosomes be stochastically overloaded during G1, this pathway may allow the cell to deterministically remove these excess structures, returning the centromere to its steady-state arrangement. Secondly, this pathway may act as a preventative mechanism against the formation of neocentromeres, thus maintaining the integrity of the ancestral centromeric locus. The balance of p97/SENP6 homeostatic regulation may differ between a *bona fide* centromere and non-centromeric regions, such that the protecting influence

of SENP6 takes precedence at the centromere whilst the destabilising action of p97 dominates elsewhere, extracting centromeric species from non-centromeric regions. These hypotheses discussed above are collectively summarised below (Figure 5.1).

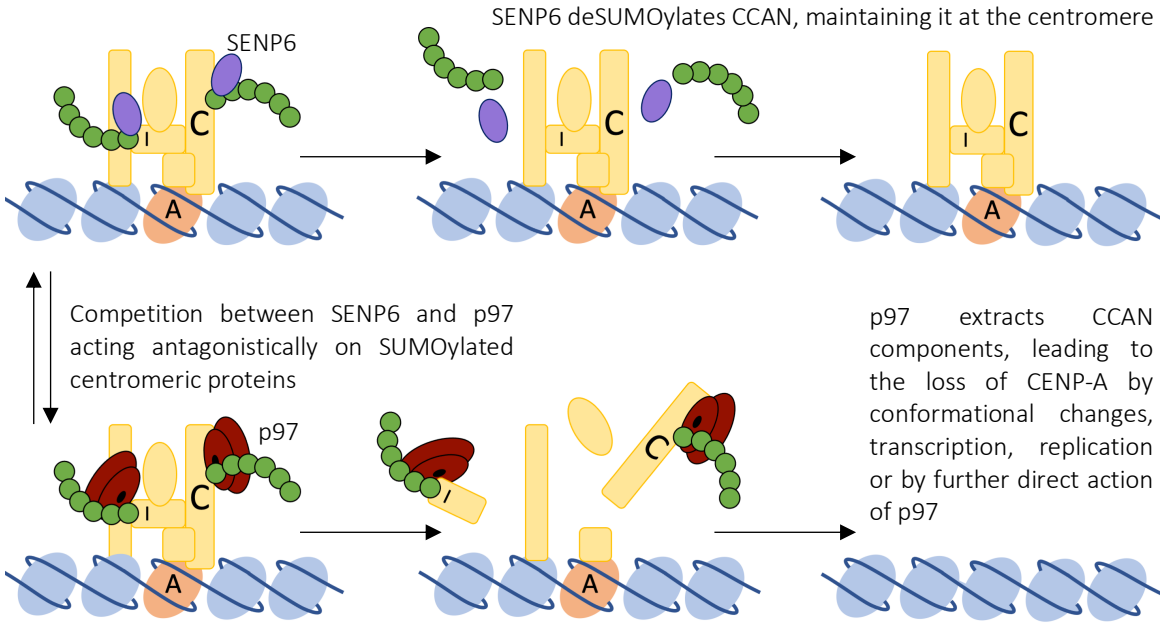


Figure 5.1 – Schematic model of the p97/SENP6 branch of the SUMO pathway at the centromere. CENP-A nucleosomes are shown in orange, and canonical H3 nucleosomes in blue. SUMO chains are shown in green, SENP6 in lilac, and p97 in red. CENP-C and CENP-I are portrayed in SUMOylated states based on the findings of Mitra *et al* and are here hypothesised as potential direct targets of p97. These are not the only candidates; other CCAN components have been previously noted as relying upon SENP6 for their maintenance at the centromere (117)

Key questions remain regarding the exact mode of action of p97/SENP6 mediated CENP-A regulation. For example, it remains unknown whether CENP-C is a direct substrate of p97. Experiments very similar to those described in Sections 4.1.3 and 4.1.4 may probe for whether co-occurrent SENP6 depletion and p97 knockdown or inhibition is capable of rescuing the loss of CENP-C at the centromere which was otherwise observed by Mitra *et al*. This would provide insights into whether p97 is required for the removal of SUMOylated CENP-C.

Further, as stated above, it is not clear whether CENP-A removal during SENP6 depletion occurs passively – through intrinsic destabilisation of nucleosome conformation in the absence of

CENP-C – or actively. Such active mechanisms may include the disruptive force of transcription or even further targeting by p97 itself. These ideas could be tested by inhibiting either transcription or p97 in cells in which CENP-C is depleted and observing the effects of this on centromeric CENP-A. This would provide a further test for whether CENP-A is a direct substrate of p97, or whether it lies downstream of these targets.

In conclusion, whereas prior literature suggested that chromatin-bound CENP-A existed in a state of maximal stability, this thesis has instead presented evidence that at least two different mechanisms are capable of destabilising CENP-A nucleosomes; p97 is one such species and destabilises CENP-A either actively or indirectly as discussed above. A separate species must be capable of directly extracting ubiquitinated CENP-A; its identity remains unknown.

Chapter 6 - Materials and Methods

6.1 - Cell Culture

All cell lines were incubated at 37°C, 5% CO_2, and trypsinised using TrypLE Express phenol red (ThermoFisher). 1X DPBS (ThermoFisher) was used for washing. HeLa CENP-A-SNAP cells originally produced by Lars Jansen, Department of Biochemistry, University of Oxford (91). HeLa SENP6-AID-EGFP (CENP-A-SNAP) cells originally produced by Sreyoshi Mitra, Department of Biochemistry, University of Oxford (112). DLD1 CENP-A-SNAP cells were a gift from Danielle Fachinetti, Institut Curie, PSL Research University (186). Growth media for all cell lines indicated below.

HeLa CENP-A-SNAP Growth Media; 1X Dulbecco's Modified Eagle Medium containing 25 mM D-Glucose, 4 mM glutamine, 1 mM sodium pyruvate (ThermoFisher) and supplemented with 10% v/v new-born calf serum (ThermoFisher), 100 U mL^{-1} penicillin, 100 µg mL^{-1} puromycin, 1 µg mL^{-1} blasticidin.

HeLa SENP6-AID-EGFP (CENP-A-SNAP) Growth Media; 1X Dulbecco's Modified Eagle Medium containing 25 mM D-Glucose, 4 mM glutamine, 1 mM sodium pyruvate (ThermoFisher) and supplemented with 10% v/v new-born calf serum (ThermoFisher), 100 U mL^{-1} penicillin, 100 µg mL^{-1} puromycin, 1 µg mL^{-1} blasticidin, 1 µg mL^{-1} puromycin, 500 µg mL^{-1} neomycin.

DLD-1 CENP-A-AID Growth Media; 1X Dulbecco's Modified Eagle Medium containing 25 mM D-Glucose, 4 mM glutamine, 1 mM sodium pyruvate (ThermoFisher) and supplemented with 10% v/v foetal bovine serum (ThermoFisher).

During active experimental protocols, antibiotic-free variants of the media above were used throughout to ensure that antibiotic use did not affect results. The growth conditions outlined above are referred to as 'complete media' (CM) throughout protocols below.

6.2 – RNAi

All siRNAs used were Silencer Select reagents (Ambion ThermoFisher Scientific). Sequences are given below (5' → 3')

siNeg9: Sense – UACGACCGGUCUAUCGUAGtt, Antisense - CUACGAUAGACCGGUCGUAtt

siSENP6: Sense – CAGACUAAACUAUAGCGAUtt, Antisense - AUCGCUAUAGUUUAGUCUGat

siMis18α: Sense – GAAGAUGUCUUGAAAGCAUtt, Antisense - AUGCUUUCAAGACAUCUUCca

sip97-1: Sense – GAAUAGAGUUGUUCGGAAUtt, Antisense - AUUCCGAACAACUCUAUUCat

sip97-2: Sense – GGCUCGUGGAGGUAACAUUtt, Antisense - AAUGUUACCUCCACGAGCCtt

siRNA stocks were maintained at 2 µM. Transfection mixtures containing 96% v/v GlutaMAX supplemented OptiMEM Reduced Serum Medium (ThermoFisher), 1.5% v/v Lipofectamine RNAiMAX (ThermoFisher) and 2.5% v/v 2 µM siRNA stocks (final working concentration of 5 nM) were incubated at room temperature for 25 minutes and mixed with CM and suspended cells (final volume 500 µL per sample, final cell count $3x10^4$ cells per sample) as per manufacturer's instructions and in-house optimisation data (196).

6.3 – CENP-A-SNAP Experiments

6.3.1 – Pulse-Chase Protocol

Pulse-Chase experiments were carried out as described in Bodor *et al* (116) with the exception that the working concentration of fluorescent SNAP-substrate was doubled in order to improve fluorescent signal. In brief, HeLa CENP-A-SNAP cells were grown as above, then re-seeded in

6-well plates ($4.5x10^5$ cells $well^{-1}$ x 3 wells) and incubated for 24 hours. Cells were then pulse labelled with CM (800 µL $well^{-1}$) containing 4 µM tetra-methyl-rhodamine-conjugated SNAP substrate ('TMR-Star', New England Biolabs) for 15 minutes, 37°C, washed twice in 1X DPBS, and incubated at 37°C in CM for a further 30 minutes. They were then washed twice again in 1X DPBS in order to remove any residual traces of TMR-Star. Cells were then quenched in CM containing 2 µM bromothenylpteridine (BTP, New England Biolabs) for 30 minutes at 37°C. This treatment with a non-fluorescent SNAP prevents the unintended fluorescent labelling of any further CENP-A-SNAP. Cells were then re-seeded ($3x10^4$ cells $sample^{-1}$) in 500 µL CM containing relevant transfection reagents (Section 6.2) on poly-lysine treated glass coverslips and in 24-well plates and incubated for 48 hours. Two coverslips were seeded per siRNA condition for later analysis by microscopy, and two wells were seeded per siRNA condition to be pooled for analysis by Western blot. Following this period, cells were washed twice with 1X DPBS. Samples grown on coverslips were fixed in 4% paraformaldehyde for 10 minutes and quenched with Tris-Cl buffer (pH 7.5) before storage in 1X DPBS at 4°C until beginning immunofluorescence protocols (Section 6.4). Samples grown in 24-well plates were resuspended, pooled, counted, and spun down (2000 x g, 5 min). CM was aspirated, and the pellet was frozen (-80°C) until Western blot analysis.

6.3.2 – Modified Pulse-Chase Protocol

Modified Pulse-Chase experiments proceeded as per Section 6.3.1 above, with the exception that cells were not simultaneously seeded and transfected following SNAP-labelling. Instead, cells were labelled as above, seeded, and incubated for 24 hours. Media was then exchanged, with new media containing transfection reagents (see below) and cells were incubated for a further 48 hours. Collection and analysis then proceeded as per Section 6.3.1

6.3.3 – Pulse-Chase Protocol Alongside Thymidine Arrest

These experiments were carried out exactly as described above in Section 6.3.1, with the exception that CM containing deoxythymidine (final concentration 2 mM) was added simultaneously alongside re-seeding and transfection, and so was present throughout the 48-hour chase period.

6.3.4 – Quench-Chase-Pulse Protocol

Experiments again proceeded according to Bodor *et al* (116). In brief, HeLa CENP-A-SNAP cells were grown as above, re-seeded in 6-well plates ($4.5x10^5$ cells $well^{-1}$ x 3 wells) and incubated for 24 hours. Following this, cells were quenched in CM containing 2 µM bromothenylpteridine (BTP, New England Biolabs) for 30 minutes at 37°C. They were then washed twice with CM and incubated for a further 30 minutes before re-seeding ($3x10^4$ cells $sample^{-1}$) in 500 µL CM containing relevant transfection reagents (Section 6.2) on poly-lysine treated glass coverslips and in 24-well plates. Once again, two coverslips were seeded per siRNA condition for later analysis by microscopy, and two wells were seeded per siRNA condition for analysis by Western Blot. Following incubation for 48 hours, cells were pulse-labelled by incubating in CM containing 2 µM TMR-Star for 15 minutes before washing twice in CM and re-incubating in CM alone for a further 30 minutes to remove any residual unreacted TMR-Star. Fixation of coverslips for microscopy and harvesting of pellets for Western blotting then proceeded as described in Section 6.3.1.

6.4 – Immunofluorescence

Immunofluorescence protocols proceeded as per Bodor *et al* (116). Fixed cells on poly-lysine coated glass coverslips were permeabilised in 1X DPBS containing 0.1% v/v Triton-X-100 (ThermoFisher) ('PBS-TX'). Coverslips were incubated in a humid chamber at 37°C for 1 hour in relevant primary antibodies at the following dilutions. Primary Antibodies: mouse monoclonal anti-CENP-A, 1:500 (gifted by Kinya Yoda, Nagoya University) (197), rabbit polyclonal

anti-CENP-B, 1:1000 (Abcam ab25734). Coverslips were then washed 3 times in PBS-TX and incubated in a dark, humid chamber at 37°C for 45 minutes in relevant secondary antibodies at 1:200 dilution. Secondary antibodies: fluorescein conjugated anti-rabbit IgG (Rockland Immunochemicals #612-702-717), rhodamine conjugated AffiniPure anti-rabbit (Jackson Immunoresearch #111-025-144), fluorescein conjugated AffiniPure anti-mouse (Jackson Immunoresearch #715-095-151). Samples were again washed 3 times in PBS-TX before staining with 4',6-diamidino-2-phenylindole ('DAPI') (Sigma-Aldrich) for 5 minutes at room temperature. Slides were mounted in Mowiol and stored at 4°C until imaging.

6.5 – Immunoblotting

Cell pellets were dissolved in 1X Sample Buffer (Laemmli) containing 5% v/v β-mercaptoethanol and boiled for 5 minutes to denature proteins and create a whole-cell lysate. Extracts were separated by SDS-PAGE (BioRad Mini-PROTEAN Tetra System) and transferred to nitrocellulose membranes (BioRad Transblot Turbo). Antibody incubation proceeded according to the following dilutions. Primary Antibodies: rat monoclonal anti-α tubulin, 1:1000 (Santa Cruz Biotechnology SC-53029), rabbit polyclonal anti-VCP [anti-p97], 1:1000 (Cell Signaling Technology #2648). Secondary Antibodies: DyLight680-coupled anti-rat, 1:10,000 (Rockland Immunochemicals #612-144-120), IRDye 800CW anti-rabbit IgG, 1:10,000 (LI-COR #926-32211). Fluorescence was detected using a near-infrared scanner (LI-COR Biosciences Odyssey Fc) and quantified using ImageStudio.

6.6 – Microscopy and Image Analysis

All imaging was performed on Leica Microsystems DMI 6000B inverted-light microscope at 63X magnification using a 1.4 NA oil objective (HC PLAN APO) to capture 0.2 µm Z-stacks with a Hamamatsu Flash Orca 4.0 sCMOS camera. Images were quantified using ImageJ macros. CRaQ is described and made available in Bodor *et al* (116). In brief, the maximum projection of the imaged

Z-stacks is calculated in each channel. Centromeres are then detected in the reference channel and quantified in the data channel by placing a small box around the centroid position of each centromeric focus. The peak intensity value within each box is measured and corrected for background fluorescence by subtracting the minimum pixel value within that same area.

The DAPI mask macro used to quantify EdU fluorescence (Section 3.3.2) and nucleic SENP6 levels (Section 4.1.3) was based upon CRaQ, modified in-house to calculate ROIs based upon the entire nucleus, rather than specifying centromeric foci.

6.7 – Flow Cytometry

HeLa CENP-A-SNAP cells were transfected co-occurrent to seeding in 10 cm petri dishes ($6.75x10^5$ cells $sample^{-1}$) as per manufacturers protocols described above (Section 6.2) and incubated for 48 hours. Cells were then washed with 1X DPBS, resuspended in CM, and counted. Samples were taken for analysis via Western blot, and the remaining cells washed in 1X DPBS again, spun down (400 x g, 5 min) and resuspended dropwise in 2 mL cold 70% (v/v in ddH_2O) ethanol whilst vortexing. Samples were then stored at 4°C for at least 30 minutes in order to fix cells, resuspended in 1X DPBS and treated with 100 µg mL^{-1} RNAse A (Invitrogen) at 37°C for 1 hour before staining with 50 µg mL^{-1} propidium iodide. Samples were analysed using a BD Fortessa X20 flow cytometer (Sir William Dunn School of Pathology, University of Oxford) controlled by FlowJo software to measure forward-scattering, side-scattering, and propidium iodide fluorescence at 561 nm. A minimum of $1x10^4$ cells were analysed per condition. Flowing Software 2 was used for subsequent hierarchical gating. Gaussian distributions of resultant histograms were calculated using Prism 9 (see Section 3.2).

6.8 – EdU Staining

Use of 5-ethynyl-2'-deoxyuridine ('EdU') staining as described in Section 3.3.2 was performed according to manufacturer's instructions (Click-iT EdU Alexa Fluor 647 Imaging Kit, Invitrogen). In brief, samples were incubated for 10 minutes in CM containing 10 μM EdU before being washed, fixed, and incubated at 37°C with a buffered reaction cocktail containing $CuSO_4$ and a fluorophore coupled azide. They were washed and stained with DAPI as per Section 6.4. EdU-conjugated fluorescence was measured at 700 nm.

6.9 – Drug Treatment

During experiments described in Chapter 4, cells were seeded on poly-lysine coated coverslips at a density of $3x10^4$ cells $coverslip^{-1}$ and induced at relevant timepoints with indole-3-acetic acid ('IAA') and NMS-873 (Sigma-Aldrich) added to CM at a final concentration of 1 mM.

6.10 – Miscellaneous

Thesis word processed using Microsoft Word. Original figures made using Microsoft PowerPoint, ImageJ, Prism 9, and ChemDraw 20. References managed using Zotero.

All figures original work unless otherwise indicated.

Bibliography

1. Scholey JM, Brust-Mascher I, Mogilner A. Cell division. Nature. 2003 Apr;422(6933):746–52.

2. Schatten H. Mitosis. In: Brenner's Encyclopedia of Genetics [Internet]. Elsevier; 2013 [cited 2020 Dec 28]. p. 448–51. Available from: https://linkinghub.elsevier.com/retrieve/pii/B9780123749840009621

3. Lennarz WJ, Lane MD, editors. Encyclopedia of biological chemistry [Internet]. 1st ed. Amsterdam ; Boston: Elsevier/Academic Press; 2004. Available from: https://www.sciencedirect.com/science/referenceworks/9780123786319

4. Marston AL, Amon A. Meiosis: cell-cycle controls shuffle and deal. Nat Rev Mol Cell Biol. 2004 Dec;5(12):983–97.

5. Leonard AC, Grimwade JE. Chromosome Replication and Segregation. In: Reference Module in Biomedical Sciences [Internet]. Elsevier; 2019 [cited 2020 Apr 5]. p. B9780128012383023000. Available from: https://linkinghub.elsevier.com/retrieve/pii/B9780128012383023515

6. Uhlmann F. Chromosome cohesion and segregation in mitosis and meiosis. Curr Opin Cell Biol. 2001 Dec;13(6):754–61.

7. Yanagida M. Basic mechanism of eukaryotic chromosome segregation. Philos Trans R Soc B Biol Sci. 2005 Mar 29;360(1455):609–21.

8. Zachos G. Regulating Cytokinesis. In: Encyclopedia of Cell Biology [Internet]. Elsevier; 2016 [cited 2020 Dec 28]. p. 494–503. Available from: https://linkinghub.elsevier.com/retrieve/pii/B9780123944474300657

9. Marston AL. Chromosome Segregation in Budding Yeast: Sister Chromatid Cohesion and Related Mechanisms. Genetics. 2014 Jan;196(1):31–63.

10. Brooker AS, Berkowitz KM. The Roles of Cohesins in Mitosis, Meiosis, and Human Health and Disease. In: Noguchi E, Gadaleta MC, editors. Cell Cycle Control [Internet]. New York, NY: Springer New York; 2014 [cited 2020 May 12]. p. 229–66. (Methods in Molecular Biology; vol. 1170). Available from: http://link.springer.com/10.1007/978-1-4939-0888-2_11

11. Ocampo-Hafalla MT, Katou Y, Shirahige K, Uhlmann F. Displacement and re-accumulation of centromeric cohesin during transient pre-anaphase centromere splitting. Chromosoma. 2007 Nov 12;116(6):531–44.

12. Eckert CA, Gravdahl DJ, Megee PC. The enhancement of pericentromeric cohesin association by conserved kinetochore components promotes high-fidelity chromosome segregation and is sensitive to microtubule-based tension. Genes Dev. 2007 Feb 1;21(3):278–91.

13. Hinshaw SM, Harrison SC. Kinetochore Function from the Bottom Up. Trends Cell Biol. 2018 Jan;28(1):22–33.

14. Hyman AA, Mitchison TJ. Modulation of microtubule stability by kinetochores in vitro. J Cell Biol. 1990 May 1;110(5):1607–16.

15. Gadde S, Heald R. Mechanisms and Molecules of the Mitotic Spindle. Curr Biol. 2004 Sep;14(18):R797–805.

16. Maciejowski J, Drechsler H, Grundner-Culemann K, Ballister ER, Rodriguez-Rodriguez J-A, Rodriguez-Bravo V, et al. Mps1 Regulates Kinetochore-Microtubule Attachment Stability via the Ska Complex to Ensure Error-Free Chromosome Segregation. Dev Cell. 2017 Apr;41(2):143-156.e6.

17. Santaguida S, Musacchio A. The life and miracles of kinetochores. EMBO J. 2009 Sep 2;28(17):2511–31.

18. Kops GJPL, Weaver BAA, Cleveland DW. On the road to cancer: aneuploidy and the mitotic checkpoint. Nat Rev Cancer. 2005 Oct;5(10):773–85.

19. Aravamudhan P, Goldfarb AA, Joglekar AP. The kinetochore encodes a mechanical switch to disrupt spindle assembly checkpoint signalling. Nat Cell Biol. 2015 Jul;17(7):868–79.

20. Introduction to the Cell Cycle. In: Cell Biology [Internet]. Elsevier; 2017 [cited 2020 Dec 28]. p. 697–711. Available from: https://linkinghub.elsevier.com/retrieve/pii/B9780323341264000402

21. Kiyomitsu T, Obuse C, Yanagida M. Human Blinkin/AF15q14 Is Required for Chromosome Alignment and the Mitotic Checkpoint through Direct Interaction with Bub1 and BubR1. Dev Cell. 2007 Nov;13(5):663–76.

22. Li Y, Gorbea C, Mahaffey D, Rechsteiner M, Benezra R. MAD2 associates with the cyclosome/anaphase-promoting complex and inhibits its activity. Proc Natl Acad Sci. 1997 Nov 11;94(23):12431–6.

23. Fang G, Yu H, Kirschner MW. The checkpoint protein MAD2 and the mitotic regulator CDC20 form a ternary complex with the anaphase-promoting complex to control anaphase initiation. Genes Dev. 1998 Jun 15;12(12):1871–83.

24. Sudakin V, Chan GKT, Yen TJ. Checkpoint inhibition of the APC/C in HeLa cells is mediated by a complex of BUBR1, BUB3, CDC20, and MAD2. J Cell Biol. 2001 Sep 3;154(5):925–36.

25. Glickman MH, Ciechanover A. The Ubiquitin-Proteasome Proteolytic Pathway: Destruction for the Sake of Construction. Physiol Rev. 2002 Apr 1;82(2):373–428.

26. Cohen-Fix O, Peters JM, Kirschner MW, Koshland D. Anaphase initiation in Saccharomyces cerevisiae is controlled by the APC-dependent degradation of the anaphase inhibitor Pds1p. Genes Dev. 1996 Dec 15;10(24):3081–93.

27. Uhlmann F, Lottspeich F, Nasmyth K. Sister-chromatid separation at anaphase onset is promoted by cleavage of the cohesin subunit Scc1. Nature. 1999 Jul;400(6739):37–42.

28. Hershko A. Mechanisms and regulation of the degradation of cyclin B. Hunt RT, Nasmyth KA, Diffley J, editors. Philos Trans R Soc Lond B Biol Sci. 1999 Sep 29;354(1389):1571–6.

29. Foley EA, Kapoor TM. Microtubule attachment and spindle assembly checkpoint signalling at the kinetochore. Nat Rev Mol Cell Biol. 2013 Jan;14(1):25–37.

30. Lara-Gonzalez P, Westhorpe FG, Taylor SS. The Spindle Assembly Checkpoint. Curr Biol. 2012 Nov;22(22):R966–80.

31. Black BE, Jansen LET, Foltz DR, Cleveland DW. Centromere Identity, Function, and Epigenetic Propagation across Cell Divisions. Cold Spring Harb Symp Quant Biol. 2010 Jan 1;75(0):403–18.

32. Talbert PB, Henikoff S. What makes a centromere? Exp Cell Res. 2020 Apr;389(2):111895.

33. Waizenegger IC, Hauf S, Meinke A, Peters J-M. Two Distinct Pathways Remove Mammalian Cohesin from Chromosome Arms in Prophase and from Centromeres in Anaphase. Cell. 2000 Oct;103(3):399–410.

34. Sekulic N, Black BE. Molecular underpinnings of centromere identity and maintenance. Trends Biochem Sci. 2012 Jun;37(6):220–9.

35. Cheeseman IM, Desai A. Molecular architecture of the kinetochore–microtubule interface. Nat Rev Mol Cell Biol. 2008 Jan;9(1):33–46.

36. Hori T, Amano M, Suzuki A, Backer CB, Welburn JP, Dong Y, et al. CCAN Makes Multiple Contacts with Centromeric DNA to Provide Distinct Pathways to the Outer Kinetochore. Cell. 2008 Dec;135(6):1039–52.

37. Hara M, Fukagawa T. Critical Foundation of the Kinetochore: The Constitutive Centromere-Associated Network (CCAN). In: Black BE, editor. Centromeres and Kinetochores [Internet]. Cham: Springer International Publishing; 2017 [cited 2020 May 23]. p. 29–57. (Progress in Molecular and Subcellular Biology; vol. 56). Available from: http://link.springer.com/10.1007/978-3-319-58592-5_2

38. Carbon J, Clarke L. Structural and Functional Analysis of a Yeast Centromere (CEN3). J Cell Sci. 1984 Jan 1;1984(Supplement 1):43–58.

39. Fitzgerald-Hayes M, Clarke L, Carbon J. Nucleotide sequence comparisons and functional analysis of yeast centromere DNAs. Cell. 1982 May;29(1):235–44.

40. Ohzeki J, Larionov V, Earnshaw WC, Masumoto H. Genetic and epigenetic regulation of centromeres: a look at HAC formation. Chromosome Res. 2015 Feb;23(1):87–103.

41. Wong CYY, Lee BCH, Yuen KWY. Epigenetic regulation of centromere function. Cell Mol Life Sci [Internet]. 2020 Feb 1 [cited 2020 May 6]; Available from: http://link.springer.com/10.1007/s00018-020-03460-8

42. Wu C -t. Genes, Genetics, and Epigenetics: A Correspondence. Science. 2001 Aug 10;293(5532):1103–5.

43. Dupont C, Armant D, Brenner C. Epigenetics: Definition, Mechanisms and Clinical Perspective. Semin Reprod Med. 2009 Sep;27(05):351–7.

44. Nagaki K, Talbert PB, Zhong CX, Dawe RK, Henikoff S, Jiang J. Chromatin Immunoprecipitation Reveals That the 180-bp Satellite Repeat Is the Key Functional DNA Element of Arabidopsis thaliana Centromeres. Genetics. 2003 Mar;163(3):1221–5.

45. Haaf T, Ward DC. Structural analysis of α-satellite DNA and centromere proteins using extended chromatin and chromosomes. Hum Mol Genet. 1994;3(5):697–709.

46. Willard HF. Centromeres of mammalian chromosomes. Trends Genet. 1990;6:410–6.

47. Sullivan BA, Schwartz S. Identification of centromeric antigens in dicentric Robertsonian translocations: CENP-C and CENP-E are necessary components of functional centromeres. Hum Mol Genet. 1995;4(12):2189–97.

48. Earnshaw WC, Migeon BR. Three related centromere proteins are absent from the inactive centromere of a stable isodicentric chromosome. Chromosoma. 1985 Aug;92(4):290–6.

49. Murillo-Pineda M, Jansen LET. Genetics, epigenetics and back again: Lessons learned from neocentromeres. Exp Cell Res. 2020 Apr;389(2):111909.

50. Voullaire LE, Slater HR, Petrovic V, Choo A. A Functional Marker Centromere with No Detectable Alpha-Satellite, Satellite Ill, or CENP-B Protein: Activation of a Latent Centromere? Am J Hum Genet. 1993 Jun;52(6):1153–63.

51. Depinet T. Characterization of neo-centromeres in marker chromosomes lacking detectable alpha-satellite DNA. Hum Mol Genet. 1997 Aug 1;6(8):1195–204.

52. Luger K, Mäder AW, Richmond RK, Sargent DF, Richmond TJ. Crystal structure of the nucleosome core particle at 2.8 Å resolution. Nature. 1997 Sep;389(6648):251–60.

53. Kornberg RD. Chromatin Structure: A Repeating Unit of Histones and DNA. Science. 1974 May 24;184(4139):868–71.

54. Worcel A, Han S, Wong ML. Assembly of newly replicated chromatin. Cell. 1978 Nov;15(3):969–77.

55. Sogo JM, Stahl H, Koller Th, Knippers R. Structure of replicating simian virus 40 minichromosomes. J Mol Biol. 1986 May;189(1):189–204.

56. Ransom M, Dennehey BK, Tyler JK. Chaperoning Histones during DNA Replication and Repair. Cell. 2010 Jan;140(2):183–95.

57. Smith S, Stillman B. Purification and characterization of CAF-I, a human cell factor required for chromatin assembly during DNA replication in vitro. Cell. 1989 Jul;58(1):15–25.

58. Verreault A. De novo nucleosome assembly: new pieces in an old puzzle. Genes Dev. 2000 Jun 15;14(12):1430–8.

59. Tsunaka Y. Alteration of the nucleosomal DNA path in the crystal structure of a human nucleosome core particle. Nucleic Acids Res. 2005 Jun 2;33(10):3424–34.

60. RCSB PDB - 2CV5: Crystal structure of human nucleosome core particle [Internet]. [cited 2020 Dec 29]. Available from: https://www.rcsb.org/structure/2cv5

61. Sehnal D, Rose A, Koca J, Burley S, Velankar S. Mol*: Towards a Common Library and Tools for Web Molecular Graphics. Workshop Mol Graph Vis Anal Mol Data. 2018;5 pages.

62. Deal RB, Henikoff JG, Henikoff S. Genome-Wide Kinetics of Nucleosome Turnover Determined by Metabolic Labeling of Histones. Science. 2010 May 28;328(5982):1161–4.

63. Kraushaar DC, Jin W, Maunakea A, Abraham B, Ha M, Zhao K. Genome-wide incorporation dynamics reveal distinct categories of turnover for the histone variant H3.3. Genome Biol. 2013;14(10):R121.

64. Chory EJ, Calarco JP, Hathaway NA, Bell O, Neel DS, Crabtree GR. Nucleosome Turnover Regulates Histone Methylation Patterns over the Genome. Mol Cell. 2019 Jan;73(1):61-72.e3.

65. Gurard-Levin ZA, Quivy J-P, Almouzni G. Histone Chaperones: Assisting Histone Traffic and Nucleosome Dynamics. Annu Rev Biochem. 2014 Jun 2;83(1):487–517.

66. Huang H, Strømme CB, Saredi G, Hödl M, Strandsby A, González-Aguilera C, et al. A unique binding mode enables MCM2 to chaperone histones H3–H4 at replication forks. Nat Struct Mol Biol. 2015 Aug;22(8):618–26.

67. Lai WKM, Pugh BF. Understanding nucleosome dynamics and their links to gene expression and DNA replication. Nat Rev Mol Cell Biol. 2017 Sep;18(9):548–62.

68. Annunziato AT. Split Decision: What Happens to Nucleosomes during DNA Replication? J Biol Chem. 2005 Apr;280(13):12065–8.

69. Gruss C, Wu J, Koller T, Sogo JM. Disruption of the nucleosomes at the replication fork. EMBO J. 1993 Dec;12(12):4533–45.

70. Alabert C, Groth A. Chromatin replication and epigenome maintenance. Nat Rev Mol Cell Biol. 2012 Mar;13(3):153–67.

71. Cutter AR, Hayes JJ. A brief review of nucleosome structure. FEBS Lett. 2015 Oct 7;589(20PartA):2914–22.

72. Onufriev AV, Schiessel H. The nucleosome: from structure to function through physics. Curr Opin Struct Biol. 2019 Jun;56:119–30.

73. Brahma S, Henikoff S. Epigenome Regulation by Dynamic Nucleosome Unwrapping. Trends Biochem Sci. 2020 Jan;45(1):13–26.

74. Palmer D, O'Day K, Wener M, Andrews B, Margolis R. A 17-kD centromere protein (CENP-A) copurifies with nucleosome core particles and with histones. J Cell Biol. 1987 Apr 1;104(4):805–15.

75. Palmer DK, O'Day K, Trong HL, Charbonneau H, Margolis RL. Purification of the centromere-specific protein CENP-A and demonstration that it is a distinctive histone. Proc Natl Acad Sci. 1991 May 1;88(9):3734–8.

76. Tachiwana H, Kagawa W, Shiga T, Osakabe A, Miya Y, Saito K, et al. Crystal structure of the human centromeric nucleosome containing CENP-A. Nature. 2011 Aug;476(7359):232–5.

77. Sullivan KF, Hechenberger M, Masri K. Human CENP-A contains a histone H3 related histone fold domain that is required for targeting to the centromere. J Cell Biol. 1994 Nov 1;127(3):581–92.

78. Yoda K, Ando S, Morishita S, Houmura K, Hashimoto K, Takeyasu K, et al. Human centromere protein A (CENP-A) can replace histone H3 in nucleosome reconstitution in vitro. Proc Natl Acad Sci. 2000 Jun 20;97(13):7266–71.

79. Gómez-Rodríguez M, Jansen LE. Basic properties of epigenetic systems: lessons from the centromere. Curr Opin Genet Dev. 2013 Apr;23(2):219–27.

80. Mendiburo MJ, Padeken J, Fulop S, Schepers A, Heun P. Drosophila CENH3 Is Sufficient for Centromere Formation. Science. 2011 Nov 4;334(6056):686–90.

81. Hori T, Shang W-H, Takeuchi K, Fukagawa T. The CCAN recruits CENP-A to the centromere and forms the structural core for kinetochore assembly. J Cell Biol. 2013 Jan 7;200(1):45–60.

82. Barnhart MC, Kuich PHJL, Stellfox ME, Ward JA, Bassett EA, Black BE, et al. HJURP is a CENP-A chromatin assembly factor sufficient to form a functional de novo kinetochore. J Cell Biol. 2011 Jul 25;194(2):229–43.

83. Sullivan KF. A solid foundation: functional specialization of centromeric chromatin. Curr Opin Genet Dev. 2001 Apr;11(2):182–8.

84. Cheeseman IM, Chappie JS, Wilson-Kubalek EM, Desai A. The Conserved KMN Network Constitutes the Core Microtubule-Binding Site of the Kinetochore. Cell. 2006 Dec;127(5):983–97.

85. Varma D, Salmon ED. The KMN protein network - chief conductors of the kinetochore orchestra. J Cell Sci. 2012 Dec 15;125(24):5927–36.

86. Screpanti E, De Antoni A, Alushin GM, Petrovic A, Melis T, Nogales E, et al. Direct Binding of Cenp-C to the Mis12 Complex Joins the Inner and Outer Kinetochore. Curr Biol. 2011 Mar;21(5):391–8.

87. Walczak CE, Heald R. Mechanisms of Mitotic Spindle Assembly and Function. In: International Review of Cytology [Internet]. Elsevier; 2008 [cited 2021 Jan 9]. p. 111–58. Available from: https://linkinghub.elsevier.com/retrieve/pii/S0074769607650037

88. DeLuca JG, Gall WE, Ciferri C, Cimini D, Musacchio A, Salmon ED. Kinetochore Microtubule Dynamics and Attachment Stability Are Regulated by Hec1. Cell. 2006 Dec;127(5):969–82.

89. Santaguida S, Vernieri C, Villa F, Ciliberto A, Musacchio A. Evidence that Aurora B is implicated in spindle checkpoint signalling independently of error correction: Aurora B is directly implicated in spindle checkpoint. EMBO J. 2011 Apr 20;30(8):1508–19.

90. Shelby RD, Monier K, Sullivan KF. Chromatin Assembly at Kinetochores Is Uncoupled from DNA Replication. J Cell Biol. 2000 Nov 27;151(5):1113–8.

91. Jansen LET, Black BE, Foltz DR, Cleveland DW. Propagation of centromeric chromatin requires exit from mitosis. J Cell Biol. 2007 Mar 12;176(6):795–805.

92. Dunleavy EM, Almouzni G, Karpen GH. H3.3 is deposited at centromeres in S phase as a placeholder for newly assembled CENP-A in G1 phase. Nucleus. 2011 Mar;2(2):146–57.

93. Bodor DL, Valente LP, Mata JF, Black BE, Jansen LET. Assembly in G1 phase and long-term stability are unique intrinsic features of CENP-A nucleosomes. Bloom KS, editor. Mol Biol Cell. 2013 Apr;24(7):923–32.

94. Nechemia-Arbely Y, Miga KH, Shoshani O, Aslanian A, McMahon MA, Lee AY, et al. DNA replication acts as an error correction mechanism to maintain centromere identity by restricting CENP-A to centromeres. Nat Cell Biol. 2019 Jun;21(6):743–54.

95. Mitra S, Srinivasan B, Jansen LET. Stable inheritance of CENP-A chromatin: Inner strength versus dynamic control. J Cell Biol. 2020 Oct 5;219(10):e202005099.

96. Remus D, Beuron F, Tolun G, Griffith JD, Morris EP, Diffley JFX. Concerted Loading of Mcm2–7 Double Hexamers around DNA during DNA Replication Origin Licensing. Cell. 2009 Nov;139(4):719–30.

97. Evrin C, Clarke P, Zech J, Lurz R, Sun J, Uhle S, et al. A double-hexameric MCM2-7 complex is loaded onto origin DNA during licensing of eukaryotic DNA replication. Proc Natl Acad Sci. 2009 Dec 1;106(48):20240–5.

98. Riera A, Tognetti S, Speck C. Helicase loading: How to build a MCM2-7 double-hexamer. Semin Cell Dev Biol. 2014 Jun;30:104–9.

99. Jain R, Aggarwal AK, Rechkoblit O. Eukaryotic DNA polymerases. Curr Opin Struct Biol. 2018 Dec;53:77–87.

100. Shibahara K, Stillman B. Replication-Dependent Marking of DNA by PCNA Facilitates CAF-1-Coupled Inheritance of Chromatin. Cell. 1999 Feb;96(4):575–85.

101. Krude T. Chromatin Assembly Factor 1 (CAF-1) Colocalizes with Replication Foci in HeLa Cell Nuclei. Exp Cell Res. 1995 Oct;220(2):304–11.

102. Gasser R, Koller T, Sogo JM. The Stability of Nucleosomes at the Replication Fork. J Mol Biol. 1996 May;258(2):224–39.

103. Kujirai T, Kurumizaka H. Transcription through the nucleosome. Curr Opin Struct Biol. 2020 Apr;61:42–9.

104. Wasylyk B, Thevenin G, Oudet P, Chambon P. Transcription of in vitro assembled chromatin by Escherichia coli RNA polymerase. J Mol Biol. 1979 Mar;128(3):411–40.

105. Lorch Y, LaPointe JW, Kornberg RD. Nucleosomes inhibit the initiation of transcription but allow chain elongation with the displacement of histones. Cell. 1987 Apr;49(2):203–10.

106. Cardone M, Alonso A, Pazienza M, Ventura M, Montemurro G, Carbone L, et al. Independent centromere formation in a capricious, gene-free domain of chromosome 13q21 in Old World monkeys and pigs. Genome Biol. 2006;7(10):R91.

107. Talbert PB, Henikoff S. Transcribing Centromeres: Noncoding RNAs and Kinetochore Assembly. Trends Genet. 2018 Aug;34(8):587–99.

108. Wong LH, Brettingham-Moore KH, Chan L, Quach JM, Anderson MA, Northrop EL, et al. Centromere RNA is a key component for the assembly of nucleoproteins at the nucleolus and centromere. Genome Res. 2007 Jul 10;17(8):1146–60.

109. Ferri F, Bouzinba-Segard H, Velasco G, Hubé F, Francastel C. Non-coding murine centromeric transcripts associate with and potentiate Aurora B kinase. Nucleic Acids Res. 2009 Aug;37(15):5071–80.

110. Ideue T, Cho Y, Nishimura K, Tani T. Involvement of satellite I noncoding RNA in regulation of chromosome segregation. Genes Cells. 2014 Jun;19(6):528–38.

111. Clark DJ, Felsenfeld G. A Nucleosome Core Is Transferred Out of the Path of a Transcribing Polymerase. Cell. 1992 Oct;71(1):11–22.

112. Mitra S, Bodor DL, David AF, Abdul-Zani I, Mata JF, Neumann B, et al. Genetic screening identifies a SUMO protease dynamically maintaining centromeric chromatin. Nat Commun. 2020 Dec;11(1):501.

113. Juillerat A, Gronemeyer T, Keppler A, Gendreizig S, Pick H, Vogel H, et al. Directed Evolution of O6-Alkylguanine-DNA Alkyltransferase for Efficient Labeling of Fusion Proteins with Small Molecules In Vivo. Chem Biol. 2003 Apr;10(4):313–7.

114. Pegg AE. Repair of O6-alkylguanine by alkyltransferases. Mutat Res Mutat Res. 2000 Apr;462(2–3):83–100.

115. Crivat G, Taraska JW. Imaging proteins inside cells with fluorescent tags. Trends Biotechnol. 2012 Jan;30(1):8–16.

116. Bodor DL, Rodríguez MG, Moreno N, Jansen LET. Analysis of Protein Turnover by Quantitative SNAP-Based Pulse-Chase Imaging. In: Bonifacino JS, Dasso M, Harford JB, Lippincott-Schwartz J, Yamada KM, editors. Current Protocols in Cell Biology [Internet]. Hoboken, NJ, USA: John Wiley & Sons, Inc.; 2012 [cited 2020 Apr 12]. p. cb0808s55. Available from: http://doi.wiley.com/10.1002/0471143030.cb0808s55

117. Mukhopadhyay D, Arnaoutov A, Dasso M. The SUMO protease SENP6 is essential for inner kinetochore assembly. J Cell Biol. 2010 Mar 8;188(5):681–92.

118. Creton S, Jentsch S. SnapShot: The SUMO System. Cell. 2010 Nov;143(5):848-848.e1.

119. Keiten-Schmitz J, Schunck K, Müller S. SUMO Chains Rule on Chromatin Occupancy. Front Cell Dev Biol. 2020 Jan 10;7:343.

120. Hickey CM, Wilson NR, Hochstrasser M. Function and regulation of SUMO proteases. Nat Rev Mol Cell Biol. 2012 Dec;13(12):755–66.

121. Mikolajczyk J, Drag M, Békés M, Cao JT, Ronai Z, Salvesen GS. Small Ubiquitin-related Modifier (SUMO)-specific Proteases: Profiling The Specificities and Activities of Human SENPs. J Biol Chem. 2007 Sep 7;282(36):26217–24.

122. Mukhopadhyay D, Dasso M. Modification in reverse: the SUMO proteases. Trends Biochem Sci. 2007 Jun;32(6):286–95.

123. Kunz K, Piller T, Müller S. SUMO-specific proteases and isopeptidases of the SENP family at a glance. J Cell Sci. 2018 Mar 15;131(6):jcs211904.

124. Huang C, Han Y, Wang Y, Sun X, Yan S, Yeh ETH, et al. SENP3 is responsible for HIF-1 transactivation under mild oxidative stress via p300 de-SUMOylation. EMBO J. 2009 Sep 16;28(18):2748–62.

125. Hwang EJ, Lee JM, Jeong J, Park JH, Yang Y, Lim J-S, et al. SUMOylation of RORα potentiates transcriptional activation function. Biochem Biophys Res Commun. 2009 Jan;378(3):513–7.

126. Boukhtouche F, Mariani J, Tedgui A. The "CholesteROR" Protective Pathway in the Vascular System. Arterioscler Thromb Vasc Biol. 2004 Apr;24(4):637–43.

127. Shimshon L, Michaeli A, Hadar R, Nutt SL, David Y, Navon A, et al. SUMOylation of Blimp-1 promotes its proteasomal degradation. FEBS Lett. 2011 Aug 4;585(15):2405–9.

128. Alm-Kristiansen AH, Norman IL, Matre V, Gabrielsen OS. SUMO modification regulates the transcriptional activity of FLASH. Biochem Biophys Res Commun. 2009 Sep;387(3):494–9.

129. Lindberg MJ, Popko-Scibor AE, Hansson ML, Wallberg AE. SUMO modification regulates the transcriptional activity of MAML1. FASEB J. 2010 Jul;24(7):2396–404.

130. Chang T-H, Xu S, Tailor P, Kanno T, Ozato K. The Small Ubiquitin-like Modifier-Deconjugating Enzyme Sentrin-Specific Peptidase 1 Switches IFN Regulatory Factor 8 from a Repressor to an Activator during Macrophage Activation. J Immunol. 2012 Oct 1;189(7):3548–56.

131. Di Bacco A, Ouyang J, Lee H-Y, Catic A, Ploegh H, Gill G. The SUMO-Specific Protease SENP5 Is Required for Cell Division. Mol Cell Biol. 2006 Jun 15;26(12):4489–98.

132. Li S-J, Hochstrasser M. A new protease required for cell-cycle progression in yeast. Nature. 1999 Mar;398(6724):246–51.

133. Li S-J, Hochstrasser M. The Yeast ULP2 (SMT4) Gene Encodes a Novel Protease Specific for the Ubiquitin-Like Smt3 Protein. Mol Cell Biol. 2000;20:11.

134. Harder Z, Zunino R, McBride H. Sumo1 Conjugates Mitochondrial Substrates and Participates in Mitochondrial Fission. Curr Biol. 2004 Feb;14(4):340–5.

135. Liebelt F, Jansen NS, Kumar S, Gracheva E, Claessens LA, Verlaan-de Vries M, et al. The poly-SUMO2/3 protease SENP6 enables assembly of the constitutive centromere-associated network by group deSUMOylation. Nat Commun. 2019 Dec;10(1):3987.

136. Wagner K, Kunz K, Piller T, Tascher G, Hölper S, Stehmeier P, et al. The SUMO Isopeptidase SENP6 Functions as a Rheostat of Chromatin Residency in Genome Maintenance and Chromosome Dynamics. Cell Rep. 2019 Oct;29(2):480-494.e5.

137. Ohkuni K, Takahashi Y, Fulp A, Lawrimore J, Au W-C, Pasupala N, et al. SUMO-targeted ubiquitin ligase (STUbL) Slx5 regulates proteolysis of centromeric histone H3 variant Cse4 and prevents its mislocalization to euchromatin. Cohen-Fix O, editor. Mol Biol Cell. 2016 May;27(9):1500–10.

138. Ohkuni K, Levy-Myers R, Warren J, Au W-C, Takahashi Y, Baker RE, et al. N-terminal Sumoylation of Centromeric Histone H3 Variant Cse4 Regulates Its Proteolysis To Prevent Mislocalization to Non-centromeric Chromatin. G3amp58 GenesGenomesGenetics. 2018 Apr;8(4):1215–23.

139. Ohkuni K, Suva E, Au W-C, Walker RL, Levy-Myers R, Meltzer PS, et al. Deposition of Centromeric Histone H3 Variant CENP-A/Cse4 into Chromatin Is Facilitated by Its C-Terminal Sumoylation. Genetics. 2020 Apr;214(4):839–54.

140. Zeiler M, Straube WL, Lundberg E, Uhlen M, Mann M. A Protein Epitope Signature Tag (PrEST) Library Allows SILAC-based Absolute Quantification and Multiplexed Determination of Protein Copy Numbers in Cell Lines. Mol Cell Proteomics. 2012 Mar;11(3):O111.009613.

141. Meyer H, Weihl CC. The VCP/p97 system at a glance: connecting cellular function to disease pathogenesis. J Cell Sci. 2014 Sep 15;127(18):3877–83.

142. Jentsch S, Rumpf S. Cdc48 (p97): a 'molecular gearbox' in the ubiquitin pathway? Trends Biochem Sci. 2007 Jan;32(1):6–11.

143. Ye Y. Diverse functions with a common regulator: Ubiquitin takes command of an AAA ATPase. J Struct Biol. 2006 Oct;156(1):29–40.

144. Zhang X, Shaw A, Bates PA, Newman RH, Gowen B, Orlova E, et al. Structure of the AAA ATPase p97. Mol Cell. 2000 Dec;6(6):1473–84.

145. DeLaBarre B, Brunger AT. Complete structure of p97/valosin-containing protein reveals communication between nucleotide domains. Nat Struct Mol Biol. 2003 Oct;10(10):856–63.

146. Ramadan K, Bruderer R, Spiga FM, Popp O, Baur T, Gotta M, et al. Cdc48/p97 promotes reformation of the nucleus by extracting the kinase Aurora B from chromatin. Nature. 2007 Dec;450(7173):1258–62.

147. Dobrynin G, Popp O, Romer T, Bremer S, Schmitz MHA, Gerlich DW, et al. Cdc48/p97-Ufd1-Npl4 antagonizes Aurora B during chromosome segregation in HeLa cells. J Cell Sci. 2011 May 1;124(9):1571–80.

148. Bergink S, Ammon T, Kern M, Schermelleh L, Leonhardt H, Jentsch S. Role of Cdc48/p97 as a SUMO-targeted segregase curbing Rad51–Rad52 interaction. Nat Cell Biol. 2013 May;15(5):526–32.

149. Davies JM, Brunger AT, Weis WI. Improved Structures of Full-Length p97, an AAA ATPase: Implications for Mechanisms of Nucleotide-Dependent Conformational Change. Structure. 2008 May;16(5):715–26.

150. Bank RPD. RCSB PDB - 3CF3: Structure of P97/vcp in complex with ADP [Internet]. [cited 2020 Dec 29]. Available from: https://www.rcsb.org/structure/3CF3

151. Los GV, Encell LP, McDougall MG, Hartzell DD, Karassina N, Zimprich C, et al. HaloTag: A Novel Protein Labeling Technology for Cell Imaging and Protein Analysis. ACS Chem Biol. 2008 Jun;3(6):373–82.

152. Fujita Y, Hayashi T, Kiyomitsu T, Toyoda Y, Kokubu A, Obuse C, et al. Priming of Centromere for CENP-A Recruitment by Human hMis18α, hMis18β, and M18BP1. Dev Cell. 2007 Jan;12(1):17–30.

153. Pan D, Walstein K, Take A, Bier D, Kaiser N, Musacchio A. Mechanism of centromere recruitment of the CENP-A chaperone HJURP and its implications for centromere licensing. Nat Commun. 2019 Dec;10(1):4046.

154. Sullivan KF, Glass CA. CENP-B is a highly conserved mammalian centromere protein with homology to the helix-loop-helix family of proteins. Chromosoma. 1991 Jul;100(6):360–70.

155. Gamba R, Fachinetti D. From evolution to function: Two sides of the same CENP-B coin? Exp Cell Res. 2020 May;390(2):111959.

156. Muro Y, Masumoto H, Yoda K, Nozaki N, Ohashi M, Okazaki T. Centromere Protein B Assembles Human Centromeric a-satellite DNA at the 17-bp Sequence, CENP-B Box. J Cell Biol. 1992 Feb 1;116(3):585–96.

157. Amor DJ, Bentley K, Ryan J, Perry J, Wong L, Slater H, et al. Human centromere repositioning 'in progress'. Proc Natl Acad Sci. 2004 Apr 27;101(17):6542–7.

158. Hudson DF, Fowler KJ, Earle E, Saffery R, Kalitsis P, Trowell H, et al. Centromere Protein B Null Mice are Mitotically and Meiotically Normal but Have Lower Body and Testis Weights. J Cell Biol. 1998 Apr 20;141(2):309–19.

159. Kapoor M, Montes de Oca Luna R, Liu G, Lozano G, Cummings C, Mancini M, et al. The cenpB gene is not essential in mice. Chromosoma. 1998 Dec 1;107(8):570–6.

160. Perez-Castro AV, Shamanski FL, Meneses JJ, Lovato TL, Vogel KG, Moyzis RK, et al. Centromeric Protein B Null Mice Are Viable with No Apparent Abnormalities. Dev Biol. 1998 Sep;201(2):135–43.

161. Tawaramoto MS, Park S-Y, Tanaka Y, Nureki O, Kurumizaka H, Yokoyama S. Crystal Structure of the Human Centromere Protein B (CENP-B) Dimerization Domain at 1.65-Å Resolution. J Biol Chem. 2003 Dec 19;278(51):51454–61.

162. Tanaka Y. Crystal structure of the CENP-B protein-DNA complex: the DNA-binding domains of CENP-B induce kinks in the CENP-B box DNA. EMBO J. 2001 Dec 3;20(23):6612–8.

163. Yoda K, Ando S, Okuda A, Kikuchi A, Okazaki T. In vitro assembly of the CENP-B/α-satellite DNA/core histone complex: CENP-B causes nucleosome positioning. Genes Cells. 1998 Aug;3(8):533–48.

164. Fachinetti D, Han JS, McMahon MA, Ly P, Abdullah A, Wong AJ, et al. DNA Sequence-Specific Binding of CENP-B Enhances the Fidelity of Human Centromere Function. Dev Cell. 2015 May;33(3):314–27.

165. Davies D, Allen P. DNA Analysis by Flow Cytometry. In: Macey MG, editor. Flow Cytometry [Internet]. Totowa, NJ: Humana Press; 2007 [cited 2020 Dec 21]. p. 165–79. Available from: http://link.springer.com/10.1007/978-1-59745-451-3_7

166. Givan AL. Flow Cytometry: An Introduction. In: Hawley TS, Hawley RG, editors. Flow Cytometry Protocols [Internet]. Totowa, NJ: Humana Press; 2011 [cited 2020 Dec 21]. p. 1–29. (Methods in Molecular Biology; vol. 699). Available from: http://link.springer.com/10.1007/978-1-61737-950-5_1

167. Riemer A, Dobrynin G, Dressler A, Bremer S, Soni A, Iliakis G, et al. The p97-Ufd1-Npl4 ATPase complex ensures robustness of the G_2/M checkpoint by facilitating CDC25A degradation. Cell Cycle. 2014 Mar 15;13(6):919–27.

168. Palmer N, Kaldis P. Regulation of the Embryonic Cell Cycle During Mammalian Preimplantation Development. In: Current Topics in Developmental Biology [Internet]. Elsevier; 2016 [cited 2020 Dec 25]. p. 1–53. Available from: https://linkinghub.elsevier.com/retrieve/pii/S0070215316301223

169. Fu X, Ng C, Feng D, Liang C. Cdc48p is required for the cell cycle commitment point at Start via degradation of the G1-CDK inhibitor Far1p. J Cell Biol. 2003 Oct 13;163(1):21–6.

170. Bjursell G, Reichard P. Effects of thymidine on deoxyribonucleoside triphosphate pools and deoxyribonucleic acid synthesis in Chinese hamster ovary cells. J Biol Chem. 1973 Jun 10;248(11):3904–9.

171. Ma HT, Poon RYC. Synchronization of HeLa Cells. In: Banfalvi G, editor. Cell Cycle Synchronization [Internet]. Totowa, NJ: Humana Press; 2011 [cited 2020 Dec 21]. p. 151–61. (Methods in Molecular Biology; vol. 761). Available from: http://link.springer.com/10.1007/978-1-61779-182-6_10

172. Chen G, Deng X. Cell Synchronization by Double Thymidine Block. BIO-Protoc [Internet]. 2018 [cited 2020 Dec 21];8(17). Available from: https://bio-protocol.org/e2994

173. Xeros N. Deoxyriboside Control and Synchronization of Mitosis. Nature. 1962 May;194(4829):682–3.

174. Salic A, Mitchison TJ. A chemical method for fast and sensitive detection of DNA synthesis in vivo. Proc Natl Acad Sci. 2008 Feb 19;105(7):2415–20.

175. Bradford JA, Clarke ST. Dual-Pulse Labeling Using 5-Ethynyl-2′-Deoxyuridine (EdU) and 5-Bromo-2′-Deoxyuridine (BrdU) in Flow Cytometry. Curr Protoc Cytom. 2011 Jan;Chapter 7:Unit 7.38.

176. Tornøe CW, Christensen C, Meldal M. Peptidotriazoles on Solid Phase: [1,2,3]-Triazoles by Regiospecific Copper(I)-Catalyzed 1,3-Dipolar Cycloadditions of Terminal Alkynes to Azides. J Org Chem. 2002 May;67(9):3057–64.

177. Gratzner H. Monoclonal antibody to 5-bromo- and 5-iododeoxyuridine: A new reagent for detection of DNA replication. Science. 1982 Oct 29;218(4571):474–5.

178. Buck SB, Bradford J, Gee KR, Agnew BJ, Clarke ST, Salic A. Detection of S-phase cell cycle progression using 5-ethynyl-2′-deoxyuridine incorporation with click chemistry, an alternative to using 5-bromo-2′-deoxyuridine antibodies. BioTechniques. 2008 Jun;44(7):927–9.

179. Nishimura K, Fukagawa T, Takisawa H, Kakimoto T, Kanemaki M. An auxin-based degron system for the rapid depletion of proteins in nonplant cells. Nat Methods. 2009 Dec;6(12):917–22.

180. Teale WD, Paponov IA, Palme K. Auxin in action: signalling, transport and the control of plant growth and development. Nat Rev Mol Cell Biol. 2006 Nov;7(11):847–59.

181. Ruegger M, Dewey E, Gray WM, Hobbie L, Turner J, Estelle M. The TIR1 protein of Arabidopsis functions in auxin response and is related to human SKP2 and yeast Grr1p. Genes Dev. 1998 Jan 15;12(2):198–207.

182. Gray WM, del Pozo JC, Walker L, Hobbie L, Risseeuw E, Banks T, et al. Identification of an SCF ubiquitin-ligase complex required for auxin response in Arabidopsis thaliana. Genes Dev. 1999 Jul 1;13(13):1678–91.

183. Tan X, Calderon-Villalobos LIA, Sharon M, Zheng C, Robinson CV, Estelle M, et al. Mechanism of auxin perception by the TIR1 ubiquitin ligase. Nature. 2007 Apr;446(7136):640–5.

184. Abel S, Theologis A. Early Genes and Auxin Action. Plant Physiol. 1996 May 1;111(1):9–17.

185. Holland AJ, Fachinetti D, Han JS, Cleveland DW. Inducible, reversible system for the rapid and complete degradation of proteins in mammalian cells. Proc Natl Acad Sci. 2012 Dec 4;109(49):E3350–7.

186. Hoffmann S, Dumont M, Barra V, Ly P, Nechemia-Arbely Y, McMahon MA, et al. CENP-A Is Dispensable for Mitotic Centromere Function after Initial Centromere/Kinetochore Assembly. Cell Rep. 2016 Nov;17(9):2394–404.

187. Magnaghi P, D'Alessio R, Valsasina B, Avanzi N, Rizzi S, Asa D, et al. Covalent and allosteric inhibitors of the ATPase VCP/p97 induce cancer cell death. Nat Chem Biol. 2013 Sep;9(9):548–56.

188. Saitoh H, Tomkiel J, Cooke CA, Ratrie H, Maurer M, Rothfield NF, et al. CENP-C, an autoantigen in scleroderma, is a component of the human inner kinetochore plate. Cell. 1992 Jul;70(1):115–25.

189. Orr B, Sunkel CE. Drosophila CENP-C is essential for centromere identity. Chromosoma. 2011 Feb;120(1):83–96.

190. Tanaka K, Li Chang H, Kagami A, Watanabe Y. CENP-C Functions as a Scaffold for Effectors with Essential Kinetochore Functions in Mitosis and Meiosis. Dev Cell. 2009 Sep;17(3):334–43.

191. Milks KJ, Moree B, Straight AF. Dissection of CENP-C–directed Centromere and Kinetochore Assembly. Bloom KS, editor. Mol Biol Cell. 2009 Oct;20(19):4246–55.

192. Falk SJ, Guo LY, Sekulic N, Smoak EM, Mani T, Logsdon GA, et al. CENP-C reshapes and stabilizes CENP-A nucleosomes at the centromere. Science. 2015 May 8;348(6235):699–703.

193. Carpenter AE, Jones TR, Lamprecht MR, Clarke C, Kang I, Friman O, et al. CellProfiler: image analysis software for identifying and quantifying cell phenotypes. Genome Biol. 2006;7(10):R100.

194. Seo HD, Kwon CS, Lee D. The 19S proteasome regulates subtelomere silencing and facultative heterochromatin formation in fission yeast. Curr Genet. 2018 Jun;64(3):741–52.

195. Suhandynata RT, Quan Y, Yang Y, Yuan W-T, Albuquerque CP, Zhou H. Recruitment of the Ulp2 protease to the inner kinetochore prevents its hyper-sumoylation to ensure accurate chromosome segregation. Cheeseman I, editor. PLOS Genet. 2019 Nov 20;15(11):e1008477.

196. RNAi Transfection Protocols - UK [Internet]. [cited 2021 Jan 4]. Available from: //www.thermofisher.com/uk/en/home/life-science/cell-culture/transfection/rnai-transfection/rnai-transfection-protocols.html

197. Ando S, Yang H, Nozaki N, Okazaki T, Yoda K. CENP-A, -B, and -C chromatin complex that contains the I-type alpha-satellite array constitutes the prekinetochore in HeLa cells. Mol Cell Biol. 2002 Apr;22(7):2229–41.